Optimization of opto-electronic properties of spray deposited n-type tin monosulfide thin film for photovoltaic application

Thesis submitted to

Cochin University of Science and Technology

in partial fulfillment of the requirements

for the award of the degree of

Doctor of Philosophy

By

Gisa Grace Ninan

Reg No: 4631

Thin Film Photovoltaic Division
Department of Physics
Cochin University of Science and Technology
Cochin-682 022, Kerala, India

May 2019

Optimization of opto-electronic properties of spray deposited n-type tin monosulfide thin film for photovoltaic application

PhD thesis in the field of Inorganic Photovoltaics

Author

Gisa Grace Ninan
Thin Film Photovoltaic Division
Department of Physics
Cochin University of Science and Technology
Kochi-682 022, Kerala, India
E-mail: gisagrace@gmail.com

Supervising Guide

Dr. K. P. Vijayakumar
Professor (Emeritus Scientist)
Department of Physics
Cochin University of Science and Technology
Kochi-682 022, Kerala, India
E-mail: vijayakumar.kandathil@gmail.com

May 2019

DEPARTMENT OF PHYSICS
COCHIN UNIVERSITY OF SCIENCE AND TECHNOLOGY
KOCHI - 682022, INDIA

Dr. K. P. Vijayakumar   Phone: 0484 2577404
Emeritus Scientist   E-mail: vijayakumar.kandathil@gmail.com

Certificate

Certified that the work presented in the thesis entitled **"Optimization** of opto-electronic properties of spray deposited n-type tin monosulfide **thin film for photovoltaic application"** submitted by **Mrs. Gisa Grace Ninan** is an authentic record of research work carried out by her under my supervision at the Department of Physics in partial fulfilment of the requirements for the award of degree of Doctor of Philosophy of Cochin University of Science and Technology and the work embodied in this thesis has not been included in any other thesis submitted for the award of any degree. All the relevant corrections and modifications suggested by the audience during the pre-synopsis seminar have been incorporated in the thesis and recommended by the doctoral committee.

Kochi - 22   **Dr. K.P. Vijayakumar**
May 2019   (Supervising Guide)

Declaration

    I hereby declare that the work presented in the thesis entitled "Optimization of opto-electronic properties of spray deposited n-type **tin monosulfide thin film for photovoltaic application"** is based on the original work done by me under the guidance of **Dr. K. P. Vijayakumar**, Professor (Emeritus Scientist), Department of Physics, Cochin University of Science and Technology, Kochi- 682 022, India and has not been included in any other thesis submitted for the award of any degree.

Kochi - 22
May 2019

Gisa Grace Ninan

Acknowledgements

I owe thanks to all my seniors Dr. Angel, Dr. Rajesh Menon, Dr. Sajeesh, Dr. Rajeshmon, Dr. Poornima, Dr. Deepu, Dr. Santhosh, and to my lab mates Geethu, Gincy, Sreejith, Titu, Jubi, Rajesh, Aswathy, Anshad and Jisha. Words are inadequate to thank those incredible people in my life for the invaluable help during my initials days of research and also for the love and joyful days and wonderful chats and hangouts throughout my course of research, which I would like to treasure in my life. I fondly remember the lively moments during my stay at Athulya hostel and all the joys and sorrows that we shared. I would like to thank all my friends in the hostel, especially my roommate Soumya for the wonderful time we had together and for making research period an unforgettable experience for me. I express my thanks to all other friends in Department of Physics, other departments, M. Phil. and M.Sc. students who have done their projects in our lab for the help I received from them at every time I needed.

I express my heartiest gratitude to my husband, parents, brother, in-laws and kids for their support and understanding. I am deeply indebted to my mother for being with me and helping me in overcoming personal hurdles without hesitation. She was there with me always patiently helping me to achieve my goal by taking care and perfectly bringing up my elder son Leo in my absence. I thank my father for the devoted guidance and efforts to correct grammatical mistakes and improve the language of the thesis for the completion of my dream. Thanks to my brother Joe for arranging me the facility to take SEM and EDAX measurements in TIFR and also for the encouragement and valuable suggestions. I express my heartfelt gratitude to my husband Gino for his unflagging love, patient understanding and moral support during my entire research period. I truly thank him for sticking by my side and being a great supporter when I was irritable and depressed. My heartfelt thanks to my

Preface

The ever-growing energy needs of the future, which resulted in depletion and scarcity of conventional energy resources by 21st century shifted the focus to identify new sources of energy that are eco-friendly and low cost. Sun is the unlimited, inexhaustible power source and provides unlimited non-polluting renewable energy. But even with the advanced technology of solar cells, most of the solar power goes untrapped. Today almost 90 % of photovoltaics is governed by some variations of silicon (polycrystalline, monocrystalline, ribbon silicon, etc.). There exist problems like costly high-tech purification process, low absorption due to indirect band gap and stagnation in the improvement of cell efficiency. Hence ongoing research now focuses on developing new technologies which can reduce the manufacturing costs and requirement of costly material. Based on these grounds, compound semiconductor thin films made an entry since they have direct band gap with high absorption coefficient, low cost, ease of preparation and eco-friendly. They can easily replace the expensive wafers of silicon (which accounts for almost 50 % of the manufacturing cost of modules) and complicated deposition methods, which in turn, can make it affordable to the common man. Hence depending on the purpose, device structure and processing techniques have to be modified. The work reported here is an attempt to bring about the potential of n-type SnS. The present research work reports preparation, optimization and improvisation of copper doped tin sulfide thin films. For the fabrication of SnS:Cu thin films simple, cost-effective and economically viable deposition method, namely chemical spray pyrolysis (CSP) is selected. Tin sulfide is a binary compound semiconductor made of abundant and eco-friendly tin

i

and sulfur. Again usage of binary material is more advantageous due to the easiness in controlling the chemical compositions.

Six chapters in the thesis are self-explanatory with introduction, results and references. It is devoted to the synthesis and development of the recent material SnS (n-type) thin films. A brief description of each chapter is included below. Best to our knowledge, the study on n-type SnS:Cu thin films, its characterizations, modifications and fabrication using CSP technique with the aim to use in solar cells has not been reported prior to this work.

Chapter 1 presents general introduction, highlighting the present status about energy economy problems, importance of solar energy, various aspects of photovoltaics, thin films, solar cells, its structure and various performance parameters. The chapter concludes with an elaborate description of current technological trends and the necessity for better and new alternatives. This is followed by a detailed discussion based on review of SnS thin films and SnS based solar cells mentioning the significance and scope of present work.

Chapter 2 deals with the preparation and characterization of n-type SnS:Cu thin films using Chemical Spray Pyrolysis technique (CSP). The first part of this chapter includes preparation of n-type SnS via 'precursor solvent reduction method' and the second part describes the improvement of its properties via co-doping. Structural, electrical and optical characterizations were done using X-Ray diffraction, optical absorption and Hall measurements. Need for using one day aged tin chloride precursor solution and its ability to get polycrystalline SnS is discussed initially, and this condition is selected for further studies. As the next step, n-type SnS is prepared by precursor solvent reducing method, i.e.,

by reducing the HCl required for dissolving $SnCl_2$ salt. The results obtained were also presented.

An attempt to prepare low resistive SnS is described in the second part of this chapter. For this, metal doping with Cu is tried. Doping of Cu is done by adding the required quantity of $CuCl_2.2H_2O$ into the initial spray solution. Molarity and doping percentage of copper chloride is optimized and is explained in this section. Resistivity was reduced by two orders, which is the lowest value obtained through chemical methods. Hence optimized precursor condition for the fabrication of SnS:Cu and relevant results obtained are highlighted in this chapter.

Chapter 3 gives a vivid description about various deposition conditions that has to be standardized in order to prepare good quality film. Generally, quality of thin film depends on many deposition parameters such as substrate temperature, rate of deposition, precursor selection, its molar ratio etc. Hence in this chapter steps to optimize all these parameters are discussed in detail. Initially, the substrate temperature of the film is optimized by varying the deposition temperature. Now keeping this temperature fixed, spray rate is optimized at which the film posses maximum crystallite size with optimum band gap and minimum surface roughness. Next aim is to optimize the composition ratio required for the deposition of good quality SnS:Cu thin films. For this, we initially varied cationic molarity keeping anionic molarity fixed and same way anionic molarity is varied keeping previously optimized cationic molarity fixed. From the latter studies, the better composition ratio Sn:S is found to be 1:2. Hence this chapter covers the crucial parameters required for the successful deposition of thin films along with the comprehensively evaluated results.

Chapter 4 describes new ways to improve the properties of fabricated films and also stability against various parameters is investigated. As an initial step, the precursor solvent is optimized once more to check, whether there is any change in its optimum value due to copper doping. Asthe next step, the influence due to various post-deposition treatments and its stability against various factors is checked. For this, various annealing treatments were carried out in air and vacuum. The optimum annealing time required and effect on material properties due to the inversion technique is also explained. Material stability against environmental temperature condition while preparing the precursor solution, is also checked, because even in our place there is temperature variation around 10 ^{o}C from winter to summer. From the characterizations, we obtained a remarkable conclusion, that this material can withstand the variations in precursor preparation temperature, without compromising its material properties. These properties make this material a good candidate for device fabrication. Hence present chapter gives a comprehensive idea about the material properties which is a pre-requisite, before going for solar cell fabrication.

Chapter 5 is an attempt to fabricate a novel device architecture in order to unlock the complete potential of material (SnS:Cu) and also investigated various ways for improving the output parameters. Even though various trial works on the device fabrication are still going on, till now no technique has been reported as the favoured fabrication technique. Best to our knowledge hetero-junction based on CZTS as p-layer and SnS:Cu (as described in previous chapters) as n-layer is demonstrated for the first time. Usually, in solar devices, a window layer with a large band gap and an absorber layer with a relatively narrow

band gap are used. But here in this case, two different materials (p-type CZTS having a band gap of ~1.5 eV and an n-type SnS:Cu having a band gap of ~1.4 eV) with almost similar band gap are used. Such a configuration is advantageous because here both can act as absorbers and has the possibility to function as a bifacial solar cell. But great care should be taken to optimize the thickness and other material properties since both layers play the role of absorbers. Hence initial section of this chapter highlights the fabrication of ITO/CZTS/SnS:Cu/Ag solar cells and the modification of structure by introducing a top layer (ZnO:Al) above SnS:Cu as ITO/CZTS/SnS:Cu/ZnO:Al/Ag. In the final section of this chapter, various aspects to improve the parameters is explained and analyzed. The current-voltage characteristics under illuminated conditions are also explained and presented in this chapter. The present work is a preliminary study and there is more room for further improvement and this material deserves special attention.

Chapter 6 summarizes the entire work done with relevant results highlighted. This chapter concludes with brief discussions on various problems that has to be sorted out, so as to enhance the short circuit current, efficiency and also about the possibility of fabricating heterojunctions with other organic and inorganic materials.

Contents

xi

List of Tables

List of Figures

xvii

xviii

xix

List of Publications

Journal publications

1. "Synthesis Of Spray Pyrolysed Copper Doped Tin Sulfide (SnS:Cu) Thin Films By Optimizing The Anionic Precursor Molarity", **Gisa Grace Ninan**, C. Sudha Kartha, K.P. Vijayakumar; Materials Today: Proceedings 8 (2019) 352–356.

2. "Eco-Friendly And Non-Toxic Thin Film Solar Cell Employing Spray Pyrolysed p-CZTS and n-SnS:Cu - A Novel Approach", **Gisa Grace Ninan**, M. R. Rajesh Menon, R. Geethu, D. R. Deepu, C. SudhaKartha and K. P. Vijayakumar; Journal of Materials Science: Materials in Electronics 29.23 (2018) 20455-20461.

3. "SnS:Cu Thin Film A Green Solar Absorber: A Method To Reduce Oxygen In Sprayed SnS:Cu", **Gisa Grace Ninan**, C. Sudha Kartha, K.P. Vijayakumar; Scire Science Multidisciplinary Journal 1(2017) 7-14.

4. "n-Type SnS:Cu Thin Films With High Surface Energy (111) Plane: Optimization Of Its Substrate Temperature", **Gisa Grace Ninan**, C. Sudha Kartha, K.P. Vijayakumar; International Journal of Scientific Research in Science and Technology 3 (2017) 202-205.

5. "Spray Pyrolysed SnS Thin Films In n And p type: Optimization Of Deposition Process And Characterization Of Samples", **Gisa Grace Ninan**, C. Sudha Kartha, K.P. Vijayakumar; Journal of Analytical and Applied Pyrolysis 120 (2016) 121–125.

6. "On The Preparation Of n-Type SnS:Cu Using Chemical Spray Pyrolysis For Photovoltaic Application: Effect Of Annealing", **Gisa Grace Ninan**, C.Sudha Kartha, K.P.Vijayakumar; Solar Energy Materials & Solar Cells 157 (2016) 229–233.

7. "Cu Doping: An Effective Method For Improving Optoelectronic Properties Of Sprayed SnS Thin Films", **Gisa Grace Ninan**, V. G Rajeshmon, C. Sudha Kartha, K.P. Vijayakumar; AIP Conference Proceedings 1591 (2014) 1440.

International/National Conference Papers

1. "Synthesis Of Spray Pyrolysed Copper Doped Tin Sulfide (SnS:Cu) Thin Films By Optimizing The Anionic Precursor Molarity" , **Gisa Grace Ninan**, C. Sudha Kartha, K.P. Vijayakumar. International Conference On Materials For Energy And Environment -2018, (22 – 23 February 2018), Loyola College, Chennai, Tamil Nadu

2. n-Type SnS:Cu Thin Films With High Surface Energy (111) Plane: Optimization Of Its Substrate Temperature", **Gisa Grace Ninan**, C. Sudha Kartha, K.P. Vijayakumar. International Conference On Advanced Materials (14-15 December 2017), St. Joseph's College, Thiruchirappalli, Tamil Nadiu

3. "Probing The Possibilities For n-Type SnS:Cu Thin Films With (111) Orientation As The Efficient Solar Cell Absorber Layer", **Gisa Grace Ninan**, C. Sudha Kartha, K.P. Vijayakumar; 6th National Seminar on Advances in Materials Science-2017 (NSAMS 2017), 2-3 March 2017, Mononmaniam Sundaranar University, Tirunelveli, Tamil Nadiu

4. "Synthesis And Characterization Of Copper Doped Tin Sulfide (SnS:Cu) Thin Films Through Spray Technique: Importance of Cationic Precursor Molarity", **Gisa Grace Ninan**, C. Sudha Kartha, K.P. Vijayakumar; 29th Kerala Science Congress (National Conference), 28-30 January 2017, Mar Thoma College, Thiruvalla, Kerala

5. "A Study On The Significant Aspects Of Fabrication Of SnS:Cu Thin Films Using CSP Technique For Photovoltaic Application", **Gisa Grace Ninan**, C. Sudha Kartha, K.P. Vijayakumar; National Conference (ETAP - 2016), 6-8 January, Bishop Moore College, Mavelikara

6. "Improving Optoelectronic Properties of SnS Thin Films by Optimizing Precursor Condition And Doping", **Gisa Grace Ninan** , C. Sudha Kartha, K.P. Vijayakumar; National Seminar On Recent Developments In Physics, 19-20 October 2015, NSS College, Ottapalam

7. "Investigations On The Opto-Electronic Properties Of n-Type SnS:Cu Due To Spray Rate Variation", **Gisa Grace Ninan** , C. Sudha Kartha, K.P. Vijayakumar; National Conference, Trends in Physical Sciences (TriPS-2015), 30-31 July, Sree Sankara College, Kalady

8. Ageing Of Precursor Solution: An Effective Method For Improving Optoelectronic Properties Of Sprayed SnS Thin Films", **Gisa Grace Ninan**, N Poormina, C. Sudha Kartha, K.P. Vijayakumar; International Conference, (ICEEE 2015), 5-7 February, CUSAT, Cochin

List of Abbreviations

PV	-	Photovoltaics
CSP	-	Chemical spray pyrolysis
SnS:Cu	-	Copper doped tin sulfide
XRD	-	X-ray diffraction
XPS	-	X-ray photo electron spectroscopy
AFM	-	Atomic force microscopy
RMS	-	Root mean square
SEM	-	Scanning electron microscopy
TCO	-	Transparent conducting oxide
ITO	-	Tin doped indium oxide
CZTS	-	Copper zinc tin sulfide
FF	-	Fill factor
J_{sc}	-	Short circuit current density
V_{oc}	-	Open circuit voltage
R_s	-	Series resistance
R_{sh}	-	Shunt resistance

.....ಸಾ.....

Chapter 1

AN INSIGHT TO ABSORBER LAYER, ITS PROPERTIES AND EXPERIMENTAL DETAILS

This thesis describes fabrication, characterization and optimization of thin film solar cell material 'copper doped tin sulfide' (SnS:Cu) via non-vacuum chemical spray pyrolysis technique. SnS:Cu research has attained great interest in recent times, and the field is rapidly developing. All the constituent materials used in the preparation of this compound semiconductor (namely copper, tin and sulfur) are non-toxic and are relatively abundant. Following chapters emphasis preparation conditions and characterization of SnS:Cu thin films, and also optimization of various spray parameters to improve its optoelectronic properties. The thesis concludes with a detailed discussion about trial works done to fabricate solar cell using CZTS/SnS:Cu heterojunction and possible improvements required to improve the cell.

1.1 Introduction

Sun is the major source of energy for our planet. It can be considered as an infinite powerhouse which radiates energy in all directions, of which our earth receives a part. It is calculated that sun deposits ~ 120,000 TW of radiation on earth's surface that amounts far more than the planet's energy needs. It is theoretically calculated that using solar panels with 10 % efficiency covering 0.16 % of the land

alone can provide 20 TW of power. This power is near twice the power produced by fossil energy to meet the world's present consumption [1-3].

The ability of the solar cell to convert incident solar energy into electricity without any fuel consumption, mechanical movements or byproduct formation paved the way for rapid interest and research in the field of photovoltaics. Indeed photovoltaic research started in the first half of the 19th century when Becquerel in 1839 succeeded in obtaining photovoltage with light incident on an electrode kept in electrolyte solution [4]. Then in 1883 Charles Fritts, came up with plans for making solar cells and was followed by the discovery of photovoltaic effect in selenium and finally a photovoltaic cell using selenium was fabricated, though it had a very low efficiency [5-7]. Later in 1954 David Chapin, Calvin Fuller and Gerald Pearson of Bell Labs fabricated world's first (silicon) solar cells [8]. Even with all these aforesaid developments, the solar panels are still unaffordable to the common man. Hence recent photovoltaic research mainly focuses on solar cells which are cost-effective, highly operation stable and at the same time eco-friendly. In such a scenario, studies focusing on earth-abundant photovoltaic materials can give a significant contribution. Before going into details, it is important to know what solar cells (Photovoltaic cells) are and how it functions. Solar cells convert photon energy into electrical energy at the junction between a p-type semiconductor layer and an n-type semiconductor layer. In photovoltaic terms, it is said to be a junction between an absorber and buffer layer. When photons of equal or greater energy than the band gap of absorber material fall on it, electrons in the valence band get excited to the conduction band of the absorber. This

results in the production of electron-hole pairs that cause a current to flow through an external circuit before they return to recombine and release their energy.

1.2 Thin film solar cells, its structure and major challenges

For a long time, crystalline silicon remained the king in the photovoltaic market. The silicon wafer cost remained more than 50 % of the total module cost. Replacement of these wafers by thin films using potential semiconductors can reduce the cost to a large extent, besides it gives an opportunity to establish various thin film technologies and its credentials [9].

1.2.1 Thin film solar cell structure

Thin film solar cell consists of various layers of materials with different chemical and physical properties. Because of these, chance for different defects, inter-diffusion, stress and other chemical changes can affect overall optoelectronic properties of the device [10]. The following section gives a brief description of thin film structure, various layers used and the role of each layer.

Generally, thin film solar cell consists of a substrate over which a transparent conducting oxide (TCO) is coated, atop comes the buffer layer, absorber layer and topmost is the metal contact.

1.2.1.1 TCO

It is the front contact of solar cell which is transparent to incident radiation and at the same time carries photogenerated current, produced

in the cell. Hence a wide band gap semiconductor with a band gap of about 3.3 eV and very low sheet resistivity ($\sim$ 10 Ω/sq (area resistance)) is generally selected [11]. Some of the widely used TCOs are "Tin doped Indium Oxide" (ITO), "aluminium doped Zinc Oxide" (AZO)) or "Fluorine-doped Tin Oxide" (FTO).

1.2.1.2 Buffer layer

The primary role of this layer is to form a junction with the absorber layer and at the same time being capable of admitting maximum light to reach the junction. Hence it should have minimum losses due to absorption and recombination (of minority carriers), good optical transparency (and hence larger band gap), and should have the capability to transport generated (minority) carriers easily [12]. Hence usually materials with wider band gap and minimum lattice mismatch between layers are chosen.

1.2.1.3 Absorber layer

Absorber layer plays an important role in the performance of solar cells because it is in this layer absorption of light and generation of carriers take place. Hence an optimum absorber material with high absorption coefficient and direct band gap in the range 1.2 to 1.7 eV is generally chosen [13]. Band gap around this range is large enough to reduce the density of reverse saturation current and at the same time small enough to absorb an appreciable range of the solar spectrum. Some of the widely used absorbers are CdTe, $CuInS_2$ (CIS), CIGS etc. The toxicity of Cd along with high cost and rarity of indium and tellurium

highlights the importance of new materials like CZTS, CIS, CZS, CTS and SnS which are currently active areas of photovoltaic research.

1.3 Basic concepts and physics of solar cells

A solar cell is a device that can convert light energy directly into electrical energy and is generally a p-n junction diode. The p-n junction is invented in around 1950, and within four years in 1954, Pearson discovered Si solar cell. Solar cells are interconnected in series or parallel to form solar modules to meet power requirements.

1.3.1 Working of Solar cell

This section outlines a brief idea about the working and the processes involved in a solar cell. For the conversion of sunlight to electricity, the following processes have to take place

a) Photon absorption

b) Carrier generation

c) Carrier separation

Electrons are excited to a higher state by absorbing energy from photons absorbed by it. This energy can be extracted more efficiently if there exists an energy gap. In the case of semiconductors, the excited state is separated from its ground state by the above-mentioned band gap and hence can be considered as good candidates for such systems. Semiconductors with band gap between 0.5 eV to 3 eV can absorb the visible light for exciting electrons across the energy gap. Absorption of light can also be enhanced by increasing thickness of absorber material with good charge collection. This can be achieved only with materials

having required optoelectronic properties. To separate the carriers formed in the process, intrinsic asymmetry in band gaps, the density of states, electron affinity, difference in work functions created by spatial variations etc. are required [10,14]. The possible ways to achieve this is to form a junction of two different materials or that of the same material treated differently. When p-type and n-type material is brought together, carriers diffuse across the junction, and they leave behind fixed charges on both sides produced by ionized atoms. Since after diffusion of electrons across the junction, there will not be any mobile carriers present in the region, it is known as 'depletion region'. An equilibrium condition is reached because diffusion of carriers is opposed by electric field created by imbalance of charges on either side of the junction. Now, when we illuminate the junction, electron-hole pairs are created in all the p-region, n-region and depletion region. But the pairs are separated by the electric field in the junction that drives the minority charge carriers across the junction. Once the carriers are separated, in order to do electrical work, it should be able to travel through the external circuit without resistance. This is achieved by using materials (for cell fabrication) that have low series resistance, high shunt resistance, good ohmic contact with the external circuit and fewer recombination losses. A combination of p and n-type semiconductor can give a "built-in electric field" in the junction and thus an asymmetry is made which will allow holes to flow from n side to p-side and electrons vice versa when the p-n junction is illuminated. The current flowing from n-side to p-side when illuminated is termed "light generated current (I_L)".

1.3.2 Solar cell performance parameters

To be very simple, the electrical properties shown by a solar cell can be explained as a parallel connection of a diode and a current source, where the current source includes all the process of converting light energy to electrical energy [15]. The current-voltage graph of a solar cell has positive voltage and negative current value that it shows up in the 4th quadrant of the graph. When a solar cell is illuminated (Figure 1.1 (b)) the intercept of electrical characteristics with vertical axis gives short circuit current (I_{sc}) and intercept with horizontal axis gives open circuit voltage (V_{oc}). The power density is calculated as the product of the current density and voltage. The voltage and current corresponding to the maximum power output are represented as V_m and I_m respectively. Fill factor (FF), and efficiency (η) of solar cell are other two significant parameters. Fill factor determines quality of I-V characteristics and efficiency is the ratio of output power to input power. The upcoming section gives a detailed idea about all the above parameters. Figure 1.1(a) and Figure 1.1(b) represent equivalent circuit of a solar cell and the current-voltage characteristics of solar cell on illumination.

(a)   **(b)**
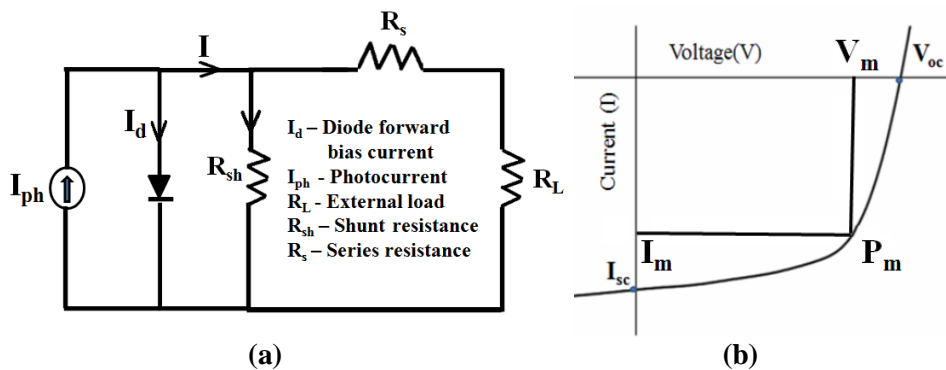
Figure 1.1 Equivalent circuit and I-V characteristics of solar cell

The solar cell equation which typically relates solar device parameters with output voltage and current is given by $I = I_L - I_0 \exp[qV/kT] - [V/R_{sh}]$ where I_L is the photogenerated current, I_0 is the cell reverse saturation current, q the charge of electron, V is the voltage, I is the current, R_s and R_{sh} the series and shunt resistance respectively, k the Boltzmann constant, and T is the temperature. Out of these I_0, R_s and R_{sh} are the diode parameters which give the performance parameters of solar cell, namely short circuit current (I_{sc}), open circuit voltage (V_{oc}), efficiency (η) and fill factor (*FF*).

1.3.2.1 Short circuit current (I_{sc})

It is the maximum current that a solar cell can produce when the terminals are short-circuited. Figure 1.2 represents the schematic diagram of short circuit condition.
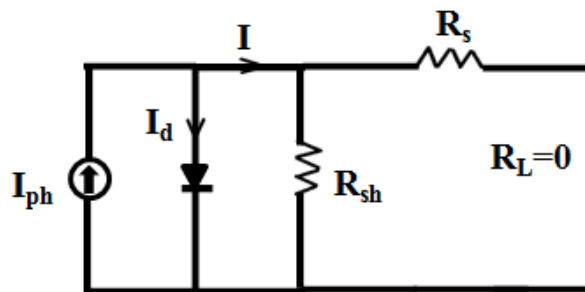
Figure 1.2 Schematic diagram of short circuit condition

It is calculated by the incident light spectrum and the solar cell area. The dependence of short circuit current on cell area can be removed by using short circuit current density (J_{sc}) term in general. Thus the maximum current output that a photovoltaic cell can provide depends mainly on optical properties of the material selected and collection probability of the

cell. The major optical property on which J_{sc} depends strongly is the absorber material band gap. Low band gap material absorbs a larger number of photons compared to large band gap material, and therefore J_{sc} will decrease with increase in band gap energy. The collection probability depends mainly on minority carrier lifetime and surface passivation.

1.3.2.2 Open circuit voltage (V_{oc})

Maximum output voltage that can be obtained from a solar cell is the open circuit voltage (V_{oc}) and is represented by Figure 1.3. It is measured as the voltage between the solar cell terminals when no current is drawn.
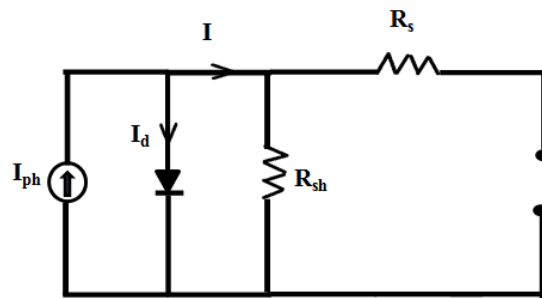
Figure 1.3 Schematic diagram of open circuit condition

Under open circuit condition, (which means there is no external contact between the n-type and the p-type) regions, no net current can flow inside the p-n junction. V_{oc} is given by the equation $V_{oc} \approx nkT/q \ln [I_L/I_0 + 1]$ [14]. This equation is derived from the characteristic equation by neglecting the final term. The term is neglected because the shunt resistance is assumed to be very high and V_{oc} depends mainly on light generated current. In general, V_{oc} will be less than that of the material band gap. V_{oc} will be greater only if I_0 is lower and since I_0 depends

mainly on the recombination rate of the device, V_{oc} can also be considered as a measure of recombination in the solar cell.

1.3.2.3 Fill factor (FF)

The maximum power that can be obtained from a solar cell is determined by a parameter called "fill factor (FF)". Fill factor can be measured as the ratio between maximum power output from the device and product of J_{sc} and $V_{oc.}$ i.e., $FF = V_m J_m / V_{oc} J_{sc}$ [14]. FF also plays an important role in determining the efficiency of the device because even with same J_{sc} and V_{oc} it is the FF which determines the maximum power (P_{max}) that can be collected from the device using the equation $P_{max} = V_{oc} J_{sc} FF$.

1.3.2.4 Efficiency (η)

Efficiency is the most widely used parameter to study the performance of various solar devices. In general, it is the ratio of output power to input power (P_{in}). The efficiency of solar cells mainly depends on the incident intensity of sunlight, solar spectrum and also the temperature of the solar device. Hence usually "Standard Test Conditions (STC)" is considered while measuring efficiency. STC points AM 1.5 spectrum with an irradiance of 1000 W/m^2 at temperature 25° C. Efficiency is given by the equation $\eta = V_{oc} J_{sc} FF / P_{in}$. From the equation, it is clear that efficiency depends directly on the V_{oc} and J_{sc}. For a solar cell, V_{oc} increases with band gap, and J_{sc} decreases with band gap and hence the selection of optimum band gap is essential to attain maximum solar cell efficiency.

Apart from the above mentioned primary parameters, the other two parameters considered in the present study are series resistance (R_s) and

shunt resistance (R_{sh}). These are important parameters for solar cell performance under given temperature and illumination intensity and is determined by various analytical methods [16].

1.3.2.5 Series resistance (R_s)

Series resistance in solar cells includes all types of resistances such as resistance between semiconductor and metal contact, resistance due to metal contact and also resistance due to all other components present along the current flowing path [17]. R_s affects fill factor and short circuit current. It is suggested that R_s should be zero for an ideal solar device. R_s can be calculated by finding the slope of the I-V curve at open-circuit voltage region. Variation of the I-V curve with an increase of R_s is shown in Figure 1.4. As R_s increases, I-V curve deviates more, and at the very high value, it becomes a straight line due to the voltage drop happening within the solar cell. Increase in R_s reduces I_{sc}, but the V_{oc} remains constant because the voltage drop in the device is zero under open circuit condition where there is no current flow.
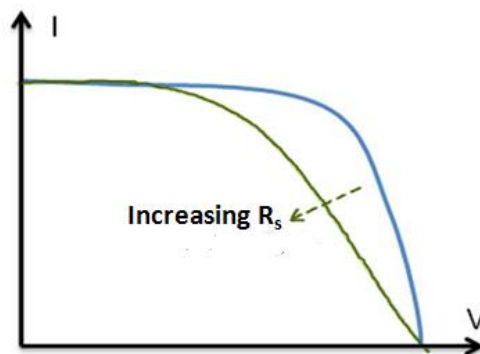
Figure 1.4 Consequence of increasing series resistance on the I-V curve

1.3.2.6 Shunt resistance (R_{sh})

The current leakage through edges of solar cell or through cell and between the contacts of different polarity gives rise to shunt resistance [18]. Low shunt resistance provides an alternate path for the generated current and causes power loss in solar cells. As a result, the I-V curve of the voltage-controlled portion begins to sag towards origin as shown in Figure 1.5. This results in a significant reduction of V_{oc} and also terminal current I.
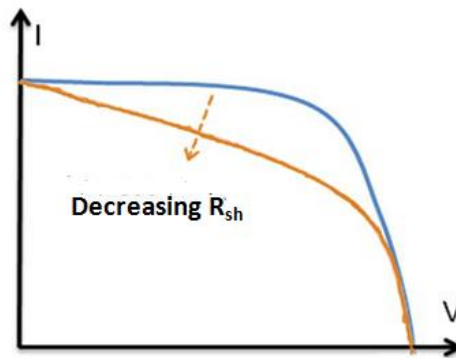
Figure 1.5 Consequence of decreasing shunt resistance on the I-V curve

Hence for an ideal solar cell, R_s should be zero and R_{sh} should be infinity, that there will not be any voltage drop across the load and no leakage path for the generated current to bypass the load.

1.4 Basic hindrances for the better performance of thin film solar devices

Various materials can be used for device fabrication, though the reported efficiencies are much lower than what can be attained. This mainly arises due to engineering problems. Theoretically, efficiency is computed

by assuming various considerations; for example, the output current is proportional to number of photons incident with energy higher than the material band gap with no series or shunt resistances affecting the fill factor [19]. But practically, all devices have carrier and resistive losses [20]. By knowing theoretical efficiency and by minimizing unavoidable losses, one can improve practical efficiencies obtained.

Some of the factors which affect solar device performance are lattice mismatch, electron affinity mismatch, thickness of various layers, substrate properties, grid contacts etc. Density of interface states formed in a material is determined by lattice mismatch, and hence it is always better to choose materials which have lattices well matched. When the electron crosses the interface of two materials, the magnitude of barrier they experience is determined by electron affinity difference and hence fewer mismatches in electron affinity are better. The thickness of each layer plays an important role in solar cell fabrication. For example, in the case of absorber layer, the product of thickness and absorbance should be optimum to ensure maximum carrier generation by absorption of useful solar spectrum. Thickness of absorber layer should be less than or equal to minority carrier diffusion length. Properties of the substrate are very important because growth mode and adherence to surface are determined by substrate characteristics. It is better to have matching thermal expansion constants between the material being deposited and substrate used. Usually, deposition takes place at a temperature much above the room temperature, and if there is a large difference in thermal expansion between both materials, it can cause stresses (destructive) while cooling. If the substrate is used as back contact, it is ideal to make

it reflecting so that the incident photons can be used effectively by assisting multiple passages of photons through the absorber layer. Grid contact plays a crucial role in controlling the efficiency of solar cell. Grid should be designed in such a way that it should reduce series resistance and at the same time possesses ohmic contact with the material layer. Transmission through grids and the spacing between them should also be optimum.

1.5 Requirement for extensive research in alternative photovoltaic thin film materials

As mentioned in the above sections, for large scale cost-effective production, thin film solar cells should satisfy major requirements like non-toxicity, material abundance, optimum transport and optical properties, inexpensive and easy to manufacture etc. Apart from silicon, CdTe and CIGS are forerunners in thin films. But the toxicity of cadmium and rarity of tellurium and indium hinders their large scale production. Moreover, the manufacturing techniques used in chalcopyrite films are very sophisticated. For example, deposition of CIGS involves 3-stage complex procedure and is vacuum based methods which are difficult to be maintained during large scale production [21]. Non-vacuum techniques were also developed for CIGS deposition, but a substantial reduction in the quality of films is observed [22]. Hence current research mainly focuses on developing solar cell materials which use low cost, non-vacuum cell fabrication techniques to obtain required material properties.

In the present work, we introduce a novel approach of depositing n-type absorber. Most of the studies on tin chalcogenide thin films focus

mainly on p-type SnS and n-type SnS_2. These two are widely used because of their optoelectronic properties suitable for solar cell fabrication. Very few works have been reported the use of n-type SnS, and so far no groups have done extensive studies on its material properties or its potential to become an absorber layer in photovoltaic devices. We optimized the material properties of these films prepared using non-vacuum, simple and cost-effective "Chemical Spray Pyrolysis" technique (CSP).

1.6 A brief review on SnS thin film

In general, SnS exists as a p-type material. The study of SnS is about a century old from the time of Herzenberg, a German mineralogist in 1932 first identified it [23]. Recently, researchers are focusing on optimizing n-type SnS, and the present thesis work is also devoted for bringing out the potential of n-type SnS. This section gives an insight into the structure of n-type SnS, review on its material properties, the effect of doping and finally solar cell fabrication with n-type polycrystalline SnS.

1.6.1 SnS structure

Tin chalcogenides which come under the IV-VI semiconducting compounds generally crystallize in orthorhombic structure and are isomorphous. According to Hofmann, each Sn atom is coordinated to three S atoms, and there will be eight atoms per unit cell with a layered structure [24-27]. The presence of double-layer structure in SnS where S and Sn atoms are bonded covalently within the layers, and the layers are

bonded with weak van der Waals force provide a chemically inert surface. This defect-tolerant surface is considered to be a great blessing because it can reduce losses due to carrier recombination at defects in p-n junction grain boundaries.

1.6.2 SnS thin films

Various chemical and physical methods used for fabrication of p and n-type SnS include, chemical bath deposition [28], SILAR [28], electrochemical deposition [29], dip deposition [28], sol-gel method [30], vacuum evaporation [31], atomic layer deposition [32], brush plating [33], radio frequency sputtering [34], pulse electro-deposition [35], chemical spray pyrolysis (CSP) [36-39] etc. In the coming section, research carried out so far on n-type SnS using various deposition methods are explained in chronological order. The material properties are found to vary considerably depending on the deposition parameters, and mode of deposition, all these are discussed below. The effect due to post-annealing treatments, doping and other variations done is also discussed.

The study on n-type SnS started in 1987 by Pramanik *et al.* [40]; in this paper, SnS films are prepared using chemical method on glass substrates. Structural, optical and electrical studies were carried out to confirm the material and found that films are amorphous. Later in 1988, Maheshwar *et al.* [41] prepared SnS samples by passing hydrogen sulfide through stannous chloride. The obtained samples showed n-type nature, and he first put forward the reason for this to be thermal decomposition, which results in "tin-rich" or "sulfur-deficient" n-SnS. In

1989 Ristov *et al.* [42] fabricated SnS thin films using chemical deposition method. He observed that conductivity changes from p-type to n-type on annealing for a short time without any change in its composition. He also proposed a similar explanation that excess of tin in the sample resulted in n-type conduction since the acceptor levels which are normally present in the lattice are created by the tin vacancies. It was in 2000; the first spray pyrolysed n-SnS samples were synthesized by Thangaraju *et al.* [43]; the obtained films were amorphous and were highly resistive. Later in 2005, Koteeswara *et al.* [44] succeeded in preparing polycrystalline SnS by varying the preparation temperature. He argued that pyrolytic temperature determines the conductivity type of the films caused by stoichiometry variation in the films (Sn/S ratio). In 2007, the same group reported preparation of n-type SnS by varying precursor concentrations [45]. It was reported that, at particular concentrations, there exists a region called 'phase conversion regions', where the film shows both p-type and n-type nature. In the same year, itself the group reported that using thermal evaporation technique n-type SnS can be synthesized by varying Sn∕S ratio which can be achieved by varying the source to substrate distance at a particular temperature [31].

Shuying *et al.* [35] prepared SnS films on ITO substrates using pulse-form electro-deposition. He reported that tin vacancies result in p-type conductivity, whereas sulfur vacancies result in n-type conduction. Later in 2010, a new approach called "doping" was tried to obtain n-type SnS and was first reported by Dussan *et al.* [46]. He tried substituting Sn with Bi to obtain SnS:Bi n-type samples. The paper suggests that doping of Bi above 50 % gives n-type films whereas below 50 % gives p-type

Optimization of opto-electronic properties of spray deposited n-type tin monosulfide thin film for photovoltaic application

17

films. In the same year, Sajeesh *et al.* obtained n-type SnS using CSP technique and he carried out the material studies and explained the presence of excess tin in the film as the reason for showing this n-type nature [36]. Later in 2012, again Prasert *et al.* [47] doped antimony to obtain n-type SnS but could not succeed in preparing low resistive films and hence was unable to confirm the conducting nature fully. In 2013, Chung *et al.* [30] reported that change in conductivity is due to the difference in ratio between the Sn^{4+} and Sn^{2+} concentrations. This paper also suggested the difficulty in precise control over the n-type SnS with desirable properties. Isovalent ion substitution is also tried by Fanyong *et al.* [48]. The paper explains the substitution of large Pb^{2+} ion at the place of Sn^{2+} ion that increases SnS interlayer distance to help the formation of Sn/Pb interstitial that acts as donors. The paper also reminds that this is possible only under sulfur poor condition. In 2016, the computational study of SnS was carried out by Yu Kumaga *et al.* [49], and in this study, properties of SnS was studied from first-principles using generalised-gradient approximation (GGA) with Heyd-Scuseria-Ernzerhof hybrid functional (HSE06), and GW0 approximation. Some of the conclusions drawn from this work are:

1) It is quite difficult to fabricate n-type SnS without doping.

2) Acceptors are formed by tin vacancies whereas donors are formed by sulfur vacancies.

This substantiates the argument that p-type SnS is formed in tin poor condition and vice versa in n-type SnS. In the same year, Jacob *et al.* [50] prepared tin sulfide films using chemical spray pyrolysis and suggested

variation of in-situ carrier gas pressure can result in n-type SnS films. Here also, the existence of 'tin-rich' condition is considered to be the reason for n-type conduction. Only a few works have been done on device fabrication. Now coming to device fabrication using n-type SnS thin film, Maheshwar *et al.* [41] in 1988 first reported a device fabricated using n-type SnS. He prepared n-type SnS by passing H_2S gas through acidic stannous chloride solution, and he studied its photo-electrochemical behaviour. He observed that this material is stable against photo-corrosion and obtained an efficiency of 0.63 % with the cell structure n-SnS/Ce^{4+}, Ce^{3+}/Pt.

G. Yue *et al.* in 2012 prepared p-n homojunction photovoltaic cell using SnS nanowire over aluminium foil substrate. The device showed an efficiency of 1.95 % with high short circuit current density of 7.64 mA cm^{-2} [51]. Later in 2013, Chung-Cheng *et al.* done a detailed study on electrical properties of hetero-junction between n-type SnS and p-type Si. The effect due to sulfide treatment on p-Si is checked. It is found that the sulfide treatment can reduce series resistance and hence can improve the efficiency of solar cells [52]. In 2018 our group reported the solar cell device fabrication with configuration ITO/CZTS/SnS:Cu/ZnO:Al/Ag. The device had an open-circuit voltage of 810 mV, short circuit current density of 0.87 mA cm^{-2} like other CZTS device [53].

1.7 Deposition techniques used in the present study

Once the material is selected, one has to select a viable, simple deposition technique. Various physical and chemical methods are reported in earlier works for the deposition of tin-chalcogenide thin film,

as mentioned above. Comparing the other deposition techniques, thin films deposited via CSP technique exhibited good device properties and performance [54]. This method is well known from several decades in the field of solar cell fabrication and glass industry [55, 56]. Possibility for easy deposition over a large area is one among the highlights of this method [57]. The fact that it is a non-vacuum technique and it does not require very high-quality substrates, ease in doping, possibility of preparing films with required composition, possibility of preparing multilayered films, simplicity in stoichiometry tailoring, no dimension or surface profile restrictions about substrate material and cost-effective deposition (especially on equipment and energy requirement) lead us to choose this method as the deposition technique for the present study. We have used an automated chemical spray coating unit (Figure 1.6 (a)) manufactured with the help of a company M/s. Hollmark, Kalamassery, India. A brief description of its instrumentation is presented below.

1.7.1 Chemical spray pyrolysis

Chemical spray pyrolysis method is employed for the production of thick and thin films of various ceramic materials and the production of powdered samples. CSP equipment mainly consists of a substrate heater, atomizer, spray rate controller, precursor container and temperature controller (Figure 1.6 (b)).

(a) **(b)**
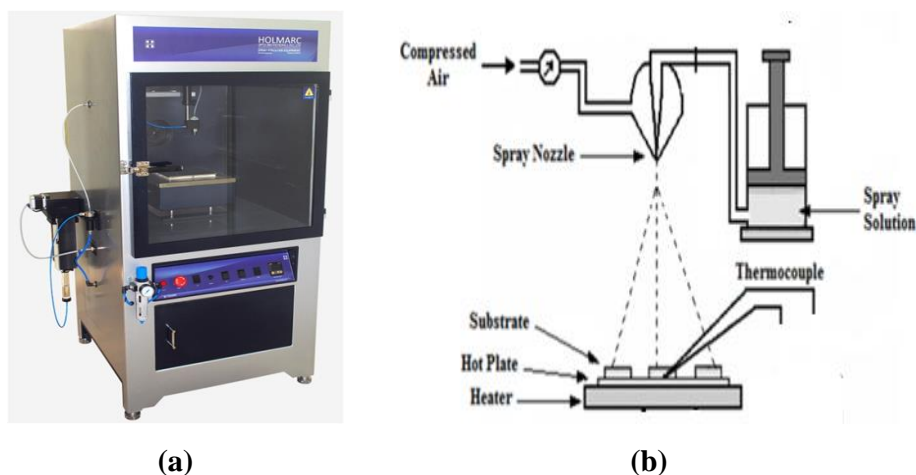
Figure 1.6 **(a)** Chemical spray coating unit and
(b) Schematic representation of CSP

Out of various atomizers, namely air blast, electrostatic and ultrasonic [58,59], we have used the air blast atomizer in which precursor solution is exposed to compressed air stream for the deposition. A circular plate with thickness 6 mm and 15 cm diameter were used as a hot plat, and heating assembly that could provide uniform temperature up to 500 ^{o}C with a maximum variation of $\pm$ 5 °C was used. A K-type thermocouple that could detect substrate surface temperature is linked to a temperature controller with 10A on/off relay circuit to keep the substrate temperature constant during spraying. Spray rate could be controlled precisely from 1 ml/min to 20 ml/min with the help of a dispensing unit with screw gauge and syringe action principle. The dispensing rate was maintained constant with a stepper motor controlled by a microprocessor. All the connecting tubes and containers were made of corrosion free teflon material. The spray head consists of a needle and air nozzle through which solution and compressed air were dispensed at

right angles. Required pressure was produced using 0.5 HP compressor and was fed to the nozzle using a mechanical pressure gauge. Substrate, heater and spray head were fixed inside a chamber with provision to remove solvent vapour and gaseous byproducts by an exhaust fan. Spraying area over the substrate was determined by employing double stepper motor mechanism where spray head could scan large area of around 15 cm X 15 cm. Speed of 'X' and 'Y' axis scan could also be controlled.

Deposition of thin films using chemical spray pyrolysis technique mainly involves two steps

1) The spraying of precursor solution onto the preheated substrate

2) The thermal decomposition of droplets reaching the substrate surface

Important parameters that decide the film properties include deposition temperature, precursor solution used, solvent used and its concentration, spray rate, height difference between heater and spray head, angle in which spray falls, carrier gas pressure etc. [60]. Optimization of each parameter is explained in the coming chapters.

1.7.2 Vacuum evaporation

Vacuum technique was mainly used in the present study for post-deposition annealing treatment on prepared films and also for electrode coating during the devices fabrication. The resistive heating method was adopted to vaporise the material. We used 200 A molybdenum source

supplied by HHV Pvt. Ltd, India in a boat structure, where the material to be evaporated could be kept. Vacuum of 2×10^{-5} Torr was created, and on vaporisation, the atoms evaporated from the material get deposited on to the substrate [61].

1.8 Characterization techniques used for the present study

Film property and its quality are determined using various characterization tools and this is very important if we are selecting a new material for device fabrication. Hence this section briefly explains characterization tools used for the present study.

1.8.1 Stylus profilometer for thickness measurement

As the name 'thin film photovoltaic' suggests, thickness plays an important role in film properties. Film thickness can be characterized using various mechanical and optical methods. In the present work, Dektak 6M stylus profilometer was used to measure surface topography profiling, line roughness and waviness thickness well below 100 Å [62]. The samples were allowed to move beneath a stylus with a diamond tip and measurements were taken electromechanically. Scan speed, length and stylus force were set appropriately. Linear variable differential transformer (LVDT) was coupled mechanically to this stylus, and as the stylus rides over the sample surface, variations were translated. Electrical signals were produced with respect to changes in core position of LVDT and these signals were converted into digital format using high precision analogue to digital converter. In order to measure film thickness, films were deposited with masked region, which creates a step

on the film surface. By calculating the vertical movement of the stylus thickness could be measured accurately.

1.8.2 Structural characterizations

Various techniques were used for conducting structural studies and they are described in the coming section

1.8.2.1 X-ray diffraction technique (XRD)

XRD pattern in our study was obtained using Rigaku (D.Max.C) X-ray diffractometer with Cu Kα line (λ = 1.5405 Å) as source radiation along with Ni filter operating at 30 kV and 20 mA. All samples were scanned in the range 10° to 60° with a scan speed of 5°/min. XRD analysis provides insight about secondary phase formation and material crystallinity. It is considered as fingerprint of a substance because each substance has a specific diffraction pattern and even in a mixture of various substances, the diffraction pattern can be used to determine the composition. But in order for diffraction to happen in a crystal, the Braggs condition $n\lambda = 2d \sin\theta$ has to be satisfied. Here λ is X-ray wavelength used, n is diffraction order, θ is 'glancing angle'; d is interplanar spacing [63]. A detector that collects diffracted radiation records the pattern. The XRD analysis gives information about crystal orientation, structure, size, composition and stress in the prepared samples [64]. By comparing with standard powder diffraction patterns published by Joint Committee on Powder Diffraction Standards (JCPDS), (also known as "International Centre for Diffraction Data (ICDD)"), the experimentally obtained data can be analyzed.

1.8.2.2 Raman spectroscopy

In this thesis, Raman analysis is carried out at room temperature employing back scattering mode. The analysis was carried out using JobinYvon Horibra LABRAM-HR visible micro Raman system at a resolution of 2 mm. The wavelength of 632.8 nm using a Helium-Neon laser was used as the excitation source.

Raman analysis is vibrational spectroscopic technique based on Raman Effect. This technique was first reported by Raman in 192, and it sheds light on the crystal structure, presence of secondary phases, phonon confinement, grain size and can even detect both inorganic and organic species present in the sample [65]. Raman spectra consist of two types of scattering; stokes shifted scattering and anti-stokes shifted scattering. In stokes shifted scattering, the incident photon imparts some of its incident energy in the form of phonon to the lattice and emerges as low energy photon. Whereas in anti-stokes scattering the photon absorbs phonon and emerges as high energy photon. The latter one is much weaker and hence usually stokes mode scattering is monitored. Raman measurements were carried out by incidenting laser beam (pump) on to the sample surface. The weak scattered signal from the sample was passed through a double monochromator to cancel out Rayleigh scattered light and was then allowed to fall on a photodetector. The photodetector records the Raman shifted wavelengths. This analysis also gives idea about amorphous, polycrystalline and single crystal materials depending on the broadness of the Raman lines.

1.8.3 Optical absorption and transmittance studies

In the present work, transmittance and band gap of films were measured using UV-Vis-NIR spectrometer (JASCO V 570 model). The band gap of each film was computed, taking into consideration their thicknesses [66]. Absorption studies were carried out for all the samples in the wavelength range of 190-2500 nm. Usually, semiconductors have high absorption coefficients, and they strongly absorb light in the visible region. In its pure state, at a certain wavelength, the absorption coefficient rapidly drops and material become mostly transparent. This drop of absorption is known as 'lattice absorption edge' or 'fundamental absorption edge'. The electronic transition occurs between valence and conduction bands. It can be direct or indirect transition, allowed or forbidden depending on the transition probability (p). The relation between the band gap (E_g) and the absorption coefficient (α) of the film as function of photon energy is given by the equation $\alpha h\nu = A (h\nu - E_g)$ p, where A is a constant and hν is photon energy [67-69].

By plotting "(αhν)p" against photon energy, we can determine nature of the transition. Direct allowed and direct forbidden transitions are represented by values p = 1/2 and p = 1/3 whereas indirect allowed and indirect forbidden transitions are represented by p = 2 and p = 3 respectively. In the present work, band gap of all the samples were determined by extrapolating linear portion of $(\alpha h\nu)^2$ versus hν graph towards intercept of hν axis. The entire plot was found to be linear and hence confirmed that transition is direct allowed in all cases.

1.8.4 Morphological studies

Film topography using SEM and AFM techniques are explained in this section

1.8.4.1 Scanning electron microscopy (SEM)

Zeiss ULTRA plus scanning electron microscope (SEM) system was employed for morphological characterization of films. The SEM images were acquired with the help of an in-lens detector and SE2 detector, which analyzes backscattered electrons and secondary electrons respectively. The measurements were taken at accelerating voltage of typically 5 keV.

SEM gives structural, microstructural and morphological information over the sample surface [70]. In SEM analysis, the sample surface is scanned by an electron beam, which passes through the scanning coils and objective lenses. These lenses deflect the beam horizontally and vertically over the sample surface. When a focused electron beam falls over a material surface, the kinetic energy of the falling electron is shared to a large number of electrons in the material to liberate avalanche of electrons from the material. These backscattered or secondary electrons are detected to obtain the image. The initial beam of electrons is produced with the help of field emission cathode or by thermal emission source. There are mainly three types of principal images which are produced in SEM. These are backscattered electron images, secondary electron images and elemental X-ray maps. If the electrons exit the sample with energy more than 50 eV, they are referred to be backscattered electron, and if the emitted electrons have energy less than 50 eV, they are considered as secondary electrons. These two

types of scattered electrons are conventionally selected for imaging purposes and the detectors are placed accordingly to collect them. For secondary electron imaging, the samples should be electrically conductive to obtain high-resolution imaging. Use of electrons gives magnifications greater than 100,000X and 100 times more field depths than optical microscope because of smaller wavelength and high penetration capability of electrons compared to photons. This high spatial resolution possibility in micrometer and nanometer scales makes scanning electron microscopes a powerful tool compared to optical microscopes that can give a faithful reproduction of surface features by mapping secondary electrons coming from the film surface layer.

1.8.4.2 Atomic force microscopy (AFM)

Imaging using AFM has an advantage that it can be used to study the surface morphology of insulators as well as semiconducting or even conducting surfaces. For the present study 'Nanosurf easyScan 2' AFM system was used and the obtained data were analyzed using WSxM software.

In the AFM set up that we used, a sharp tip with a diameter less than 100 Å scans the sample surface and moves up and down depending on the contour of the film surface. The tip which scans the selected area of the sample is attached to a cantilever beam. Depending on the surface non-uniformity, the scanning probe is deflected and this variation is read into a dual element photodiode by a laser beam attached to the back of the cantilever of the probe. Dual element photodiode produces voltage corresponding to the difference in light intensities obtained from lower

and upper photodetectors. This feedback is then processed by computer software to generate the topography map.

1.8.5 Electrical characterization by Hall effect

To calculate the electrical properties like carrier density, resistivity, mobility and polarity of carriers, we used Hall effect measurement method. In the present work, we have used four probe van der Pauw configuration with AC modulation of magnetic field at room temperature using Ecopia model No HMS-3000 (magnetic field = 0.57 T) that is capable of current measurement in the range 1–20 mA.

Hall measurement system works on the Hall effect principle. When magnetic field is applied perpendicular to the direction of current flowing through conductor, mutually perpendicular electric field will be produced across the conductor. This phenomenon is called Hall effect. The voltage produced by the field is called "Hall voltage (V_H)" given by the equation. $V_H = R_H IB/d$ where R_H is Hall coefficient which is constant of proportionality for the potential gradient and the current density, I is current, B is the magnetic field and d is the dimension of the sample [70,71]. This Hall voltage is also proportional to the carrier mobility, and its sign depends on the majority charge carriers (holes or electrons). Hall voltage can be used for calculating Hall mobility and carrier concentration of a semiconductor.

1.8.6 Compositional analysis

In the present work, the composition and atomic percentage is calculated using EDAX and XPS technique.

1.8.6.1 Energy dispersive X-ray analysis (EDAX)

Energy dispersive X-ray (EDAX) is usually integrated with SEM and is used for finding elemental composition present over an "area of interest" in the film. In the present study, samples were analyzed using EDAX, in which the excitation was done using the electrons with 5 - 20 keV. When beam of electrons is bombarded on the film, they may knock out some of the electrons from the material. This creates a vacancy in the inner shell and high energy electrons from the outer shell may jump down, releasing its extra energy as X-rays. Initial and final shell from which the electron is transferred can be calculated from the amount of energy released and will be unique for an element. By calculating the energy of emitted X-rays, the identity of an atom can be established and how frequently X-rays are emitted from each energy level. The intensity peak at any energy level is indicative of the concentration of some elements present in the film. Higher the intensity of peak, greater will be the concentration of that element in the film. For the present work, the same SEM machine (mentioned above) was used for EDAX analysis.

1.8.6.2 X-ray photoelectron spectroscopy (XPS)

Composition of prepared samples was obtained from X-ray photoelectron spectroscopy (XPS) data with the help of Kratos Analytical AMICUS spectrometer with Mg Kα/Al Kα dual anode X-ray source. Depth wise information about the film was obtained, by argon ion etching and correspondingly recording the XPS spectra.

XPS works on the principle that when X-rays of known energy (hν) are irradiated on to the surface of the sample, electrons with binding

energy E_b are ejected out for all the $E_b < h\nu$. Kinetic energy E_k of such emitted electrons are measured as $E_k = h\nu - E_b - \Phi_\varphi$, where, Φ_φ is the work function of the material. This term can be eliminated since we can compensate for this value electronically and so the equation becomes

$$E_k = h\nu - E_b \text{ OR } E_b = h\nu - E_k$$

Binding energy (BE) represents atomic orbital energies which is a characteristic of each element. Higher BE is noted for atoms with higher oxidation state because of extra columbic interaction between core ion and photoemitted electron and hence XPS can discriminate various chemical environment and oxidation states. This is considered as major strength of this technique. All these measurements are carried out in near ultra-high vacuum environment to avoid interference from other gas collisions with the photoelectrons. Quantitative results and identification of chemical states can be estimated from the peak areas, heights and also from the separations and position of peak obtained [72].

1.9 Significance of the thesis

This thesis highlights fabrication of n-type eco-friendly and non-toxic absorber material namely, SnS, which can be used as either absorber or window layer; this makes optical absorption to take place even in absorber (as the band gap is sufficiently low). Material properties were improved by doping and employing other post-deposition techniques to make it suitable for device fabrication. Only a few papers on this study are available in the literature and there is still a long way to go to attain the material's predicted potential. In the thesis, a

different device structure is tried to improve the parameters of the fabricated device. Usually, in solar devices, window layer with large band gap and absorber layer with a relatively narrow band gap are used. But here in our case, we have used two different materials with an almost similar band gap. For this, we have selected the well-studied material 'CZTS' as p-layer. Such a configuration is advantageous because here both act as absorbers and has a huge possibility to function as a bifacial solar cell. Further modification in the cell structure is done by introducing a top layer of ZnO:Al and also by various other optimization studies. On comparing with the open circuit voltage (V_{oc}) and fill factor (FF) obtained for high efficiency solar cells so far published by 'progress in photovoltaics', we could say that we have almost reached near to their V_{oc} and FF values using our easy fabrication technique and also with our thinner n and p-layers [73]. Present work is a preliminary study and enhancement of J_{sc} is required to bring out the complete potential of this material so as to improve the efficiency further.

References

[1] Service, Robert F. "Solar energy. Is it time to shoot for the sun?." *Science (New York, NY)* 309.5734 (2005): 548.

[2] Popov, Dimityr. "An option for solar thermal repowering of fossil fuel fired power plants." *Solar Energy* 85.2 (2011): 344-349.

[3] Eisenberg, Richard, and Daniel G. Nocera. "Preface: Overview of the forum on solar and renewable energy." *Inorganic chemistry* 44.20 (2005): 6799-6801.

[4]   Becquerel, M. E. "Mémoire sur les effets électriques produits sous l'influence des rayons solaires." *Comptes rendus hebdomadaires des séances de l'Académie des sciences* 9 (1839): 561-567.

[5]   Smith, Willoughby. *The action of light on selenium*. 1876.

[6]   Fritts, Charles E. "On a new form of selenium cell, and some electrical discoveries made by its use." *American Journal of Science* 156 (1883): 465-472.

[7]   Adams, William Grylls, and R. Evans Day. "The action of light on selenium." *Proceedings of the Royal Society of London* 25.171-178 (1877): 113-117.

[8]   Chapin, Daryl M., C. S. Fuller, and G. L. Pearson. "A new silicon p-n junction photocell for converting solar radiation into electrical power." *Journal of Applied Physics* 25.5 (1954): 676-677.

[9]   Green, Martin A. "Thin-film solar cells: review of materials, technologies and commercial status." *Journal of Materials Science: Materials in Electronics* 18.1 (2007): 15-19.

[10]   Nelson, Jenny. "Imperial College Press." *The physics of solar cells* (2003).

[11]   Hartnagel, Hans, *Semiconducting transparent thin films*. CRC Press, 1995.

[12]   M. Mathew, PhD Thesis, Cochin University of Science and Technology, India (2009).

[13]   Bube, Richard H., and Richard Howard Bube. "Photovoltaic materials" (1998).

[14]   Markvart, Tom, Augustin McEvoy, and Luis Castaner, eds. *Practical handbook of photovoltaics: fundamentals and applications*. Elsevier, 2003.

[15] Lorenzo, Eduardo. *Solar electricity: engineering of photovoltaic systems*. Earthscan/James & James, 1994.

[16] Khan, Firoz, S. N. Singh, and M. Husain. "Determination of diode parameters of a silicon solar cell from variation of slopes of the I–V curve at open circuit and short circuit conditions with the intensity of illumination." *Semiconductor Science and Technology* 25.1 (2009): 015002.

[17] Solanki, Chetan Singh. *Solar photovoltaics: fundamentals, technologies and applications*. PHI Learning Pvt. Ltd., 2015.

[18] Rajesh, G., Muthukumarasamy, N., Subramaniam, E. P., Agilan, S., & Velauthapillai, D. (2013). Synthesis of Cu 2 ZnSnS 4 thin films by dip-coating method without sulphurization. *Journal of sol-gel science and technology*, *66*(2), 288-292.

[19] Kazmerski, Lawrence L. "Electrical properties of polycrystalline semiconductor thin films." *Polycrystalline and amorphous thin films and devices*. Academic Press, 1980. 59-133.

[20] Markvart, Tom, Augustin McEvoy, and Luis Castaner, eds. *Practical handbook of photovoltaics: fundamentals and applications*. Elsevier, 2003.

[21] Jackson, P., Hariskos, D., Lotter, E., Paetel, S., Wuerz, R., Menner, R., ... & Powalla, M. (2011). New world record efficiency for Cu (In, Ga) Se2 thin-film solar cells beyond 20%. *Progress in Photovoltaics: Research and Applications*, *19*(7), 894-897.

[22] Kaneshiro, J., Gaillard, N., Rocheleau, R., & Miller, E. (2010). Advances in copper-chalcopyrite thin films for solar energy conversion. *Solar Energy Materials and Solar Cells*, *94*(1), 12-16.

[23] Herzenberg, R. "Kolbeckina, un nuevo mineral de estaño—Buenos Aires." *Rev. Miner* 4 (1932): 33-35.

[24] Baldwin, K. R., and C. J. E. Smith. "Repair of metal coatings using environmentally compliant brush-plating solutions." *Plating and surface finishing* 84.7 (1997): 23-28.

[25] Hofmann, W. "W. Hofmann, Z. Kristallogr. 91, 161 (1935)." *Z. Kristallogr.* 91 (1935): 161.

[26] Okazaki, Atsushi, and Ikuhiko Ueda. "The crystal structure of stannous selenide SnSe." *Journal of the Physical Society of Japan* 11.4 (1956): 470-470.

[27] Jiang, Tong, and Geoffrey A. Ozin. "New directions in tin sulfide materials chemistry." *Journal of materials chemistry* 8.5 (1998): 1099-1108.

[28] Chaki, Sunil H., Mahesh D. Chaudhary, and M. P. Deshpande. "SnS thin films deposited by chemical bath deposition, dip coating and SILAR techniques." *Journal of Semiconductors* 37.5 (2016): 053001.

[29] Kafashan, Hosein, Farid Jamali-Sheini, Reza Ebrahimi-Kahrizsangi, and Ramin Yousefi. "Influence of growth conditions on the electrochemical synthesis of SnS thin films and their optical properties." *International Journal of Minerals, Metallurgy, and Materials* 23, no. 3 (2016): 348-357.

[30] Huang, Chung-Cheng, Yow-Jon Lin, Cheng-Yu Chuang, Chia-Jyi Liu, and Yao-Wei Yang. "Conduction-type control of SnSx films prepared by the sol–gel method for different sulfur contents." *Journal of Alloys and Compounds* 553 (2013): 208-211

[31] Devika, M., N. Koteeswara Reddy, D. Sreekantha Reddy, S. Venkatramana Reddy, K. Ramesh, E. S. R. Gopal, K. R. Gunasekhar, V. Ganesan, and Y. B. Hahn. "Optimization of the distance between source and substrate for device-grade SnS films grown by the thermal evaporation technique." *Journal of Physics: Condensed Matter* 19, no. 30 (2007): 306003.

[32] Sinsermsuksakul, Prasert, Jaeyeong Heo, Wontae Noh, Adam S. Hock, and Roy G. Gordon. "Atomic layer deposition of tin monosulfide thin films." *Advanced Energy Materials* 1, no. 6 (2011): 1116-1125.

[33] Subramanian, B., C. Sanjeeviraja, and M. Jayachandran. "Photoelectrochemical characteristics of brush plated tin sulfide thin films." *Solar energy materials and solar cells* 79.1 (2003): 57-65.

[34] Hartman, Katy, J. L. Johnson, Mariana I. Bertoni, Daniel Recht, Michael J. Aziz, Michael A. Scarpulla, and Tonio Buonassisi. "SnS thin-films by RF sputtering at room temperature." *Thin Solid Films* 519, no. 21 (2011): 7421-7424.

[35] Cheng, Shuying, *et al.* "The structure and properties of SnS thin films prepared by pulse electro-deposition." *Materials Letters* 61.6 (2007): 1408-1412.

[36] Sajeesh, T. H., Anita R. Warrier, C. Sudha Kartha, and K. P. Vijayakumar. "Optimization of parameters of chemical spray pyrolysis technique to get n and p-type layers of SnS." *Thin Solid Films* 518, no. 15 (2010): 4370-4374.

[37] Reddy, N. Koteswara, and KT Ramakrishna Reddy. "Growth of polycrystalline SnS films by spray pyrolysis." *Thin solid films* 325, no. 1-2 (1998): 4-6.

[38] Reddy, KT Ramakrishna, P. Purandar Reddy, R. W. Miles, and P. K. Datta. "Investigations on SnS films deposited by spray pyrolysis." *Optical materials* 17, no. 1-2 (2001): 295-298.

[39] Sajeesh, T. H., K. B. Jinesh, M. Rao, C. Sudha Kartha, and K. P. Vijayakumar. "Defect levels in SnS thin films prepared using chemical spray pyrolysis." *physica status solidi (a)* 209, no. 7 (2012): 1274-1278.

[40] Pramanik, P., P. K. Basu, and S. Biswas. "Preparation and characterization of chemically deposited tin (II) sulphide thin films." *Thin Solid Films* 150.2-3 (1987): 269-276.

[41] Sharon, Maheshwar, and Krishnan Basavaswaran. "Photoelectrochemical behaviour of tin monosulphide." *Solar cells* 25.2 (1988): 97-107.

[42] Ristov, M., G. J. Sinadinovski, I. Grozdanov, and M. Mitreski. "Chemical deposition of tin (II) sulphide thin films." *Thin Solid Films* 173, no. 1 (1989): 53-58.

[43] Thangaraju, B., and P. Kaliannan. "Spray pyrolytic deposition and characterization of SnS and SnS2 thin films." *Journal of Physics D: Applied Physics* 33.9 (2000): 1054.

[44] Reddy, N. Koteeswara, and KT Ramakrishna Reddy. "Electrical properties of spray pyrolytic tin sulfide films." *Solid-state electronics* 49.6 (2005): 902-906.

[45] Reddy, N. Koteeswara, and KT Ramakrishna Reddy. "Preparation and characterisation of sprayed tin sulphide films grown at different precursor concentrations." *Materials Chemistry and Physics* 102.1 (2007): 13-18.

[46] Dussan, A., F. Mesa, and G. Gordillo. "Effect of substitution of Sn for Bi on structural and electrical transport properties of SnS thin films." *Journal of materials science* 45.9 (2010): 2403-2407.

[47] Sinsermsuksakul, Prasert, Rupak Chakraborty, Sang Bok Kim, Steven M. Heald, Tonio Buonassisi, and Roy G. Gordon. "Antimony-doped tin (II) sulfide thin films." *Chemistry of Materials* 24, no. 23 (2012): 4556-4562.

[48] Ran, Fan-Yong, Zewen Xiao, Yoshitake Toda, Hidenori Hiramatsu, Hideo Hosono, and Toshio Kamiya. "n-type conversion of SnS by isovalent ion substitution: Geometrical doping as a new doping route." *Scientific reports* 5 (2015): 10428.

[49] Kumagai, Yu, Lee A. Burton, Aron Walsh, and Fumiyasu Oba. "Electronic Structure and Defect Physics of Tin Sulfides: SnS, Sn 2 S 3, and Sn S 2." *Physical Review Applied* 6, no. 1 (2016): 014009.

[50] Andrade-Arvizu, Jacob A., M. F. García-Sánchez, M. Courel-Piedrahita, F. Pulgarín-Agudelo, E. Santiago-Jaimes, E. Valencia-Resendiz, A. Arce-Plaza, and O. Vigil-Galán. "Suited growth parameters inducing type of conductivity conversions on chemical spray pyrolysis synthesized SnS thin films." *Journal of analytical and applied pyrolysis* 121 (2016): 347-359.

[51] Yue, Guanghui, Youdao Lin, Xin Wen, Laisen Wang, and Dongliang Peng. "SnS homojunction nanowire-based solar cells." *Journal of Materials Chemistry* 22, no. 32 (2012): 16437-16441.

[52] Huang, Chung-Cheng, Yow-Jon Lin, Chia-Jyi Liu, and Yao-Wei Yang. "Photovoltaic properties of n-type SnS contact on the unpolished p-type Si surfaces with and without sulfide treatment." *Microelectronic Engineering* 110 (2013): 21-24.

[53] Katagiri, Hironori, Kazuo Jimbo, Win Shwe Maw, Koichiro Oishi, Makoto Yamazaki, Hideaki Araki, and Akiko Takeuchi. "Development of CZTS-based thin film solar cells." *Thin Solid Films* 517, no. 7 (2009): 2455-2460.

[54] Reddy, KT Ramakrishna, N. Koteswara Reddy, and R. W. Miles. "Photovoltaic properties of SnS based solar cells." *Solar energy materials and solar cells* 90.18-19 (2006): 3041-3046.

[55] Mochel, John M. "Electrically conducting coatings on glass and other ceramic bodies." U.S. Patent No. 2,564,707. 21 Aug. 1951.

[56] Hill, James E., and Rhodes R. Chamberlin. "Process for making conductive film." U.S. Patent No. 3,148,084. 8 Sep. 1964.

[57] T.V. Vimalkumar, PhD Thesis, Cochin University of Science and Technology, India (2011).

[58] Balkenende, A. R., A. A. M. B. Bogaerts, J. J. Scholtz, R. R. M. Tijburg, and H. X. Willems. "Thin MgO layers for effective hopping transport of electrons." *Philips journal of research* 50, no. 3-4 (1996): 365-373.

[59] Chen, C. H., and E. M. Kelder. "PJJM vanderPut, J. Schoonman." *J. Mater. Chem* 6.5 (1996).

[60] Kim, Soo Gil, Kook Hyun Choi, Jae Hwan Eun, Hyeong Joon Kim, and Cheol Seung Hwang. "Effects of additives on properties of MgO thin films by electrostatic spray deposition." *Thin Solid Films* 377 (2000): 694-698.

[61] Chopra, Kasturi L. "Thin film phenomena." (1969).

[62] Maissel, Leon I., and Reinhard Glang. "Handbook of thin film technology." *New York: McGraw-Hill, 1970, edited by Maissel, Leon I.; Glang, Reinhard* (1970).

[63] Kittel, Charles, Paul McEuen, and Paul McEuen. *Introduction to solid state physics*. Vol. 8. New York: Wiley, 1996.

[64] Somorjai, Gabor A. *The structure and chemistry of solid surfaces: proceedings of the Fourth International Materials Symposium. Held at the University of California, Berkeley, June 17-21, 1968*. Vol. 4. John Wiley & Sons, 1969.

[65] Raman, Chandrasekhara Venkata, and Kariamanikkam Srinivasa Krishnan. "A new type of secondary radiation." *Nature* 121.3048 (1928): 501.

[66] Jacques, I. "Optical Processes in Semiconductors." (1971).

[67] Goswami, A. *Thin film fundamentals*. New Age International, 1996.

[68] Heavens, Oliver S. *Optical properties of thin solid films*. Courier Corporation, 1991.

[69] Bube, Richard H. *Photoelectronic properties of semiconductors*. Cambridge University Press, 1992.

[70] Schroder, Dieter K. *Semiconductor material and device characterization*. John Wiley & Sons, 2006.

[71] Petersen, Dirch H., Ole Hansen, Rong Lin, and Peter F. Nielsen. "Micro-four-point probe Hall effect measurement method." *Journal of Applied Physics* 104, no. 1 (2008): 013710.

[72] Moulder, John F. "Handbook of X-ray photoelectron spectroscopy." *Physical electronics* (1995): 230-232.

[73] Green, Martin A., Yoshihiro Hishikawa, Ewan D. Dunlop, Dean H. Levi, Jochen Hohl-Ebinger, and Anita WY Ho-Baillie. "Solar cell efficiency tables (version 52)." *Progress in Photovoltaics: Research and Applications* 26, no. 7 (2018): 427-436.

Chapter 2

DEPOSITION OF n-TYPE SnS, SnS:Cu

2.1 Introduction

Recently there has been a lot of interest in the development of cost-effective and eco-friendly solar cells utilizing easily available materials. In this direction, SnS is considered as a new suitable contender that can be prepared using easily adoptable deposition techniques. Considering beneficial aspects of chemical spray pyrolysis (CSP) technique mentioned in the previous chapter, the method is selected for deposition of SnS layer in this work. CSP which is suitable for large area deposition is low cost as well as simple, with possibility for easy doping and flexibility in stoichiometry tailoring. For the same reason, CSP with optimized deposition parameters is a popular tool in thin-film solar device fabrication [1]. Quality and performance of any photovoltaic device depend on material properties from which they are made of [2]. The present study focuses on depositing n-type SnS with suitable optoelectronic properties required for solar cell fabrication. A review on various studies so far done for/on n-type SnS is already presented in the previous chapter. Since structural, morphological, optical and compositional knowledge of the material is important for device fabrication, we start by investigating methods to prepare low resistive n-type SnS with required optoelectronic properties.

In this chapter, we describe the selection of precursors and preparation of n-type thin films by decreasing precursor solvent volume. Resistivity of so prepared samples was further reduced by doping with $CuCl_2.2H_2O$ followed by optimization of doping percentage. All the optimized conditions were fixed after a detailed investigation on its structural, optical and electrical properties and it will be discussed in this chapter.

2.2 Preparation of precursors

The precursors chosen, the precursor salts used, the solvent used for dissolving these salts, the concentration of precursor solution etc are some factors that determine properties of sprayed thin films. There are reports suggesting that, when an alcoholic or acidic medium is used as precursor solvent, material properties will change. For example, in the case of ZnO, transparency is increased when ethanol is used instead of water as a solvent for zinc acetate [3]. A change in surface morphology is reported by Chen *et al.* due to the addition of acetic acid along with the precursor solution [4]. In the present study, we have selected chloride based precursor since presence of chlorine is known to maintain the n-type nature of SnS [5]. It is also reported that films prepared using chloride based precursors are more photosensitive and crystalline [6, 7]. Chemical modification of precursor solution might be the reason for these changes. Current section deals with cationic and anionic precursor preparation selected for developing Sn_xS_y thin films.

2.2.1 Cationic precursor

Chemical chosen for cationic precursor was dihydrated stannous chloride ($SnCl_2.2H_2O$). The previous optimization studies done on p-type SnS and low material cost prompted us to select $SnCl_2$ instead of $SnCl_4$. We used $SnCl_2.2H_2O$ (Merck, assay = 99 % , M.W = 225.25 g/mol) as cationic precursor. $SnCl_2.2H_2O$ did not give clear solution while dissolving in deionised water and precipitated due to the formation of hydroxide. Stirring of solution for long hours or ultrasonicating the solution also did not give a positive result in achieving a clear solution. Hence we used the reported method of dissolving cationic precursor either in acidic or alkaline medium to get a clear solution [8-10]. Dissolving $SnCl_2.2H_2O$ in pure HCl is also known to give clear aqueous solution by suppressing the $Sn(OH)_2$ (hydroxide) formation (gel like white precipitate) when water reacts with Sn, and this retains Sn content in the precursor solution [11]. We used (35 % assay and 11.32 M) HCl as the initial solvent for dissolving the cationic precursor. The salt was initially dissolved in few milliliters of HCl and then diluted with water to obtain the required molarity. We started with already reported optimization methods used for p-type SnS where 11.282 g of $SnCl_2.2H_2O$ was dissolved in 20 ml of HCl which was made-up to 100 ml with de-ionised water to get stock solution of 0.5 M and then modified the quantity of HCl to get n-type SnS [11].

2.2.2 Anionic precursor

Anionic precursor selected was thiourea ($CS(NH_2)_2$; (Merck, M.W = 76.12 g/mol, assay = 99 %). Precipitation of metallic hydroxides

and sulfides can be avoided by using thiourea (TU) as a source for sulfur in the spraying solution [12]. We used 7.62 g of TU salt dissolved in 100 ml of de-ionized water to prepare 1 M TU stock solution. The desired precursor solution was prepared from this stock solution by using equation "m_1 v_1 = m_2 v_2" where molarity of stock solution is m_1 and v_1 is the volume of stock solution. Desired molarity and volume are m_2 and v_2, respectively. Films were fabricated using the above-mentioned stock solution molarity and volume.

2.2.3 SnS fabrication

For the fabrication of SnS, we started by taking 0.1 M $SnCl_2.H_2O$ from the prepared (0.5 M) stock solution and 0.2 M TU from the (1 M) stock solution. Because of high vapour pressure of sulfur, (that results in loss of sulfur during the pyrolytic reduction due to increased evaporation), molarity of TU was kept in the ratio 1:2 [13,14]. It is also reported that sulfur incorporation will not improve beyond a limit even if we increase sulfur concentration in the solution [15]. Thus knowledge about film properties with various deposition conditions is very vital. Structural, morphological and optoelectronic properties of films were optimized by varying deposition parameters of the CSP technique. Due to unavailability of related studies, an extensive study was required on various parameters of spray pyrolysed SnS:Cu thin film fabrication.

2.3   Effect due to ageing of precursor solution
2.3.1 Experimental details

Since it is already reported that same parameters (as mentioned above) can be used for preparing n-type SnS [16], all deposition

parameters were initially kept same as that of p-type SnS. Films were prepared using an aqueous solution of tin chloride and thiourea in the ratio 1:2. As mentioned above, tin chloride ($SnCl_2.2H_2O$) precursor solution was prepared by employing 'two-step' process: the salt was dissolved in HCl initially, and then it was diluted using deionized water. Initially, we tried preparing SnS using freshly prepared tin chloride precursor. But the SnS films obtained were highly resistive and amorphous. To tackle this problem, various methods were tried and finally decided to use $SnCl_2$ precursor which was aged for one day for the preparation. This method was able to give reliable results. There are reports which emphasize improvement of material and transport properties with ageing of spray solution [17]. So far, to our knowledge, no groups have studied effect of precursor ageing on structural, electrical and optical properties of spray pyrolysed SnS thin films. We prepared two sets of tin chloride solutions: One set was aged for one day (24 hours), while the other was prepared and used immediately for fabricating thin films. The films prepared using tin chloride solution aged for one day was compared with those prepared using freshly prepared tin chloride solution. The samples were named "standard" (S) and "instant" (I) respectively. The films were prepared on ordinary soda lime glass substrates. Molarity of the precursors was set to keep the ratio of tin and sulfur as 1:2. Samples were deposited at a spray rate of 2 ml/min with substrate temperature 375 ^{o}C > T < 400 ^{o}C, using compressed air (pressure ~1.5 bar) as the carrier gas. The total volume of solution sprayed was 30 ml.

2.3.2 Material characterization

2.3.2.1 Structural analysis

Figure 2.1 represents the XRD pattern obtained for "instant" (I) and "standard" (S) SnS thin films.
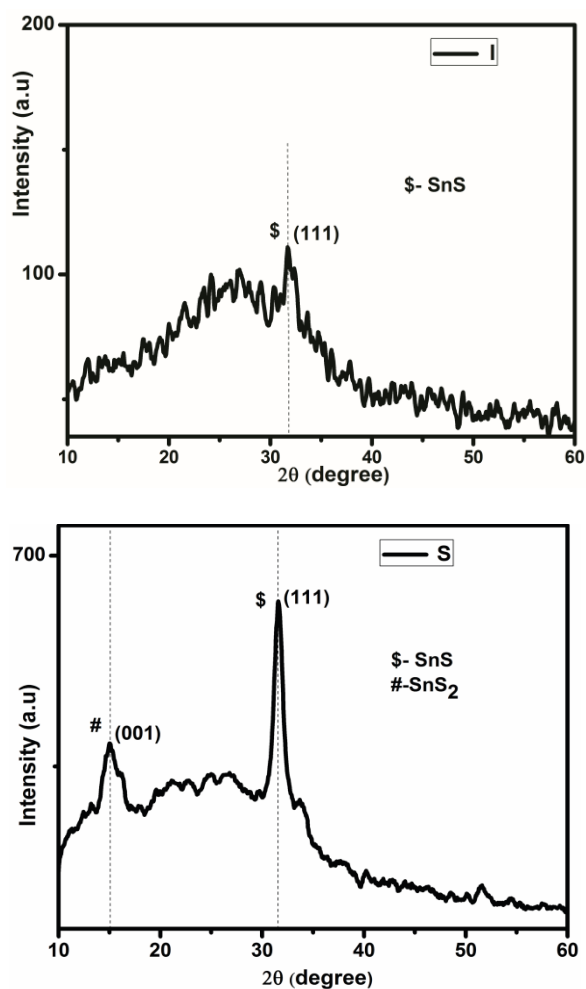
Figure 2.1 X-ray diffractograms of instant (I) and standard (S) SnS samples

It is clear from Figure 2.1 that "standard" sample is polycrystalline whereas "instant" sample is comparatively amorphous. The standard sample has preferential orientation along (111) plane corresponding to a 2θ value of 31.5^0 (JCPDS: 75-0925) and is crystallized in orthorhombic structure. Presence of SnS_2 phase with $2\theta = 15^0$ is also detected here (JCPDS: 83-1705).

2.3.2.2 Optical analysis

The optical band gap for both samples was determined using '$(\alpha h\nu)^2$ versus $h\nu$' plot (thickness of film 650 nm included) and is shown in Figure 2.2. It is almost the same for both "instant" and "standard" samples and is around 1.4 eV (1.37 eV for "standard "and 1.42 eV for "instant"). Good absorption coefficient ($> 10^5\,cm^{-1}$) is obtained for both samples. The direct band gap nature is confirmed from the linearity of the graph obtained.
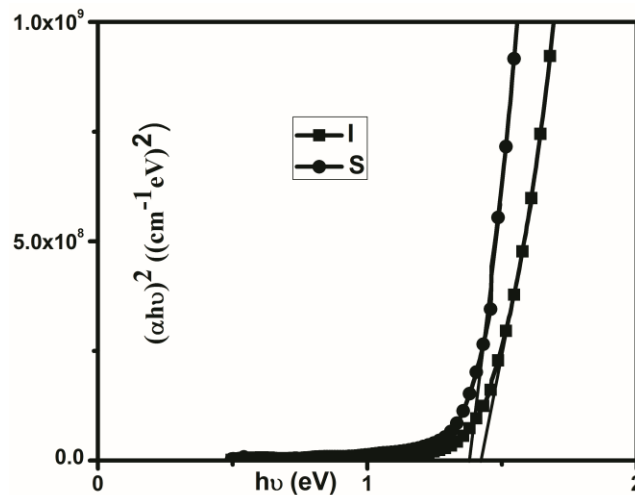
Figure 2.2 '$(\alpha h\nu)^2$ versus $h\nu$' plot of instant (I) and standard (S) SnS samples

2.3.2.3 Electrical analysis

Using Hall measurements, resistivity is found to be around 105 Ω.cm for "instant" and 1.4 Ω.cm for "standard" film. The decrease in resistivity of the standard film might be attributed to the increase in film crystallinity [18].

Because of its highly resistive and amorphous nature, preparation of films using instant $SnCl_2$ is not selected for further studies and the standard samples which exhibited better optoelectronic properties are chosen for further studies hereafter.

2.4 Optimization of precursor solvent to obtain n-type SnS

In this section, we explain structural and optoelectronic studies done to confirm the formation of n-type SnS in detail. In the CSP technique, we kept tin concentration a bit higher so as to compensate for tin vacancies which are responsible for p-type conduction. This method is known to be a successful technique even from 2010 [16] as the n-type nature is due to cation interstitials or anion vacancies and vice-versa for p-type conductivity [19-21]

2.4.1 Experimental details

Using the optimized standard solution, SnS samples are prepared by varying concentration of precursor solvent HCl. As mentioned above, $SnCl_2$ precursor solution is prepared by employing a 'two-step' process: the salt is dissolved in HCl initially and then it is diluted using deionized water. We had observed that a higher concentration of HCl used for dissolving tin chloride could badly affect device fabrication. Hence we tried reducing the HCl quantity from the reported value of 20 ml [11].

Quantity of HCl that is used for dissolving $SnCl_2$ salt is varied as 2 ml, 5 ml, 10 ml and 15 ml and samples are prepared under "standard" condition. Reduction of HCl below 2 ml has resulted in precipitation due to tin hydroxide formation and increase in HCl above 15 ml is found to result in inferior device performance. All other parameters of CSP are kept the same as mentioned above. Total volume of solution that is sprayed is 30 ml. The samples are referred to as B2, B5, B10, B15 respectively.

2.4.1.1 Structural analysis

X-ray diffractograms of samples are depicted in Figure 2.3. The (111) plane of SnS remains predominant irrespective of solvent variation. However, another phase of SnS_2 corresponding to (001) plane at 2θ value 15.0^0 (JCPDS: 83-1705) has emerged as the HCl concentration is increased beyond 5 ml. For SnS thin films that are used for PV applications, most devices are known to have the (111) orientation [22].
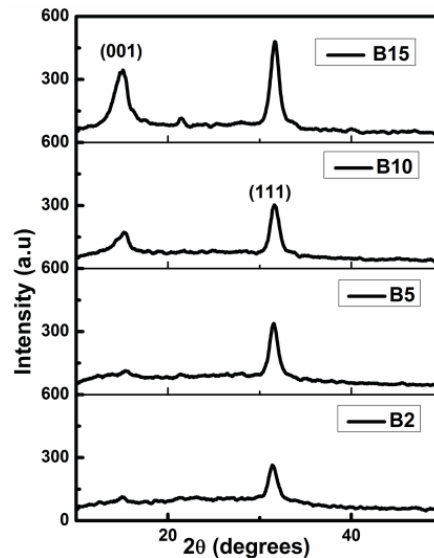
Figure 2.3 The XRD diffractograms of samples B2 to B15

Using Scherrer's formula D = $0.9\lambda/ \beta \, Cos\theta$, where, *D* is the average grain size, λ is the X-ray wavelength, β is the full-width at half-maximum (FWHM) of XRD peaks and θ is the Bragg angle, grain size of the films are calculated [23]. Average grain size for this set is found to be around 14 nm. Number of grains per unit area (N) is calculated using the equation $N=t/D^3$(per unit area) where 't' is the film thickness, and 'D' is the grain size [23]. It is found to be $\sim 2.3*10^{17}$. These are tabulated in Table 2.1 below

Table 2.1 Crystallite size and number of grains calculated for all the samples

Sample name	Crystallite size (nm)	Number of grains (per cm^2) $*10^{13}$
B2	13	2.7
B5	16	1.46
B10	14	2.18
B15	14	2.18

To further understand phase purity of samples, Raman analysis was carried out. Figure 2.4 represents Raman spectra obtained using exciting radiation of 632.8 nm. IV-VI compounds like GeS, SnSe, SnS etc. generally have an orthorhombic structure with eight atoms per unit cell. In such an orthorhombic structure, irreducible representations of 24 vibrational modes at the centre of the Brillouin zone can be represented by:

$$\Gamma = 4A_g + 2B_{1g} + 4B_{2g} + 2B_{3g} + 2A_u + 4B_{1u} + 2B_{2u} + 4B_{3u}$$

It is already reported that 21 optical phonons with 12 Raman active modes ($2B_{1g}$, $2B_{3g}$, $4A_g$ and $4B_{2g}$), 7 infrared active modes ($3B_{1u}$, $1B_{2u}$ and

$3B_{3u}$) and 2 inactive modes ($2A_u$) [24-27]. It is easy to distinguish formation of other phases since the Raman spectrum of each tin binary sulfide (SnS, Sn_2S_3, SnS_2) has distinct peak positions. The Raman peaks of single crystal SnS are at 96 cm^{-1} and 220 cm^{-1} respectively [28]. Our analysis showed two peaks at 96 cm^{-1} and 224 cm^{-1} which belong to that of SnS thin film [16]. Slight variation from the Raman peak position here may be attributed to the restricted ordering by grain boundaries [29]. The shift at 224 cm^{-1} corresponds to Ag mode [30]. Sajeesh et al. observed Raman shifts at 224 cm^{-1} in the case of spray deposited SnS thin films [16]. Liu *et al.* reported Raman mode of SnS nanowires at 223 cm^{-1} which corresponds to the 2Ag modes [31]. Even for GeS the Ag mode is observed at 224 cm^{-1} [32].
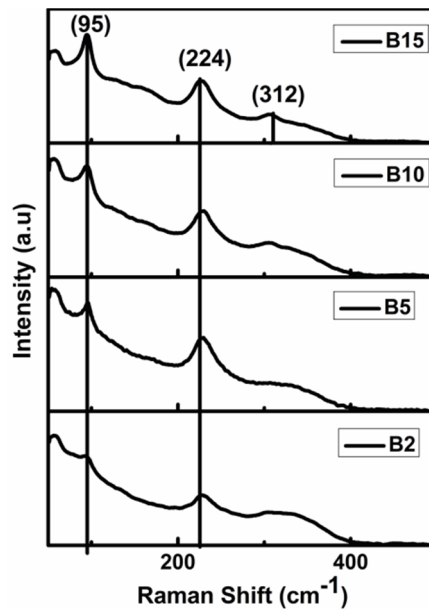
Figure 2.4 The Raman spectra of samples from B2 to B15.

The Raman vibrational mode of SnS_2 at 312 cm^{-1} is obtained for higher HCl concentration, which also validates the XRD result obtained [28].

2.4.1.2 Optical analysis

To estimate band gaps obtained for the samples, absorption measurements are done in the wavelength range of 190-2500 nm.Using Tauc's plot the bandgap is calculated for B2, B5, B10 and B15 samples and obtained as 1.43 eV, 1.34 eV, 1.45 eV, and 1.43 eV respectively (Figure 2.5 (a)).
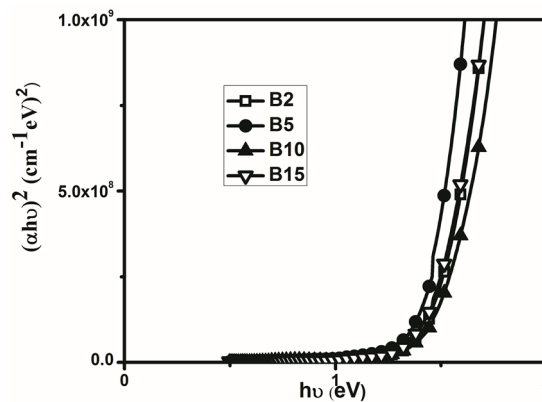
Figure 2.5 (a) $(\alpha h\nu)^2$ versus $h\nu$ plot of samples B2 to B15

Decrease in band gap for B5 sample might be due to improved crystallinity and grain size. Band gap of a single crystal is known to be higher than that of corresponding sprayed films due to the appearance of nearly exponential absorption tail which arises as a result of density of states tail formation at band edge [33]. All samples have high absorption coefficient ($>10^5$cm^{-1}) which implies that the material (within a micrometer thickness) can absorb almost 99 % of incoming photons.

This emphasises the possibility of saving the material and material cost compared to Si, which requires more than 300 μm thickness [34].

Figure 2.6 shows transmittance spectra of the samples taken in the wavelength range 300 to 2000 nm. The fringes obtained confirm uniformity of the films prepared. It is seen that transmittance of the film increases with wavelength and minimum transmittance is obtained for B5 sample.
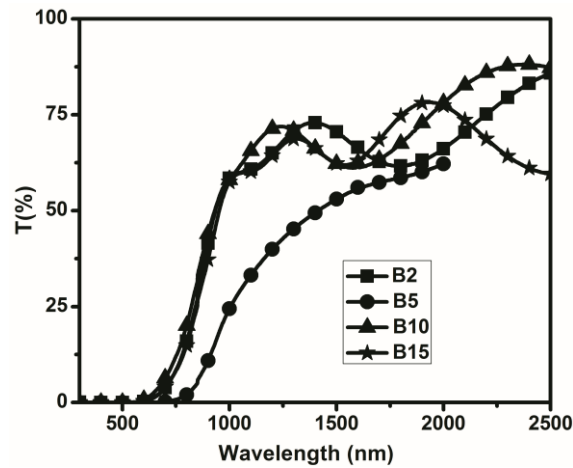
Figure 2.6. The transmittance spectra obtained for samples B2 to B15

2.4.1.3 Electrical characterization

To investigate electrical properties, Hall measurements are carried out. Carrier concentration, resistivity, mobility and polarity obtained are depicted in Table 2.2. A change in polarity from p-type to n-type is observed with a reduction of HCl concentration. However, in all the samples, resistivity is found to be high.

Table 2.2 Electrical measurements

Sample Name	Carrier Concentration (/cm^3) (*10^{17})	Resistivity (ohm.cm)	Mobility (cm^2/V.s)	Polarity
B2	12	98	0.53	n
B5*	4.9	335	0.38	n
B10	2.3	352	0.77	p
B15	1.3	540	0.89	p

(* In the case of B5 samples, majority showed n-type nature. The electrical measurement values obtained for p-type sample had carrier concentration = $15*10^{17}$/cm^3, resistivity = 347 ohm.cm and mobility = 0.12 cm^2/V.s)

From the present study, possibility of preparing the n-type SnS without affecting structural or optical properties was thus confirmed.

2.5 Effect of doping on n-type SnS and its optimization

One of the advantages with semiconductors is the possibility to control Fermi level position and facility to impart desirable properties by adding suitable elements as 'impurity' during its synthesis. These impurities are called "dopants" and the process of adding these dopants to semiconductors is known as "doping". This process can induce dramatic changes in material properties. Using CSP technique, the process of doping is quite easy, and hence it is possible to study its effect on material properties by varying doping concentration, molarity, concentration etc. The main objective of doping in present work was to enhance the conductivity of SnS fabricated via CSP technique to a certain level to use in device fabrication.

Doping of SnS with various elements like Bi, Sb, Pb, Cl, Al, Cu, In, Fe to improve various material properties were already tried [5, 35-41]. Presence of some dopants can also act as contaminant, which in turn affects the required properties [42] and hence, it is very important to choose the right dopant required to meet the demand. For the present study, we have selected doping with copper to meet our main aim, which is to reduce the resistivity of the material. Various studies on copper doping were carried out via various techniques and have been reported that Cu doping can enhance the carrier concentration and conductivity [43,44].

2.5.1 Experimental details

Eventhough we succeeded in synthesizing n-type SnS, its resistivity was found to be very high. From the reports mentioned in the above section, it is observed that Cu is a potential doping candidate to reduce resistivity of the material. Hence in order to enhance conductivity of SnS thin films, doping with Cu has been attempted. Copper doping is done by adding $CuCl_2.2H_2O$ (Merck, assay 99 %, M.W = 170.48 g/mol) along with the precursor spray solution. The optimum molarity of copper chloride required for doping is optimized via trial and error method and is fixed at 0.02 M. Keeping this molarity fixed, the optimum doping percentage (by varying the volume of $CuCl_2.2H_2O$ solution added) is studied by varying doping percentage from 2 to 10. The percentage is calculated with respect to that of tin chloride molarity taken in the solution. The samples are named as "Cu(Molarity)percentage" accordingly. All other deposition parameters are kept constant. The percentage varied samples thus prepared are named Cu(0.02)2%, Cu(0.02)4%, Cu(0.02)6%, Cu(0.02)8% and Cu(0.02)10% respectively.

2.5.2 Structural properties

X-ray diffraction patterns obtained for pristine (undoped) and doped SnS thin films are shown in Figure 2.7.
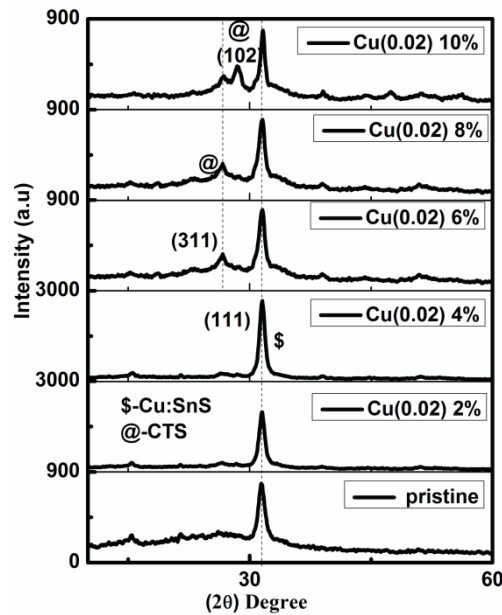
Figure 2.7 X-ray diffractograms of pristine& doped (Cu(0.02)2% to Cu(0.02)10%) samples

It is clear that all samples retained their preferential orientation of SnS (111) plane even with Cu doping. Intensity of (111) plane decreased with increase in doping percentage, and CTS (311) plane (JCPDS 71-0129) arises from 6 % doping onwards. For higher doping percentage, another plane (102) of CTS started to emerge and no other new mixed phases are observed. It is seen that as (102) plane emerges, intensity of (311) plane diminishes. Other researchers also reported similar behaviour [45,46]. For our sample, it is found that 4 % doping is optimum which is devoid of any CTS phase and has enhanced SnS plane.

2.5.3 Optical properties

Optical absorption spectra is recorded in the wavelength region of 200 -1500 nm and band gap is determined by plotting $(\alpha h\nu)^2$ versus hν (Figure 2.8(a)); the corresponding variation in band gap obtained is described in Figure 2.8(b). It is seen that on doping, the band gap decreased initially and then increased, as doping percentage increases. Similar phenomenon had been pointed out by other researchers as well [43,44]. Band gap varies from 1.3 eV to 1.6 eV when doping percentage of copper is varied, and band gap of ~1.3 eV is obtained for 4 % doping.
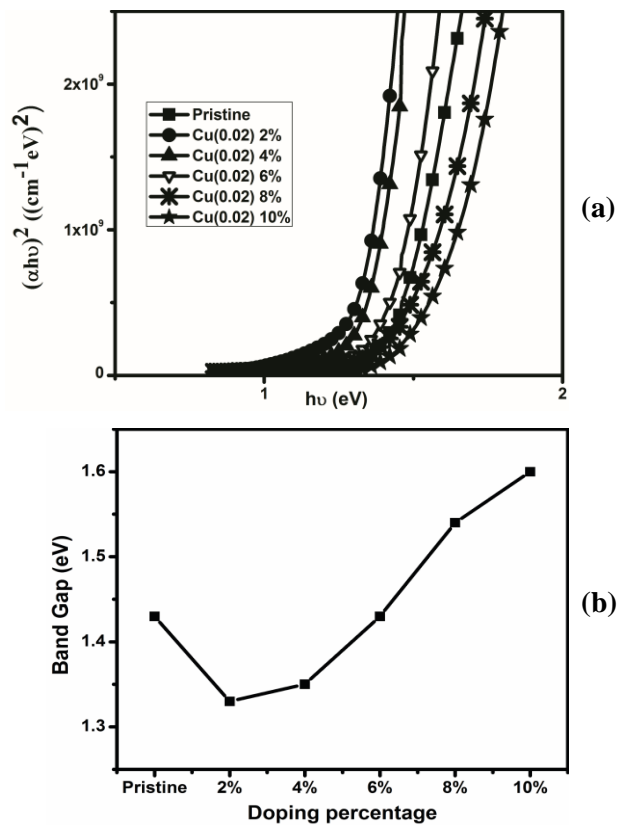
Figure 2.8 **(a)** $(\alpha h\nu)^2$ versus hν plot **(b)** Variation of band gap with doping

The decrease in band gap with doping initially might be due to the band shrinkage effect due to increased carrier concentration and due to the defects formed by unsaturated bonds in the layers which produce localized states within the band structure [47,48]. The increase in band gap with further doping percentage can be attributed to effective incorporation of copper atoms at substitutional sites [49]. The band gap increases due to the efficient placement of dopant into the SnS lattice.

2.5.4 Electrical measurements

Electrical measurements are taken using Hall measurement syste, and Figure 2.9 represents carrier concentration, resistivity and mobility obtained. All samples are found to retain their n-type nature. The pristine sample (0 % doped) has the highest resistivity and its resistivity decrease by two orders with doping.
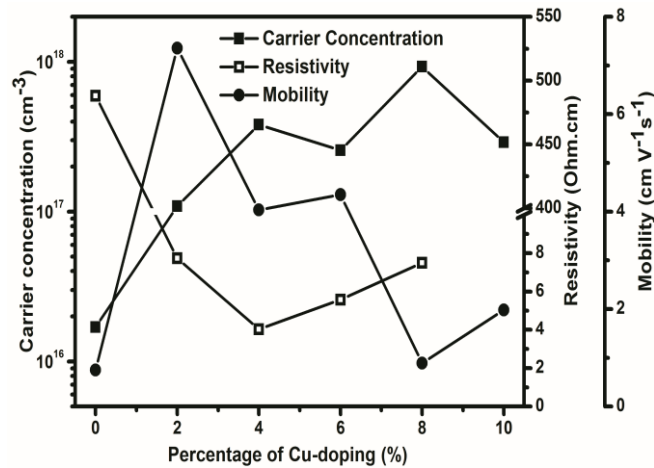
Figure 2.9 Electrical properties obtained for samples with doping percentage (0 to 10)

With further increase in doping percentage, resistivity increased slightly, with minimum resistivity for 4 % doping (4 Ωcm), which is the lowest resistivity reported for sprayed n-type SnS:Cu. On doping, free carriers are released to conduction band from the dopant. This is clear from the Hall measurement, which shows an increase in carrier concentration with doping compared to undoped samples. The studies also indicate improvement in mobility with doping. For doped samples, an increase in mobility and carrier concentration resulted in reduction of resistivity. It is seen that beyond 4 % of doping, resistivity starts increasing due to an increase in doping ions that act as scattering centers resulting in decreased carrier mobility [50,51].

2.6 Inference

In this chapter, the deposition of n-type SnS thin films using chemical spray pyrolysis technique is discussed. Structural and optoelectronic properties are improved by various methods like ageing the precursor solution ($SnCl_2.2H_2O$), optimizing the solvent quantity (quantity of HCl added) and also by proper doping ($CuCl_2.2H_2O$). The effect due to the ageing of tin chloride solution for a day is initially checked and it is found that the aged solution gives better structural properties when compared with the samples prepared 'instantly'. The samples prepared using 'one day aged solution' (named as "standard sample") are considered as the optimized case and at the next step, the precursor solvent quantity (quantity of HCl used to dissolve the salt) is varied to assess required quantity to obtain n-type SnS. The material properties are studied for HCl variation and 5 ml HCl is fixed as the

safer limit for further studies. In the present work doping is tried next and here this is done by adding the dopant to the prepared precursor spray solution. Doping is done by adding required percentages of 0.02 M $CuCl_2.2H_2O$. Doping percentage is varied from 2 % to 10 % (of tin concentration) in the precursor solution. Improvement in carrier concentration by an order and correspondingly enhanced conductivity is achieved by the doping. Variation in band gap is also observed with doping percentage. Incorporation of 4 % copper doping is found to result in minimum resistivity.

References

[1]   Patil, Pramod S. "Versatility of chemical spray pyrolysis technique." *Materials Chemistry and physics* 59.3 (1999): 185-198.

[2]   Bube, Richard H., and Richard Howard Bube. "Photovoltaic materials." (1998).

[3]   P. M. Ratheesh Kumar, PhD Thesis Cochin University of Science and Technology, India (2007).

[4]   Chen, C. H., E. M. Kelder, and J. Schoonman. "Effects of additives in electrospraying for materials preparation." *Journal of the European Ceramic Society* 18.10 (1998): 1439-1443.

[5]   Khaleel, Reem Saadi, Sami Salman Chiad, and Nadir Fadhil Habubi. "The Effect of Chlorine Concentration on the Optical Constants of SnS Thin Films." *Baghdad Science Journal* 8.2 (2011): 566-570.

[6]   Teny Theresa John, PhD Thesis, Cochin University of Science and Technology, India (2004).

[7] John, Teny Theresa, C. Sudha Kartha, K. P. Vijayakumar, T. Abe, and Y. Kashiwaba. "Preparation of indium sulfide thin films by spray pyrolysis using a new precursor indium nitrate." *Applied Surface Science* 252, no. 5 (2005): 1360-1367.

[8] Mariappan, R., T. Mahalingam, and V. Ponnuswamy. "Preparation and characterization of electrodeposited SnS thin films." *Optik-International Journal for Light and Electron Optics* 122.24 (2011): 2216-2219.

[9] Geetha, G., M. Priya, and S. Sagadevan. "Investigation of the optical and electrical properties of tin sulfide thin films." *Chalcogenide Letters* 12.11 (2015): 609-617.

[10] Ragina, A. J., K. C. Preetha, K. V. Murali, K. Deepa, and T. L. Remadevi. "Wet chemical synthesis and characterization of tin sulphide thin films from different host solutions." *Adv Appl Sci Res* 2 (2011): 438-44.

[11] Sajeesh T.H, PhD Thesis, Cochin University of Science and Technology, India (2012).

[12] Ortega-Lopez, Mauricio, and Arturo Morales-Acevedo. "Characterization of $CuInS_2$ thin films for solar cells prepared by spray pyrolysis." *Thin Solid Films* 330.2 (1998): 96-101.

[13] Devika, M., K. T. Ramakrishna Reddy, N. Koteeswara Reddy, K. Ramesh, R. Ganesan, E. S. R. Gopal, and K. R. Gunasekhar. "Microstructure dependent physical properties of evaporated tin sulfide films." *Journal of applied physics* 100, no. 2 (2006): 023518.

[14] Tiwari, A. N., D. K. Pandya, and K. L. Chopra. "Electrical and optical properties of single-phase $CuInS_2$ films prepared using spray pyrolysis." *Thin Solid Films* 130.3-4 (1985): 217-230.

[15] Tina Sebastian, PhD Thesis, Cochin University of Science and Technology, India (2009).

[16] Sajeesh, T. H., Anita R. Warrier, C. Sudha Kartha, and K. P. Vijayakumar. "Optimization of parameters of chemical spray pyrolysis technique to get n and p-type layers of SnS." *Thin Solid Films* 518, no. 15 (2010): 4370-4374.

[17] Maldonado, A., Salvador Tirado-Guerra, and M. de la L. Olvera. "Chemically sprayed ZnO:(F, Zr) thin films: effect of starting solution ageing time and substrate temperature on the physical properties." *Journal of Physics and Chemistry of Solids* 70.3-4 (2009): 571-575.

[18] Sebastian, Tina, R. Jayakrishnan, C. Sudha Kartha, and K. P Vijayakumar. "Characterization of spray pyrolysed CuInS2 thin films." *The Open Surface Science Journal* 1, no. 1 (2009).

[19] Noguchi, Hidenori, Agus Setiyadi, Hiromasa Tanamura, Takao Nagatomo, and Osamu Omoto. "Characterization of vacuum-evaporated tin sulfide film for solar cell materials." *Solar energy materials and solar cells* 35 (1994): 325-331.

[20] Reddy, N. Koteswara, and KT Ramakrishna Reddy. "Preparation and characterisation of sprayed tin sulphide films grown at different precursor concentrations." *Materials Chemistry and Physics* 102.1 (2007): 13-18.

[21] Nwofe, P. A., KT Ramakrishna Reddy, Gedi Sreedevi, J. K. Tan, Ian Forbes, and R. W. Miles. "Single phase, large grain, p-conductivity-type SnS layers produced using the thermal evaporation method." *Energy Procedia* 15 (2012): 354-360.

[22] Reddy, KT Ramakrishna, N. Koteswara Reddy, and R. W. Miles. "Photovoltaic properties of SnS based solar cells." *Solar energy materials and solar cells* 90.18-19 (2006): 3041-3046.

[23] Guneri, E., C. Ulutas, F. Kirmizigul, G. Altindemir, F. Gode, and C. Gumus. "Effect of deposition time on structural, electrical, and optical properties of SnS thin films deposited by chemical bath deposition." *Applied Surface Science* 257, no. 4 (2010): 1189-1195.

[24] Nikolic, P. M., P. Mihajlovic, and B. Lavrencic. "Splitting and coupling of lattice modes in the layer compound SnS." *Journal of Physics C: Solid State Physics* 10.11 (1977): L289.

[25] Bashkirov, S. A., "Influence of thermal treatment on the microstructure and electrical and optical properties of SnS thin films." *Physics of the Solid State* 56.7 (2014): 1310-1314.

[26] Chandrasekhar, H. R., R. G. Humphreys, U. Zwick, and M. Cardona. "Infrared and Raman spectra of the IV-VI compounds SnS and SnSe." *Physical Review B* 15, no. 4 (1977): 2177.

[27] Wiley, JoD, W. J. Buckel, and R. L. Schmidt. "Infrared reflectivity and Raman scattering in GeS." *Physical Review B* 13.6 (1976): 2489.

[28] Mathews, N. R., C. Colín García, and Ildefonso Z. Torres. "Effect of annealing on structural, optical and electrical properties of pulse electrodeposited tin sulfide films." *Materials Science in Semiconductor Processing* 16.1 (2013): 29-37.

[29] Jain, Priyal, and P. Arun. "Influence of grain size on the band-gap of annealed SnS thin films." *Thin Solid Films* 548 (2013): 241-246.

[30] Devika, M., N. Koteeswara Reddy, M. Prashantha, K. Ramesh, S. Venkatramana Reddy, Y. B. Hahn, and K. R. Gunasekhar. "The physical properties of SnS films grown on lattice-matched and amorphous substrates." *physica status solidi (a)* 207, no. 8 (2010): 1864-1869.

[31] Liu, Yingkai, Dedong Hou, and Guanghou Wang. "Synthesis and characterization of SnS nanowires in cetyltrimethylammoniumbromide (CTAB) aqueous solution." *Chemical physics letters* 379.1-2 (2003): 67-73.

[32] Chandrasekhar, H. R., R. G. Humphreys, and M. Cardona. "Pressure dependence of the Raman spectra of the IV-VI layer compounds GeS and GeSe." *Physical Review B* 16.6 (1977): 2981.

[33] Rajaram, P., R. Thangaraj, and A. K. Sharma. "A. Raza and O. P. Agnihotri." *Thin Solid Films* 100 (1983): 111.

[34] Deepa K G, PhD Thesis, Cochin University of Science and Technology, India (2008).

[35] Dussan, A., F. Mesa, and G. Gordillo. "Effect of substitution of Sn for Bi on structural and electrical transport properties of SnS thin films." *Journal of materials science* 45.9 (2010): 2403-2407.

[36] Sinsermsuksakul, Prasert, Rupak Chakraborty, Sang Bok Kim, Steven M. Heald, Tonio Buonassisi, and Roy G. Gordon. "Antimony-doped tin (II) sulfide thin films." *Chemistry of Materials* 24, no. 23 (2012): 4556-4562.

[37] Ran, Fan-Yong, Zewen Xiao, Yoshitake Toda, Hidenori Hiramatsu, Hideo Hosono, and Toshio Kamiya. "n-type conversion of SnS by isovalent ion substitution: Geometrical doping as a new doping route." *Scientific reports* 5 (2015): 10428.

[38] Kafashan, Hosein, Reza Ebrahimi-Kahrizsangi, Farid Jamali-Sheini, and Ramin Yousefi. "Effect of Al doping on the structural and optical properties of electrodeposited SnS thin films." *physica status solidi (a)* 213, no. 5 (2016): 1302-1308.

[39] Bommireddy, Purusottam Reddy, Chandra Sekhar Musalikunta, Chalapathi Uppala, and Si-Hyun Park. "Influence of Cu doping on physical properties of sol-gel processed SnS thin films." *Materials Science in Semiconductor Processing* 71 (2017): 139-144.

[40] Reghima, Meriem, Anis Akkari, Cathy Guasch, and Najoua Kamoun-Turki. "Effect of indium doping on physical properties of nanocrystallized SnS zinc blend thin films grown by chemical bath deposition." *Journal of Renewable and Sustainable Energy* 4, no. 1 (2012): 011602.

[41] Reghima, Meriem, Anis Akkari, Cathy Guasch, Michel Castagné, and Najoua Kamoun-Turki. "Synthesis and characterization of Fe-doped SnS thin films by chemical bath deposition technique for solar cells applications." *Journal of Renewable and Sustainable Energy* 5, no. 6 (2013): 063109.

[42] Steinmann, Vera, Riley E. Brandt, Rupak Chakraborty, R. Jaramillo, Matthew Young, Benjamin K. Ofori-Okai, Chuanxi Yang et al. "The impact of sodium contamination in tin sulfide thin-film solar cells." *APL Materials* 4, no. 2 (2016): 026103.

[43] Zhang, Shuai, and Shuying Cheng. "Thermally evaporated SnS:Cu thin films for solar cells." *Micro & Nano Letters* 6.7 (2011): 559-562.

[44] Kumar, K. Santhosh, A. Gowri Manohari, Chaogang Lou, T. Mahalingam, and S. Dhanapandian. "Influence of Cu dopant on the optical and electrical properties of spray deposited tin sulphide thin films." *Vacuum* 128 (2016): 226-229.

[45] Kafashan, Hosein. "Structural characterizations of pure SnS and In-doped SnS thin films using isotropic and anisotropic models." *Materials Research Express* 5.4 (2018): 046417.

[46] Kumar, PM Ratheesh, C. Sudha Kartha, K. P. Vijayakumar, T. Abe, Y. Kashiwaba, F. Singh, and D. K. Avasthi. "On the properties of indium doped ZnO thin films." *Semiconductor science and technology* 20, no. 2 (2004): 120.

[47] Minami, Tadatsugu, Toshikazu Kakumu, Yoshihiro Takeda, and Shinzo Takata. "Highly transparent and conductive ZnO/ In$_2$O$_3$ thin films prepared by dc magnetron sputtering." *Thin solid films* 290 (1996): 1-5.

[48] Devika, M., N. Koteeswara Reddy, K. Ramesh, K. R. Gunasekhar, E. S. R. Gopal, and KT Ramakrishna Reddy. "Low resistive micrometer-thick SnS: Ag films for optoelectronic applications." *Journal of the Electrochemical Society* 153, no. 8 (2006): G727-G733.

[49] Gómez-Pozos, Heberto, A. Maldonado, and M. de la L. Olvera. "Effect of the [Al/Zn] ratio in the starting solution and deposition temperature on the physical properties of sprayed ZnO: Al thin films." *Materials Letters* 61.7 (2007): 1460-1464.

[50] Igasaki, Yasuhiro, and Hiromi Saito. "The effects of deposition rate on the structural and electrical properties of ZnO: Al films deposited on (1120) oriented sapphire substrates." *Journal of Applied Physics* 70.7 (1991): 3613-3619.

[51] Meril Mathew, PhD Thesis, Cochin University of Science and Technology, India (2009).

Chapter 3

OPTIMIZATION OF CHEMICAL SPRAY PYROLYSIS PARAMETERS

3.1 Introduction

In the previous chapter, fabrication of n-type SnS thin films were explained. We experimented the preparation conditions described in the literature and also tried a few modifications to it. In this chapter, a more systematic approach, to optimize various deposition parameters so as to obtain good quality films with required optoelectronic properties, is considered. This is done with the aim to modify this eco-friendly and earth-abundant compound semiconductor for making it a better absorber. Actually, this is the major reason for selecting Sn chalcogenide absorber layer and its fabrication using chemical spray pyrolysis (CSP) technique for this study. The ease in doping and the possibility of tailoring material stoichiometry makes CSP a popular technique specifically suited for device fabrication [1,2]. Hence optimization of spray parameters is discussed seriously so as to obtain good thin films of SnS with repeatability. Apart from our work, there are very few studies available on spray deposited n-type SnS thin films. Thankaraju *et al.* [3] fabricated n-type tin sulphide thin films using spray technique. The films obtained were resistive and highly amorphous. Later in 2005 and 2007, Koteeswara

Reddy *et al.* [4,5] deposited n-type SnS by varying deposition temperature and also by varying precursor concentration. In 2010 Sajeesh *et al.* [6] reported deposition of n-type SnS using CSP by varying precursor molarity. Recently Jacob *et al.* [7] in 2016 prepared n-type SnS by varying carrier gas pressure in CSP technique. In the present work, repeatability and quality of films prepared can be confirmed, since the entire work is carried out using indigenously developed automated spray machine (detailed explanations given in 1st chapter).

3.2   Optimization of various CSP deposition parameters

The following section describes detailed investigation onthe optimization of various CSP deposition parameters. Important parameters that have to be optimized are rate at which the spray falls over the substrate, optimum pyrolytic temperature required for the decomposition of precursors to obtain the required material and the cationic and anionic molarity required. In order to study the effect of each parameter, films were deposited by varying one parameter at a time, while keeping all other conditions fixed. Structural, optical, morphological and electronic properties were compared in each case to optimize the most well-suited deposition conditions for preparing the best quality SnS:Cu thin films.

3.2.1 Optimization of substrate temperature

Optimization of substrate temperature is critical since it is the main factor which provides required energy that determines film properties in pyrolytic reduction and film formation. In general, it is observed that

crystallinity of the film is directly related to its deposition temperature [8,9]. With higher deposition temperature, there will be an increase in surface mobility of adsorbed species, and they could interact among themselves easily. This helps in the formation of films with continuous, well distinct and large grains. There are also reports that suggest higher temperature deposition as more advantageous because it provides more chances for grain recrystallization and hence, the formation of larger grains [10]. But there are also reports that insist on care to be taken about enhancing the deposition temperature beyond a limit. For example, Nair *et al.* [11], suggests that it is not advisable to deposit films at very high temperature because it can cause anionic species to re-evaporate in metal sulfide thin films. Also, at very high deposition temperatures, the sulfur from metal sulfides may re-evaporate producing metal rich surface which may oxidise with the oxygen present in atmosphere. Stelzer *et al.* [12] reported effect of deposition temperature on film surface morphology, and he found that as temperature increases, the morphology changes from cracked to dense and finally becomes porous at very high temperature. All these points to the argument that deposition temperature is a critical factor for good quality film fabrication. Variation in substrate temperature, even within various regions of the same film surface, may result in non-uniform films with varying composition and thickness. Maintenance of uniform temperature over a large area is really challenging with solid surface contacts as only less than 1 % of the actual area is used as contact area in a spray pyrolysis system. Bursts or pulse spraying are some of the methods used to maintain a reasonably constant temperature. The

following section is dedicated to explain various deposition temperature optimization techniques that are required for obtaining good uniform SnS:Cu thin films. Taking the above requirements into consideration, thin films in the present study were deposited on glass substrates by varying deposition temperature (°C) from 300 °C to 450 °C with an accuracy of ± 5 °C, and these samples were named as C300, C350, C375, C400 and C450 respectively. Structural, optical and morphological studies were done using XRD, UV-Vis spectrophotometer, SEM and AFM analysis respectively. The results obtained are discussed below in detail.

3.2.1.1 Structural analysis

Figure 3.1 depicts XRD patterns of SnS:Cu films deposited at different substrate temperatures (300 °C to 450 °C). All the samples except those prepared at 300°C had SnS (111) plane crystallized in Orthorhombic structure (JCPDS 75-0925). At a lower temperature of 300 °C, presence of Sn_2S_3 phase (JCPDS 14-0619) is observed along with SnS (120) plane and at a higher temperature of 450 °C, the SnS_2 phase (JCPDS 23-0677) became prominent. It is observed from XRD data that, at substrate temperature of 375 °C, the impurity phases are absent and that the film has better crystallinity with prominent SnS (111) plane.
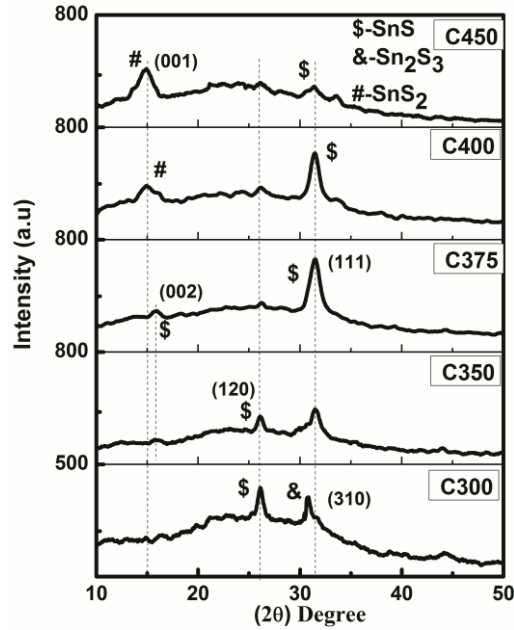
Figure 3.1 XRD pattern of films C300 to C450

It is to be noted that even with doping, no peaks corresponding to Cu_xS phase is formed. According to reports, surface energies (σ) of orthorhombic structure increases as σ (100) < σ (001) < σ (010) < σ (111) and it is also mentioned that the (111) plane will grow only when an optimum number of sulfur atoms are present around Sn atoms [13]. Hence the optimum substrate temperature for the synthesis of SnS:Cu thin films with the high energy (111) plane is fixed at 375 ^{o}C.

3.2.1.2 Thickness measurements

Thickness of the obtained Sn_xS_y films was calculated with the help of stylus thickness profiler; it was found to be decreasing from 1320 nm to 520 nm with increase in deposition temperature (Figure 3.2)
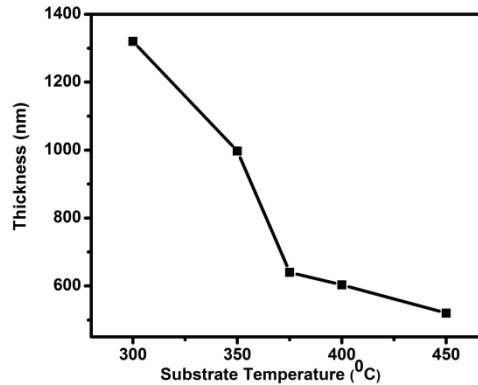
Figure 3.2 Variation of film thickness with respect to
substrate temperature

The reduction in thickness might be due to the re-evaporation of compounds due to increasing temperature. This reduction of thickness is very common in the case of CSP technique and is already reported [14].

3.2.1.3 Morphological analysis

Surface morphology of the samples showed a noticeable difference with change in temperature. The film surface is analyzed using both SEM and AFM.

A) SEM

SEM analysis reveals noticeable difference in surface morphology of the samples prepared at different deposition temperatures. Figure 3.3 shows SEM image of the samples prepared at 300 °C, 375 °C and 450 °C respectively.
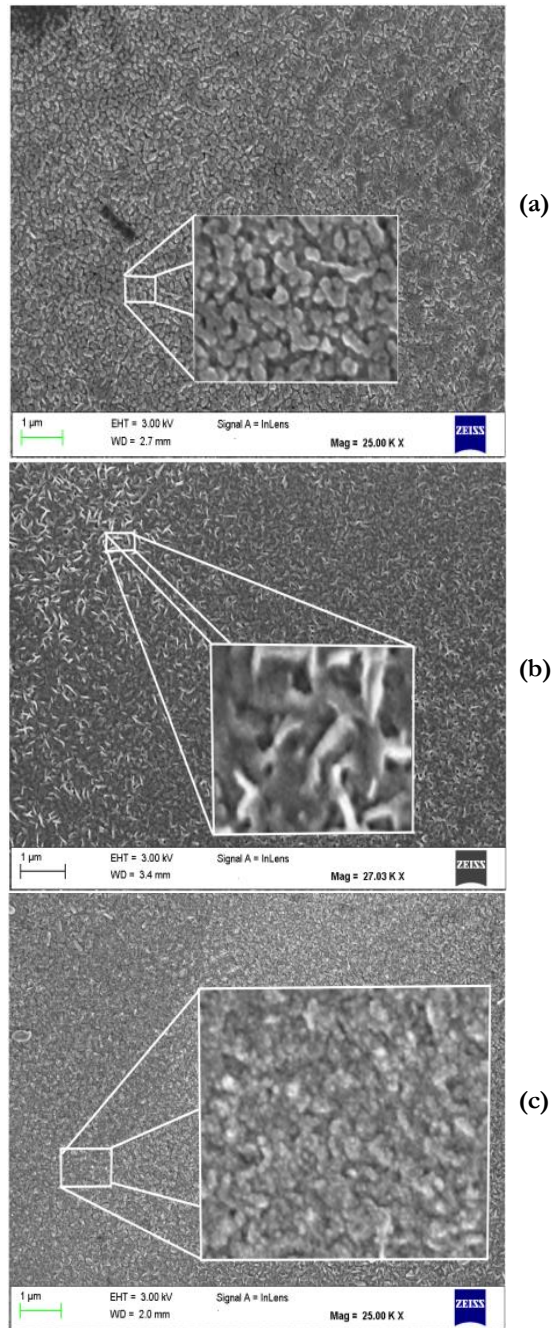
Figure 3.3 SEM images of samples prepared at
(a) 300 °C (b) 375 °C (c) 450 °C

The samples at 300 °C showed spherical grain nature whereas samples at 375 °C showed (usual) needle-like the structure of SnS:Cu; samples prepared at 450 °C showed granule structure of SnS_2. This confirmed change in film morphology with temperature. The 'needle-like structure' is already reported [6]. Interestingly Huilan Su *et al.* [15] observed almost similar 'rod-like' structure for SnS deposited via thermal reaction.

B)   AFM

Figure 3.4 represents AFM images obtained for the films prepared by varying substrate temperature. All films were found to be uniform and pinhole free. For deposition temperature greater than 400 °C, the films appeared in brownish grey colour, whereas samples prepared at 450 °C appeared more like a translucent brownish film due to the presence of SnS_2 phase at high temperature. This again confirms that surface morphology can be controlled by varying the deposition condition. Surface roughness was calculated by AFM analysis and was found to be decreasing with increase in substrate temperature up to 375 °C and thereafter it increased with increase in temperature. This might be due to improper formation of films at a higher temperature.
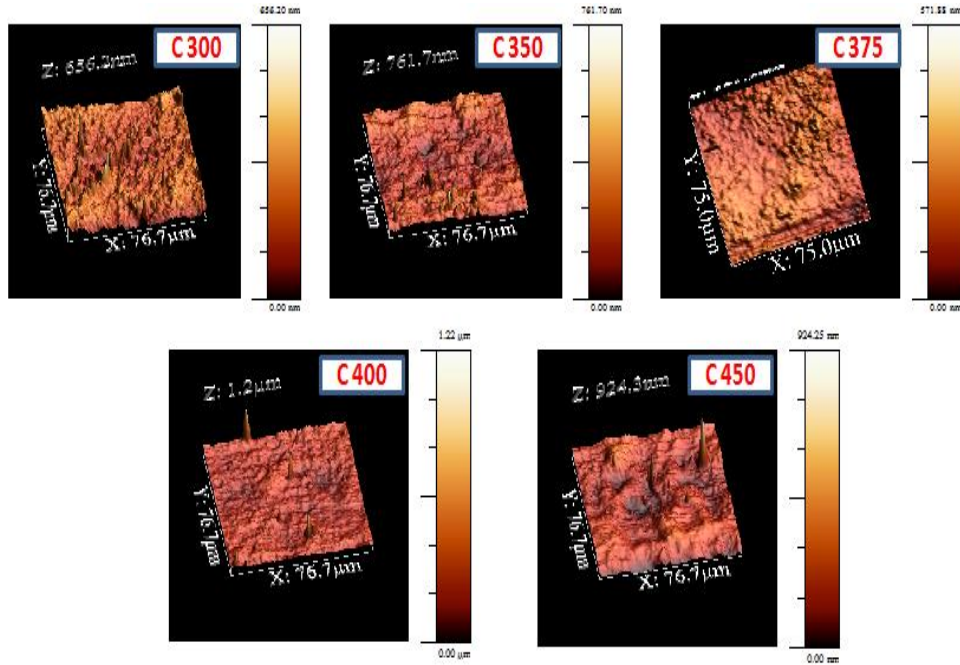
Figure 3.4 AFM images of sample prepared at different deposition temperature

RMS value of surface roughness obtained is tabulated in Table 3.1

Table 3.1 RMS roughness calculated for all the samples

Sample Name	RMS Surface roughness (nm)
C300	51
C350	45
C375	36
C400	43
C450	46

3.2.1.4 Optical characterizations

Optical band gap of all the films prepared at different substrate temperatures were determined using '$(\alpha h v)^2$ versus hv' plot (Figure 3.5 (a)).

The corresponding band gap is also shown in Figure 3.5 (b). Absorption coefficient ($> 10^5$ cm^{-1}) for all the samples was determined. Direct band gap nature of Sn_xS_y is confirmed from the linearity of the graph. The film synthesized at 375 ^{o}C was found to have band gap around 1.4 eV. For lower and higher temperature, the band gap was found to be greater than that of C375.
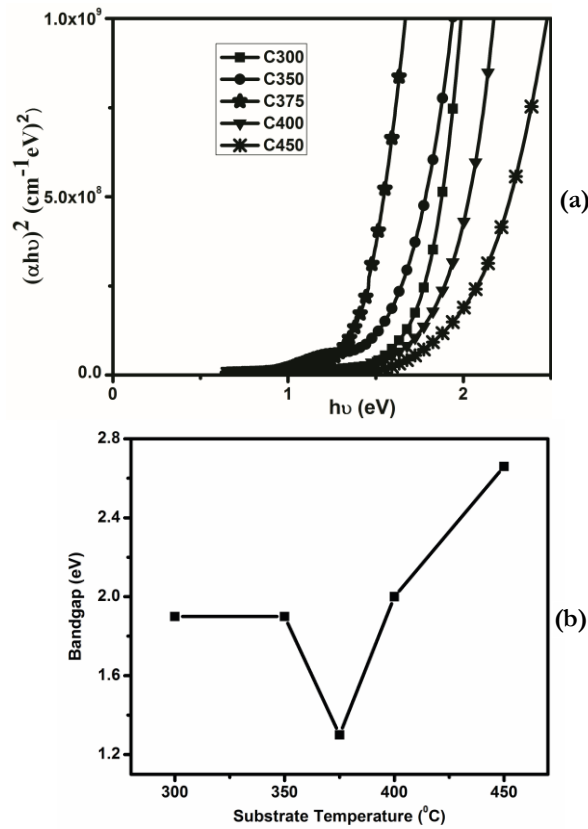
Figure 3.5 (a) $(\alpha h\nu)^2$ versus hν plot (b) Variation of band gap with deposition temperature

Variation in band gap shows its tunability by merely changing the temperature alone. From the graph obtained, it is clear that the band gap has great dependence on material composition. High band gap value obtained for lower and higher temperature is probably due to the presence of other phases like Sn_2S_3 and SnS_2 respectively [16,17].

The transmittance of each film with deposition temperature is also checked and the percentage of transmittance with respect to wavelength is depicted in Figure 3.6 (in the wavelength range 450 to 2500 nm).
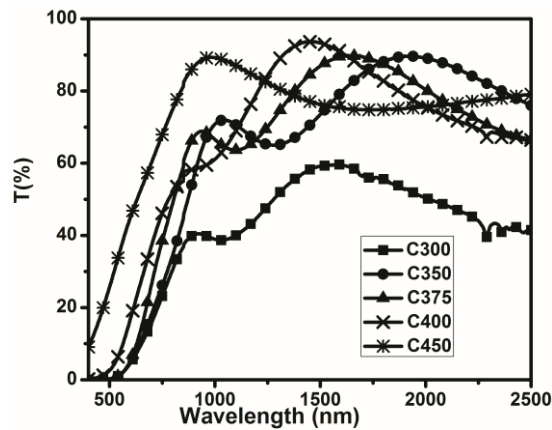
Figure 3.6 Transmittance spectra obtained for films C300 to C450

From Figure 3.6 it is clear that the transmittance (T %) is dependent on deposition temperature. The fringes obtained in the transmission spectra highlights the uniformity of the prepared samples.

3.2.1.5 Electrical characterizations

Carrier concentration, resistivity and mobility of all the samples were calculated using Hall measurement and are depicted in Figure 3.7.
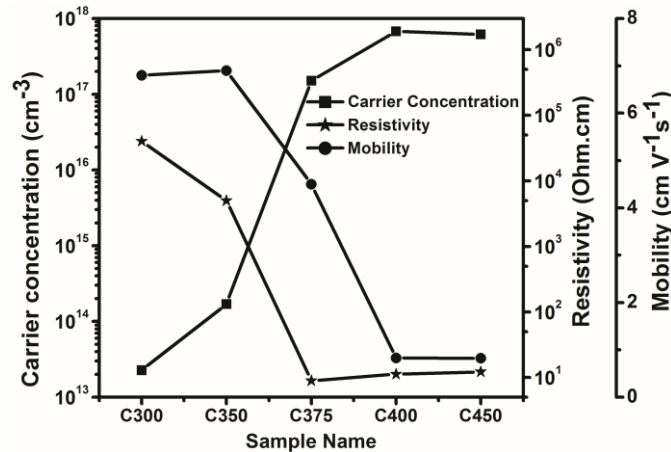
Figure 3.7 Electrical studies done on films C300 to C450

For samples prepared at substrate temperatures above 375 °C, resistivity remains low, with the minimum at 375 °C, while resistivity shows an increasing trend for the films prepared at substrate temperature below 375 °C (4×10^4 Ω.cm to 4×10^1 Ω.cm). The minimum resistivity obtained for samples prepared at 375 °C is 9 Ω.cm. A minor increase in resistivity with further increase in temperature might be due to the presence of other phases present in the sample. High resistivity for samples below 350 °C is due to highly resistive Sn_2S_3 mixed valency phase [18]. Polarity is checked for all the samples and found to be n-type irrespective of deposition temperature. Mobility showed a decreasing trend as temperature increases, whereas carrier

concentration showed an opposite nature. Based on the above studies the substrate temperature for better conducting SnS:Cu films is fixed as 375 °C.

3.2.2 Optimization of spray rate

Spray rate of the precursor solution is measured in milliliters (ml) per minute, and it very well influences morphology of deposited films. In CSP technique, optimum growth and deposition rates are mutually linked and are very vital too for device fabrication. Very high spray rates may produce rough films, whereas low rates may result in thinner films, possibly due to high re-evaporation [19]. Effect on film properties like crystallinity, resistivity, morphology and uniformity due to variation in spray rate is already reported in literature [20]. In the case of thin films fabricated using CSP technique, generally, it is observed that better crystalline films are obtained with low spray rate [19]. To the best of our knowledge, ours is the first study reporting the effect of spray rate variation on n-type SnS:Cu thin films. The study is done by keeping deposition temperature at 375 °C and varying the spray rate from 1 ml/min to 6 ml/min in uniform steps (1 ml/min, 2 ml/min, 3 ml/min, 4 ml/min and 6 ml/min); the resulting samples were referred to as D1, D2, D3, D4 and D6 respectively. Total volume of precursor solution sprayed was kept constant (20 ml) so as to minimize variation in thickness of the deposited samples.

3.2.2.1 Structural characterizations

A)   XRD

X-ray diffraction (XRD) pattern of SnS:Cu films prepared by varying spray rate are shown in Figure 3.8(a). Crystallite size was calculated using Scherer's formula and is depicted in Figure 3.8(b). Maximum grain size was obtained for sample D2 and was ~22 nm.
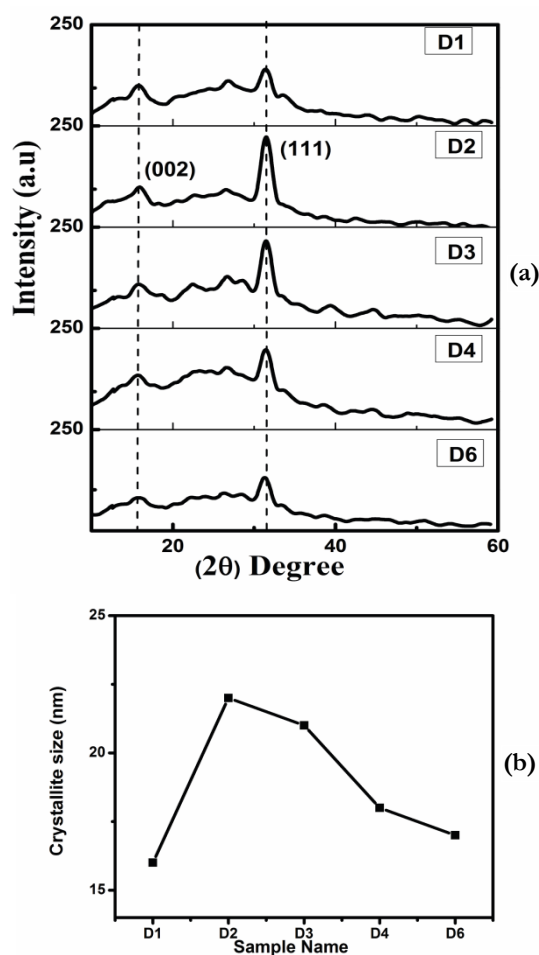
Figure 3.8(a) XRD pattern
                    (b) Crystallite size variation from D1 to D6

Preferential orientation is along the (111) plane, (corresponding to 2θ value of 31.5^O) crystallized in orthorhombic structure. No peaks were observed corresponding to the SnS_2 phase. It is seen that peak intensity of (111) plane is enhanced with maximum crystallite size for D2 sample. It is to be specifically noted that there were no peaks corresponding to Cu_xS phase. Though the spray rates were varied, total volume sprayed was kept constant, so that thickness of the layer remained uniform in all samples. Intensity of XRD (111) peak initially increased and then decreased with increase in spray rate. Low intensity for lower spray rate might be due to the re-evaporation of certain elements, and similarly, at higher spray rate, the chance for deviation in substrate temperature is high, resulting in improper film formation. The samples deposited at low spray rate were found to be preferable, but the smallest spray rate required more deposition time to fabricate films with the same thickness. Films fabricated at high spray rate will not be suitable for device fabrication since very high spray rate results in deviation of surface temperature, leading to formation of unwanted compounds. From the XRD, it is observed that, at both lower and higher spray rates, the fabricated films have low crystallinity. Crystallite size is found to be decreasing as the spray rate increased from 2 ml/min to 6 ml/min. A similar trend has been reported for $CuInS_2$ sprayed films also [19,21]. Based on the observations, spray rate of 2 ml/min, that gave maximum crystallinity, was considered to be optimum.

B) Raman analysis

Compositional and structural changes are more sensitive to Raman measurements [22]. Raman analysis was carried out to confirm the phase purity of SnS:Cu films. In the Raman spectra (Figure 3.9), only the Raman shifts due to SnS:Cu (95 cm^{-1} and 224cm^{-1}) are seen. Absence of other phases like SnS_2 (at 316cm^{-1}) and Sn_2S_3 (at 237cm^{-1}) assures that the samples are pure SnS:Cu without any contamination.
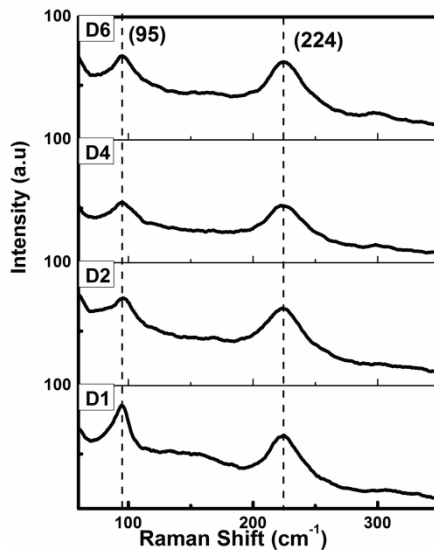
Figure 3.9 Raman analysis of D1 to D6 samples

3.2.2.2 Optical characterizations

Absorption spectra of SnS:Cu samples are shown in Figure 3.10(a). The linearity of the plots confirms direct band gap of the material. From the $(\alpha h\upsilon)^2$ versus $h\upsilon$ plot, optical band gaps of the films were also determined, and variation is shown in Figure 3.10 (b).

From the band gap versus spray rate plot, it is seen that E_g varies from 1.24 eV to 1.4 eV (D1-1.24, D2-1.35, D3-1.39, D4-1.39, D6-1.4) on varying the spray rate. Band gap of 1.3 eV was obtained for SnS:Cu thin films prepared by spraying at the rate of 2 ml/min. The absorption coefficient was found to be $> 10^4$ cm^{-1}.
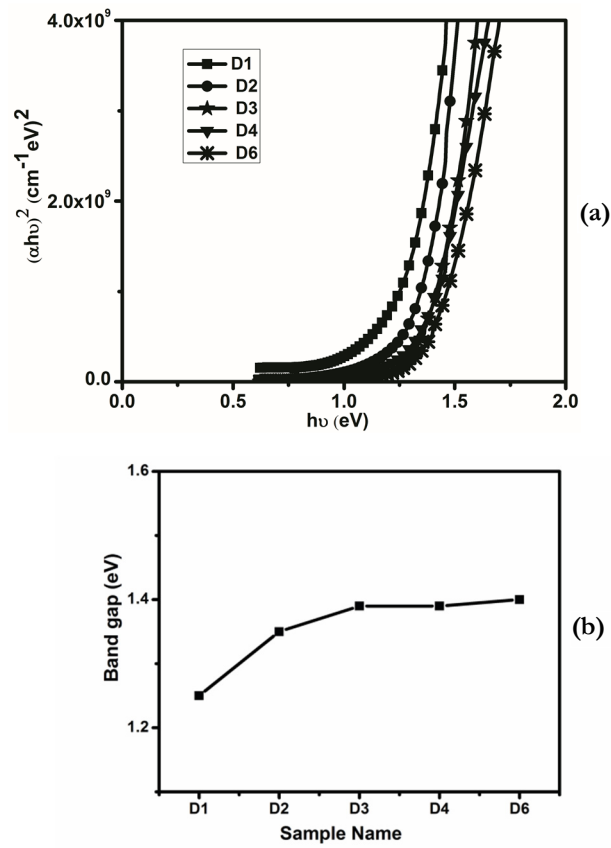
Figure 3.10 (a) $(\alpha h\nu)^2$ versus $h\nu$ plot
(b) band gap obtained for each sample

3.2.2.3 Morphological analysis

A) SEM

Topographical analysis of D2 samples were compared with that of D6 samples using SEM. (Figure 3.11). This confirmed that the entire surface of the films was free from cracks or voids. D2 sample had (the usual) "needle-like" structure of SnS:Cu whereas at 6 ml/min, it was rough "granule like" structure.
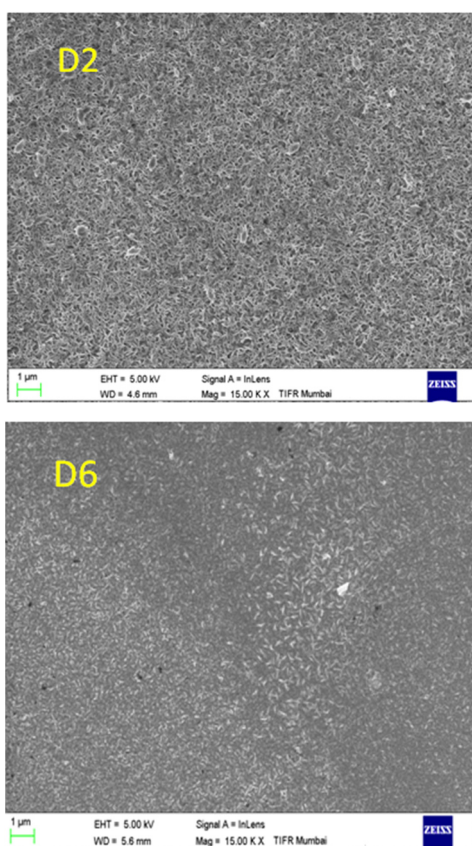
Figure 3.11 SEM of D2 and D6 film surface

B) AFM

Surface topography and roughness of all films were investigated using atomic force microscopy (Figure 3.12). All films were found to be free of pinholes and cracks. Root mean square (RMS) values of surface roughness were calculated and are tabulated in Table 3.2. Roughness of 2 ml/min sprayed samples was found to be ~30 nm.
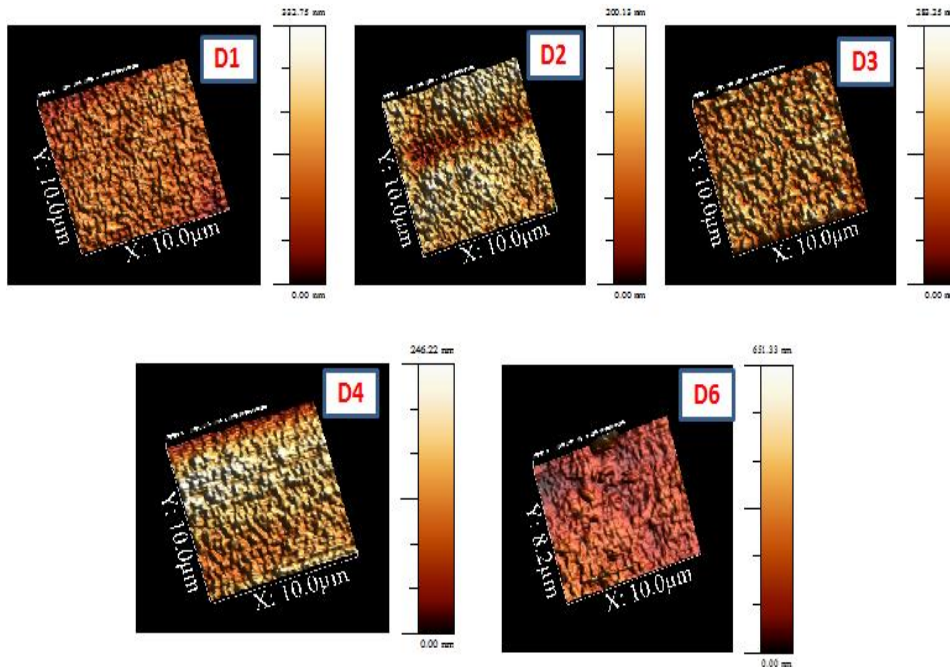
Figure 3.12 AFM image of spray rate varied samples

Table 3.2 Surface roughness of spray rate varied samples

Sample Name	RMS surface roughness (nm)
D1	28
D2	30
D3	32
D4	39
D6	54

Surface roughness increased with increase in spray rate. With higher spray rate, the probability for formation of uneven surfaces and resulting short circuits in solar cell fabrication may increase. At high spray rate, there will not be enough time for thiourea to react with atmospheric oxygen and to liberate various unwanted gases like SO_2, NO, CO_2 etc. Studies show that presence of oxygen and carbon can affect photovoltaic parameters of solar cells [23]. Hence lower spray rate is preferred; but if spray rate is very low, the time consumption will be very high to achieve a particular thickness as mentioned before. Hence depending on our requirement and deposition techniques, we have to select optimum spray rate.

3.2.2.4 Electrical studies

Electrical studies were carried out using Hall measurement for the samples and variations obtained in resistivity, carrier concentration and mobility are plotted in Figure 3.13
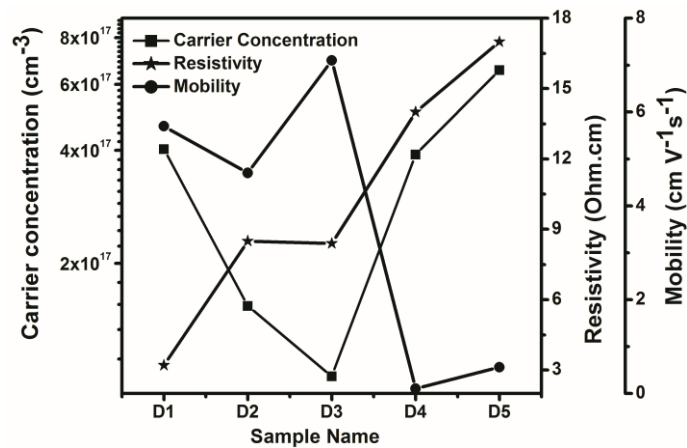
Figure 3.13 Electrical studies done on spray rate varied samples

Resistivity was minimum for 2 ml/min spray rate along with enhancement in mobility (Figure 3.13). Conductivity type for all samples was found to be n-type. Hence from the entire characterization studies, D2 sample (i.e., those prepares at 2 ml/min spray rate) was found to be optimum for further studies.

3.2.3 Cationic molarity optimization

The precursor molarity plays a major role in controlling reaction cross section of spray pyrolysed thin films, and this has a vital role in its optoelectronic properties. The molarity was chosen such that stoichiometrically uniform film could be fabricated. Low molarity will make the film non-uniform (due to less adhesion on to substrate surface), while higher value would cause the solution to precipitate making it unsuitable for spraying. In order to fabricate thin films with desired properties, optimization of precursor molarity is very essential. To determine the optimum value, copper doped SnS thin films were prepared by varying the tin molarity, keeping copper doping percentage and sulfur molarity fixed. The following section deals with interesting observations in structural, electrical and optical properties of the films obtained by varying the cationic molarity. Molarity of the tin precursor was varied keeping the doping percentage and sulfur molarity constant, as (Sn:S) 0.05:0.2, 0.075:0.2, 0.1:0.2, 0.15:0.2, 0.2:0.2 and 0.3:0.2. The substrate temperature was maintained at 375 $^{\circ}$C and spray rate at 2 ml/min. Compressed air (pressure ~1.5 bar) was used as the carrier gas. Samples were named as T(0.05), T(0.075), T(0.1), T(0.15), T(0.2) and T(0.3) respectively.

3.2.3.1 Structural analysis

A) XRD
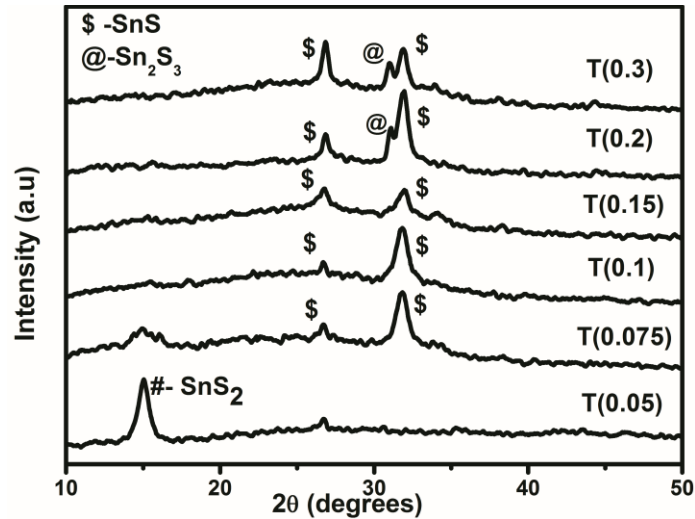
Figure 3.14 X-Ray diffractograms of T(0.05) to T(0.3) samples

XRD pattern of the samples (T(0.05) to T(0.3)) are shown in Figure 3.14. Preferential orientation was found to be along (111) plane (corresponding to 2θ value of 31.5^0) for the films that were prepared with tin molarity greater than 0.05 [JCPDS 75-0925]. For T(0.05) sample, preferential orientation was along (001) plane of SnS_2 [JCPDS-83-1705]. This might be due to very less concentration of tin in the sample. It is seen that preferential peak of (111) plane is obtained as single peak for T(0.1) film along with minor SnS (120) plane. For T (0.2) and T(0.3), there is additional peak around 31.3^0 corresponding to (210) plane of Sn_2S_3 phase [JCPDS-75-2183]. Except for the samples having very low tin molarity, all others had a prominent orientation in {111} plane. There were no peaks corresponding to the formation of Cu_xS phase.

B) Raman analysis

Raman analysis were carried out to confirm the phase purity of SnS:Cu films and the results are depicted in Figure 3.15. There were only two peaks (at 95 cm^{-1} and 224 cm^{-1}) belonging to that of SnS:Cu [24]. Raman analysis also validates the results obtained from XRD analysis.
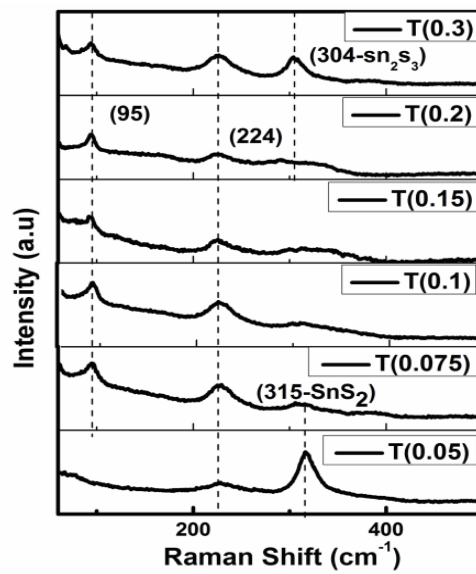
Figure 3.15 Raman analysis of T(0.05) to T(0.3) samples

Peaks of SnS$_2$ at 315 cm^{-1} and Sn$_2$S$_3$ at 304 cm^{-1} confirmed the presence of those phases at lower and higher concentrations of tin in the samples. Interestingly only T(0.1) showed pure SnS:Cu phase without any contamination.

3.2.3.2 Optical studies

Absorption spectra of SnS:Cu samples are presented in Figure 3.16. From the $(\alpha h\upsilon)^2$ versus $h\upsilon$ plot (Figure 3.16 (a)), optical band gap of the films were determined.
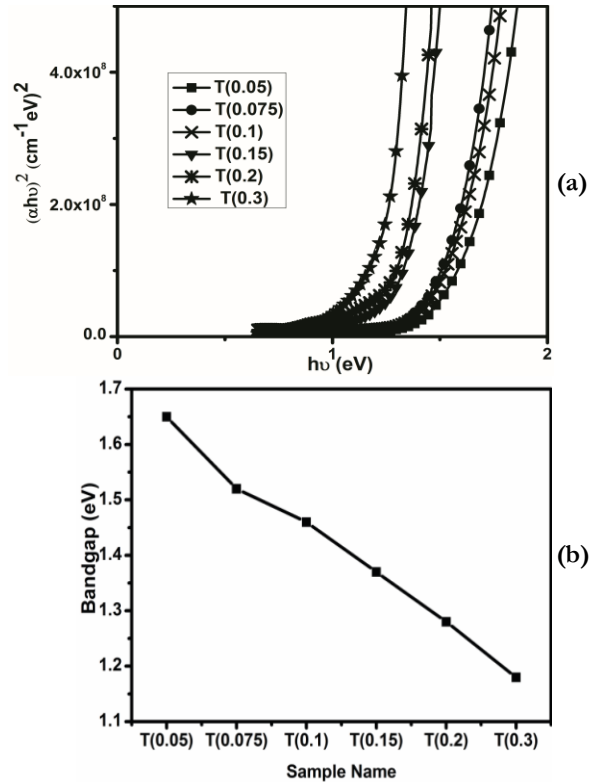
Figure 3.16 (a) $(\alpha h\nu)^2$ versus $h\nu$ plot and
(b) band gap obtained for each sample

Linearity of the plot confirmed direct band gap of the material. We can see that 'E_g' varies from 1.1 eV to 1.6 eV on varying tin molarity (Figure 3.16 (b)). For higher concentration of tin, band gap is decreasing (due to formation of Sn_2S_3) and for a lower concentration of tin, the band gap is increasing (due to the formation of SnS_2). It is already reported that presence of other phases can affect the band gap values [25]. The optimal band gap of 1.4 eV is obtained for T (0.1) SnS:Cu thin film which had absorption coefficient $> 10^4$ cm^{-1}.

3.2.3.3 Morphological characterization and thickness variation

SEM images for lower, middle and higher tin molarities were recorded and are shown in Figure 3.17. For lower molarity samples, spherical 'granule like' structure was seen that might be due to the presence of mixed phases of SnS_2 (Figure 3.17 (a)). For sample T(0.1), usual 'needle-like' structure of SnS:Cu was obtained (Figure 3.17 (b)). It is clear from XRD and Raman analysis that sample T(0.1) has phase pure SnS:Cu formation without mixed and/or impurity phases. Finally for higher molarity, (Figure 3.17 (c)) the sample was found to have 'rod like' structure.

(a)

(b)

(c)
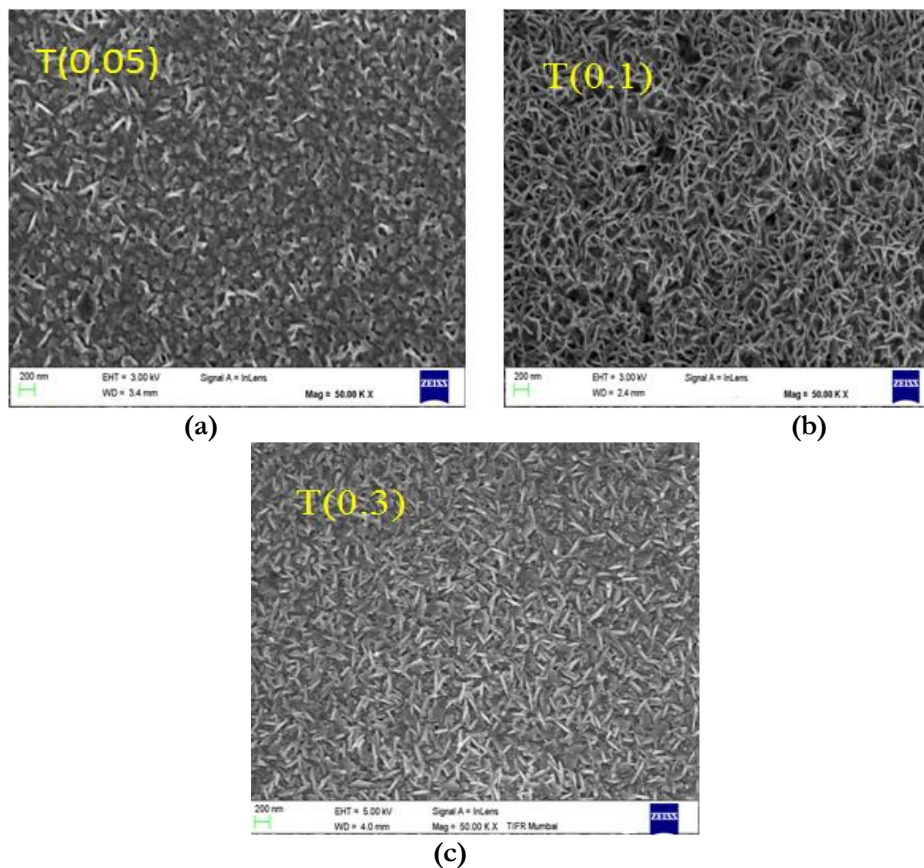
Figure 3.17 SEM image of **(a)** T(0.05) **(b)** T(0.1) **(c)** T(0.3)

Thickness of each sample was measured, and its variation is plotted in Figure 3.18. It was found that the thickness increased with increase in tin molarity.
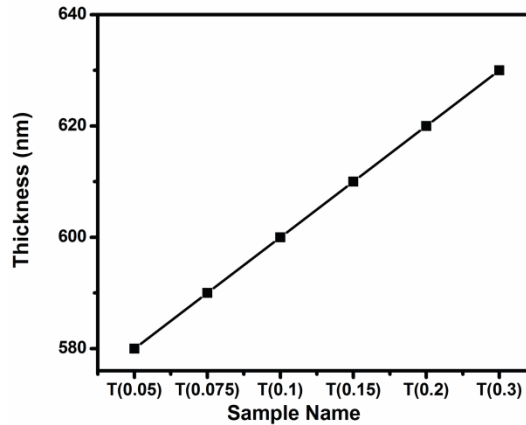
Figure 3.18 Thickness variation of T(0.05) to T(0.3) samples

3.2.3.4 Electrical characterizations

Electrical characterization was done using Hall measurement and the results obtained are shown in Figure 3.19. Resistivity was minimum for T(0.1) sample. Variations in the electrical properties might be due to the presence of mixed phases of SnS_2, Sn_2S_3 and/or due to variation of tin concentration in the samples. All the samples showed n-type nature irrespective of tin molarity.

Similar electrical nature was shown by other materials also with precursor molarity variation. The initial decrease in resistivity with an increase in precursor molarity might be caused by a decrease in trapping states due to the increase in grain size. With further increase in molarity, the resistivity increases. This may be explained as due to

immobilization of free charge carriers possibly due to the incomplete atomic bonding at grain boundaries that act as trap centers for charge carriers [26].
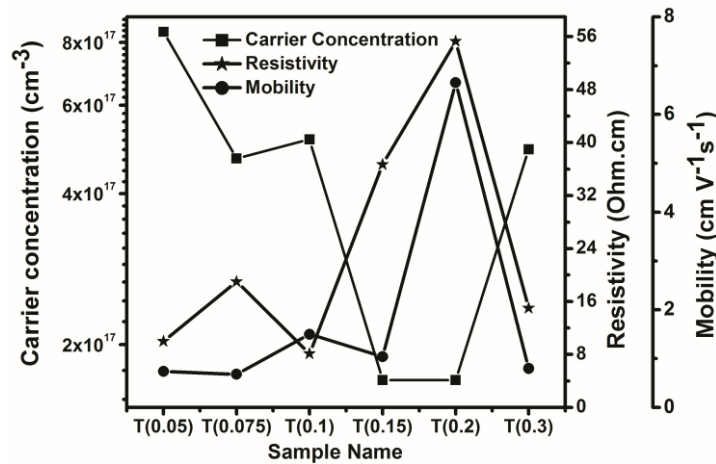
Figure 3.19 Electrical properties of T(0.05) to T(0.2) samples

The above study of varying cationic precursor molarity in sprayed SnS:Cu thin films, points out that films with molarity ratio 0.1:0.2 (i.e., T(0.1) sample), is observed to have low resistivity ~ 8 ohm.cm and band gap value of 1.4 eV.

3.2.4 Anionic molarity optimization

From the above studies, we found that better molarity of cationic precursor is 0.1 M. Now, as the next step, anionic molarity was varied, keeping cationic molarity fixed. Due to easy re-evaporation of sulfur, we compensated it by modifying the ratio of composition of n-type SnS:Cu thin films. This is supported by earlier reports that even if the starting solution is sulfur-rich, sulfur will not get incorporated into films

proportionately and hence will not improve the material properties [27]. The compound formation with desired properties mainly depends in cationic to anionic precursor ratio and hence in this section; we report results of studies on those films prepared by varying sulfur molarity while keeping percentage of copper doping and tin molarity constants. Molarity of sulfur was varied from 0.1M to 0.4 M keeping the ratio of Sn:S as 0.1:0.1, 0.1:0.2, 0.1:0.3 and 0.1:0.4 and the samples were named as S(0.1), S(0.2), S(0.3) and S(0.4) respectively. The corresponding changes in structural, electrical and optical properties of these films were studied.

3.2.4.1 Structural analysis

A) XRD

Variations in crystallinity and phase formation were, analyzed using XRD.

Figure 3.20 shows the XRD pattern of the films (S(0.1) to S(0.4)). Despite the sulfur variation, all the samples were having preferential orientation along (111) plane (corresponding to 2θ value of 31.5^0) and along (120) plane (corresponding to 2θ value of 26.0^0) of SnS [JCPDS 75-0925]. At very high Sulfur concentration, (i.e., for S(0.4) sample), SnS_2 (001) plane is observed which can be argued to be due to less tin concentration in the sample [JCPDS 23-0677].
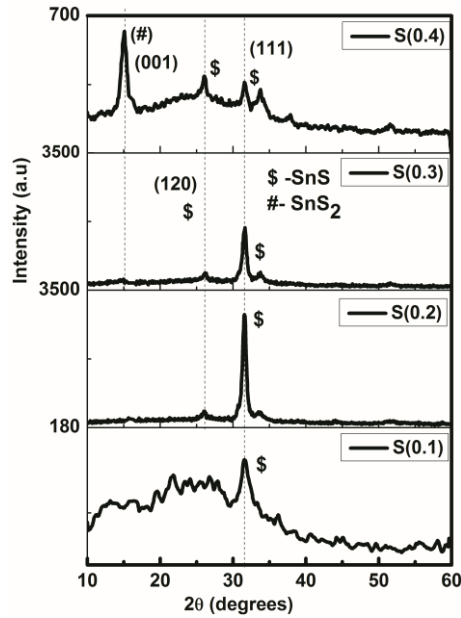
Figure 3.20 XRD pattern obtained for samples S(0.1) to S(0.4)

Absence of Sn_2S_3 in the XRD might be due to its low concentration. Maximum intensity for peak corresponding to (111) plane was obtained for S(0.2) film. Interestingly no peaks corresponding to the formation of Cu_xS phase was obtained even in samples with higher concentration of sulfur.

B) Raman analysis

The Raman shifts obtained for sulfur varied samples are represented in Figure 3.21. Phase purity of the samples was further confirmed through Raman analysis. The peaks at 95 cm^{-1} and 224 cm^{-1} belong to that of SnS:Cu [24]. The SnS_2 peak at 315 cm^{-1} and Sn_2S_3 peak at 304 cm^{-1} confirm their presence in the samples prepared with higher and lower

concentration of sulfur respectively. It is worth mentioning here that only S(0.2) sample showed pure SnS:Cu phase without any mixed phase. Interestingly both XRD and Raman analysis obtained here showed exactly opposite nature to that was observed for cationic molarity variations
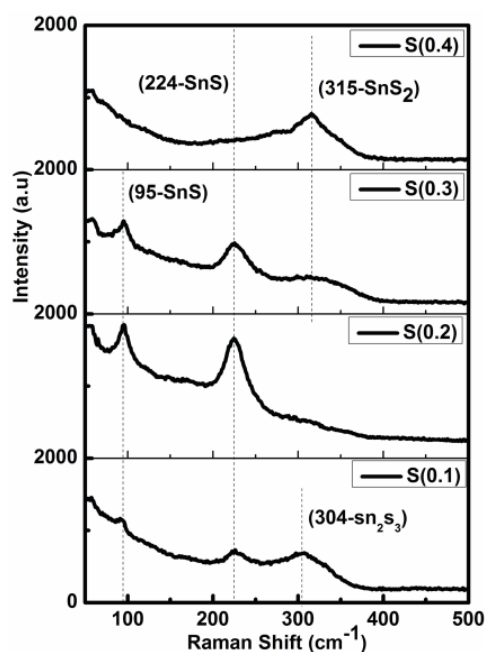
Figure 3.21 Raman shifts obtained for samples S(0.1) to S(0.4)

3.2.4.2 Optical studies

Figure 3.22 (a) depicts absorption spectr, and Figure 3.22 (b) depicts band gap variation.
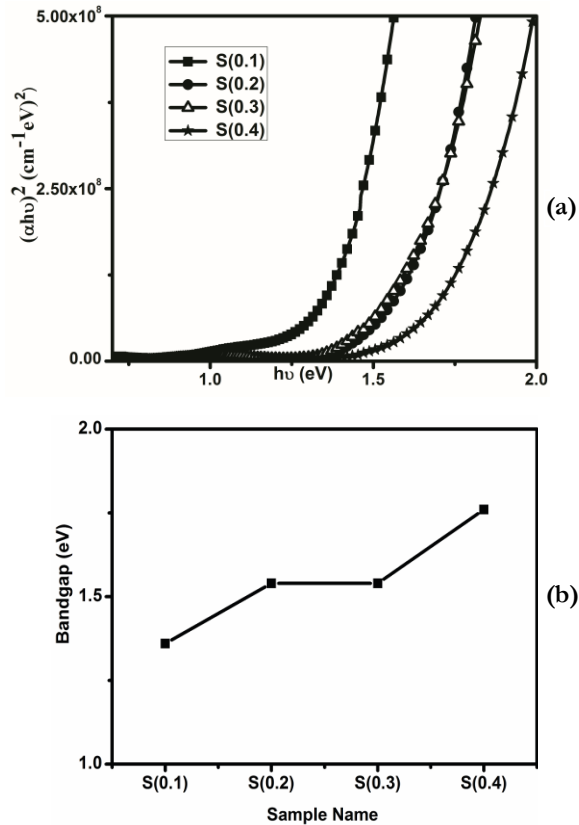
Figure 3.22 **(a)** $(\alpha h\nu)^2$ versus $h\nu$ plot and **(b)** band gap obtained for samples S(0.1) to S(0.4)

Optical band gap was determined from $(\alpha h\nu)^2$ versus $h\nu$ plot. It is clear that E_g varies from 1.3 eV to 1.7eV with increase in sulfur molarity and variation in band gap obtained here is exactly opposite to that of cationic variation. For lower concentration of sulfur, band gap was found to be decreasing due to the presence of Sn_2S_3, and for higher concentration of sulfur it increased due to the formation of SnS_2. Band gap of 1.54 eV was obtained for S(0.2) and S(0.3) samples. Absorption coefficient was found to be $> 10^4$ cm^{-1}.

3.2.4.3 SEM analysis

SEM image of S(0.2) and S(0.4) samples were compared and is shown in Figure 3.23.

(a)   **(b)**
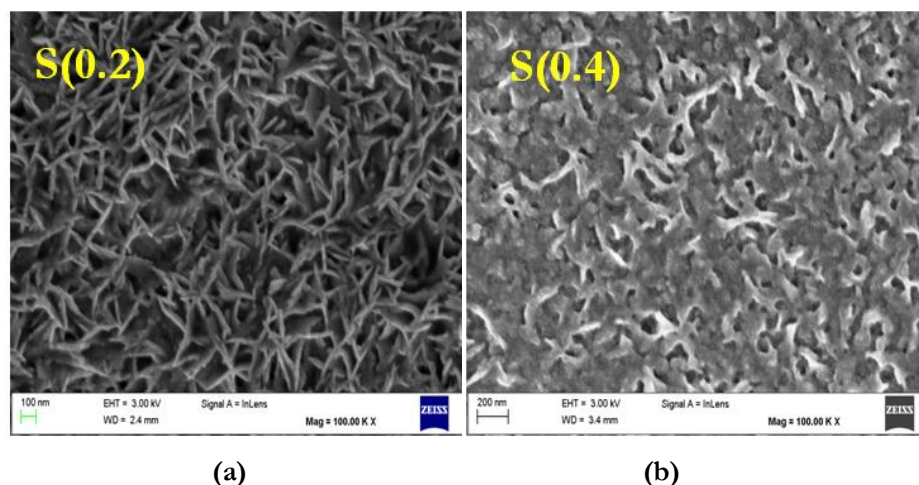
Figure 3.23 SEM image of **(a)** S(0.2) **(b)** S(0.4)

It is seen that with an increase in sulfur concentration, the morphology changes from the usual needle-like' structure of SnS:Cu to a fused structure.

3.2.4.4 Electrical studies

Resistivity of the samples is found to decrease initially and then to increase with increase in sulfur molarity. Presence of other phases like SnS_2 and Sn_2S_3 depending on sulfur concentration might be the reason for this variation. Nature for all the films was confirmed to be n-type using Hall technique. Electrical characterization confirmed that S(0.2) sample had minimum resistivity with enhanced mobility and carrier

concentration. Carrier concentration, resistivity and mobility obtained for sulfur varied samples are shown in Figure 3.24.
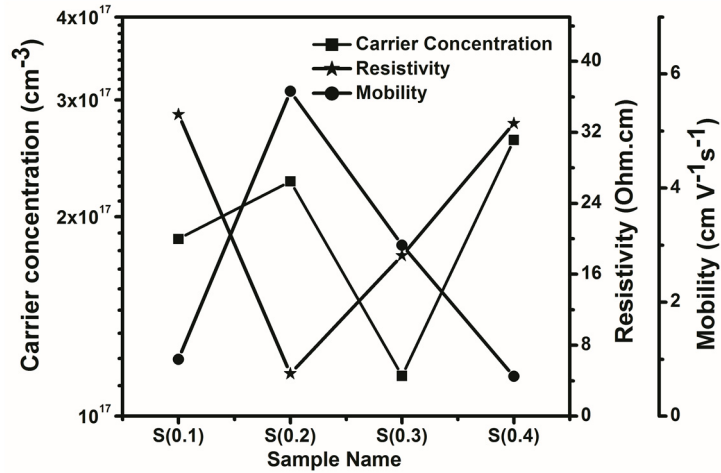
Figure 3.24 Electrical parameters obtained for samples S(0.1) to S(0.4)

3.3 Conclusion

In this chapter, all the deposition parameters were optimized in order to obtain good stoichiometric SnS:Cu films. Related literature suggests the need for systematic study on various deposition parameters like substrate temperature, spray rate, cationic molarity, anionic molarity etc. that can highly influence conductivity and other properties of the material. Hence the effect of each parameter on the properties of SnS:Cu thin films was investigated systematically. It was seen that substrate temperature is a crucial parameter in spray pyrolysis, and for each material, there is a characteristic temperature at which good quality films can be obtained. Below and above that particular temperature, deposited film contains secondary phases that adversely affect film properties.

Similarly, if spray rate is very low, higher deposition time is required for obtaining films with required thickness, and if the spray rate is very high, surface temperature of the substrate decreases and surface roughness increases, due to the lack of time to complete reaction before the arrival of subsequent layers of coating. Finally, cationic to anionic ratio was optimized as 1:2 with molarity of tin and sulfur to be 0.1 M and 0.2 M respectively. To obtain this ratio and molarity, rather than sticking to just either cationic or anionic molarity variation alone, we tried varying systematically both tin and sulfur molarities keeping the other molarity and parameters fixed. SnS:Cu thin films (ratio Sn:S = 1:2 with 4 % Cu doping) prepared considering all the above optimized deposition conditions were found to be suitable for device fabrication due to its optimum direct band gap (~1.4 eV) and very high absorption coefficient with competitively low resistivity (ohms range).

References

[1] John, Teny Theresa, S. Bini, Y. Kashiwaba, T. Abe, Y. Yasuhiro, C. Sudha Kartha, and K. P. Vijayakumar. "Characterization of spray pyrolysed indium sulfide thin films." *Semiconductor Science and Technology* 18, no. 6 (2003): 491.

[2] Patil, Pramod S. "Versatility of chemical spray pyrolysis technique." *Materials Chemistry and physics* 59.3 (1999): 185-198.

[3] Thangaraju, B., and P. Kaliannan. "Spray pyrolytic deposition and characterization of SnS and SnS$_2$ thin films." *Journal of Physics D: Applied Physics* 33.9 (2000): 1054.

[4]   Reddy, N. Koteeswara, and KT Ramakrishna Reddy. "Electrical properties of spray pyrolytic tin sulfide films." *Solid-state electronics* 49.6 (2005): 902-906.

[5]   Reddy, N. Koteeswara, and KT Ramakrishna Reddy. "Preparation and characterisation of sprayed tin sulphide films grown at different precursor concentrations." *Materials chemistry and physics* 102.1 (2007): 13-18.

[6]   Sajeesh, T. H., Anita R. Warrier, C. Sudha Kartha, and K. P. Vijayakumar. "Optimization of parameters of chemical spray pyrolysis technique to get n and p-type layers of SnS." *Thin Solid Films* 518, no. 15 (2010): 4370-4374.

[7]   Andrade-Arvizu, Jacob A., M. F. García-Sánchez, M. Courel-Piedrahita, F. Pulgarín-Agudelo, E. Santiago-Jaimes, E. Valencia-Resendiz, A. Arce-Plaza, and O. Vigil-Galán. "Suited growth parameters inducing type of conductivity conversions on chemical spray pyrolysis synthesized SnS thin films." *Journal of analytical and applied pyrolysis* 121 (2016): 347-359.

[8]   Mooney, John B., and Shirley B. Radding. "Spray pyrolysis processing." *Annual review of materials science* 12.1 (1982): 81-101.

[9]   Demian, S. E. "Optical and electrical properties of transparent conducting ZnO films prepared by spray pyrolysis." *Journal of Materials Science: Materials in Electronics* 5.6 (1994): 360-363.

[10]   Chopra, Kasturi. *Thin film device applications*. Springer Science & Business Media, 2012.

[11]   Nair, P. K., M. T. S. Nair, J. Campos, and A. Sanchez. "SnS/ SnO$_2$ conversion of chemically deposited SnS thin films." *Advanced Materials for Optics and Electronics* 1, no. 3 (1992): 117-121.

[12] Stelzer, N. H. J., and J. Schoonman. "Synthesis of terbia-doped yttria-stabilized zirconia thin films by electrostatic spray deposition (ESD)." *Journal of Materials Synthesis and Processing* 4 (1996): 429-438.

[13] Reddy, N. Koteeswara. "Growth-temperature dependent physical properties of SnS nanocrystalline thin films." *ECS Journal of Solid State Science and Technology* 2.6 (2013): P259-P263.

[14] Sebastian, Tina, Manju Gopinath, C. Sudha Kartha, K. P. Vijayakumar, T. Abe, and Y. Kashiwaba. "Role of substrate temperature in controlling properties of sprayed CuInS2 absorbers." *Solar Energy* 83, no. 9 (2009): 1683-1688.

[15] Su, Huilan, Yi Xie, Yujie Xiong, Peng Gao, and Yitai Qian. "Preparation and morphology control of rod-like nanocrystalline tin sulfides via a simple ethanol thermal route." *Journal of Solid State Chemistry* 161, no. 2 (2001): 190-196.

[16] Khadraoui, M., N. Benramdane, C. Mathieu, A. Bouzidi, R. Miloua, Z. Kebbab, K. Sahraoui, and Rachel Desfeux. "Optical and electrical properties of Sn2S3 thin films grown by spray pyrolysis." *Solid State Communications* 150, no. 5-6 (2010): 297-300.

[17] Reddy, N. Koteeswara, and KT Ramakrishna Reddy. "SnS films for photovoltaic applications: Physical investigations on sprayed SnxSy films." *Physica B: Condensed Matter* 368.1-4 (2005): 25-31.

[18] Sanchez-Juarez, A., and A. Ortiz. "Effects of precursor concentration on the optical and electrical properties of Sn_XS_Y thin films prepared by plasma-enhanced chemical vapour deposition." *Semiconductor science and technology* 17.9 (2002): 931.

[19] Sebastian, Tina, R. Jayakrishnan, C. Sudha Kartha, and K. P Vijayakumar. "Characterization of spray pyrolysed CuInS2 thin films." *The Open Surface Science Journal* 1, no. 1 (2009).

[20] Kriisa, Merike, Malle Krunks, Erki Kärber, Mart Kukk, Valdek Mikli, and Arvo Mere. "Effect of solution spray rate on the properties of chemically sprayed ZnO: In thin films." *Journal of Nanomaterials* 2013 (2013): 3.

[21] Rajeshmon.V.G, PhD. Thesis, Cochin University of Science and Technology, India (2013).

[22] Rondahl, Stina Holmgren, Fabien Pointurier, Linnea Ahlinder, Henrik Ramebäck, Olivier Marie, Brice Ravat, François Delaunay et al. "Comparing results of X-ray diffraction, μ-Raman spectroscopy and neutron diffraction when identifying chemical phases in seized nuclear material, during a comparative nuclear forensics exercise." *Journal of radioanalytical and nuclear chemistry* 315, no. 2 (2018): 395-408.

[23] Ryo, Toshihiro, Duy-Cuong Nguyen, Motohito Nakagiri, Noriaki Toyoda, Hiroaki Matsuyoshi, and Seigo Ito. "Characterization of superstrate type CuInS2 solar cells deposited by spray pyrolysis method." *Thin Solid Films* 519, no. 21 (2011): 7184-7188.

[24] Sajeesh T.H, PhD Thesis, Cochin University of Science and Technology, India (2012).

[25] Chaki, Sunil H., Mahesh D. Chaudhary, and M. P. Deshpande. "SnS thin films deposited by chemical bath deposition, dip coating and SILAR techniques." *Journal of Semiconductors* 37.5 (2016): 053001.

[26] Prathap, Pathi, YP Venkata Subbaiah, KT Ramakrishna Reddy, and R. W. Miles. "Influence of growth rate on microstructure and optoelectronic behaviour of ZnS films." *Journal of Physics D: Applied Physics* 40, no. 17 (2007): 5275.

[27] Tina Sebastian, PhD. Thesis, Cochin University of Science and Technology, India (2009).

Chapter **4**

ENGINEERING STRUCTURAL AND OPTO-ELECTRONIC PROPERTIES OF SnS:Cu FILMS

4.1 Introduction

In previous chapters, successful deposition of n-type SnS:Cu thin films and optimization of various deposition parameters were explained. Here in this chapter, effect due to post deposition treatments are analyzed to further improve properties of these prepared films. To the best of our knowledge, no groups have reported these studies on n-type SnS. The material stability with various parameters and its ability to retain material properties over long periods were also checked.

4.2 Optimization of volume of precursor solvent

This section details the need to confirm the quantity of precursor solvent (HCl) required for good quality films. As mentioned in 2nd chapter, $SnCl_2$ precursor solution was prepared by employing 'two-step' process: the salt is dissolved in HCl initially, and then it was diluted using deionized water. Final volume of the prepared precursor solution was kept fixed as 30 ml. To find optimal value of HCl quantity required after copper doping, $SnCl_2$ salt was dissolved in 11.32 M (35 % assay) HCl, whose volumes were varied from 2 ml to 15 ml. The volume was made up to 30 ml by adding the remaining with de-ionised water. These samples were named as A2, A5, A10, A15 respectively. Thin film

samples were deposited using CSP technique as explained in 3rd chapter and samples were kept for 10 minutes over heater at deposition temperature before removing it from the heater.

4.2.1 Structural characterizations

A)   XRD

Crystal structure of fabricated SnS:Cu thin films was confirmed from XRD analysis (Figure 4.1) and phase purity of the samples was confirmed from Raman analysis. It is clear that as HCl concentration increases, there is a change in predominant orientation from (111) plane (that corresponds to 2θ value of 31.5°) to (002) plane (with 2θ value 15.84°) (JCPDS: 75-0925). No peaks corresponding to formation of Cu_xS phase are seen with increase in HCl concentration. For PV applications, the (111) orientation is generally preferred for SnS thin films [1,4].
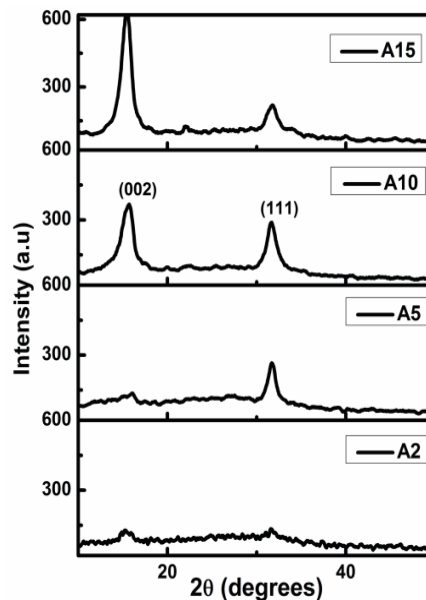
Figure 4.1 XRD pattern for A2 to A15 samples

Using Scherrer's formula, $D = 0.9 \lambda / \beta \cos \theta$, where D is the average grain size, λ is the X-ray wavelength, β is the full-width at half-maximum (FWHM) of XRD peaks, and θ is the Bragg angle, grain size of the films were calculated [5]. The average grain size was found to be around 12 nm. Number of grains per unit area (N) was calculated using the equation $N = t/D^3$ (per unit area) where 't' is the film thickness, and 'D' is the grain size [5]. It is found to be around 3.7×10^{13} (per cm^2).

B) Raman analysis

Phase purity of the film was determined from Raman analysis using exciting radiation of 632.8 nm and is presented in Figure 4.2. Raman peaks observed at 95 cm^{-1} and 224 cm^{-1} are characteristic to SnS thin films [6,7] and absence of peaks corresponding to other phases like SnS_2 (at 315 cm^{-1}, 215 cm^{-1}) and Sn_2S_3 (at 307 cm^{-1}, 251 cm^{-1}) confirms formation of pure SnS:Cu without any contamination [8,9].
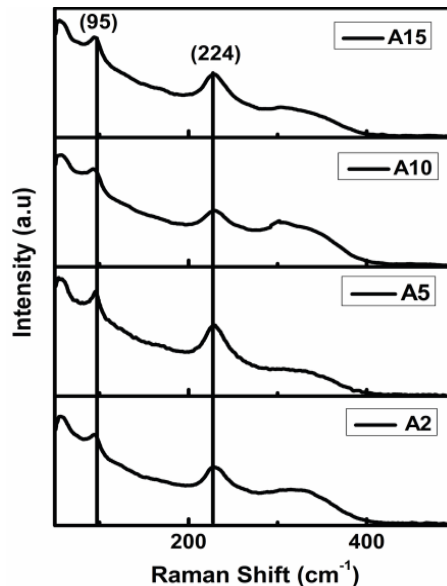
Figure 4.2 Raman pattern for A2 to A15 samples

4.2.2 Optical characterizations

A)   Evaluation of band gap

Absorption measurements were taken in wavelength range 190–2500 nm in order to evaluate the band gap. Figure 4.3 shows $\alpha h\nu^2$ against energy ($h\nu$) from which band gap was determined [10]. Optical band gaps (which are direct) exhibited a decrease in its value from 1.43 eV to 1.34 eV as HCl concentration was increased.
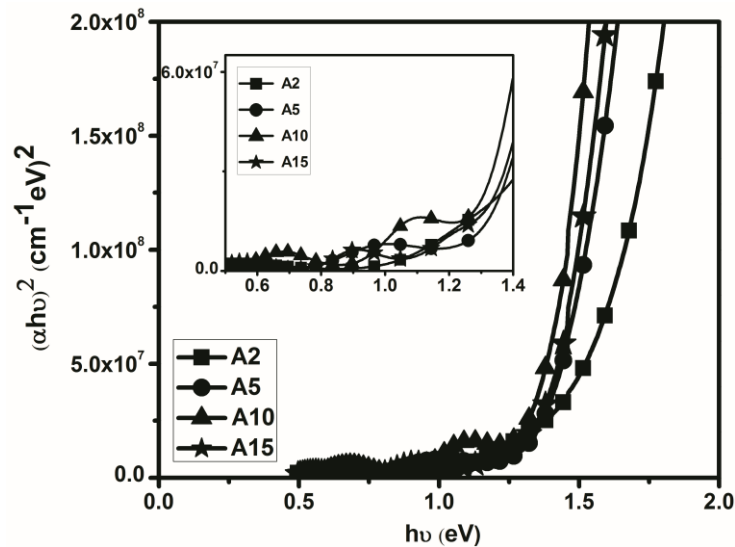
Figure 4.3 $(\alpha h\nu)^2$ versus $h\nu$ plot of A2 to A15

The inset in Figure 4.3 shows the $(\alpha h\nu)^2$ versus $h\nu$ plot of all the samples in energy region from 0.5 eV to 1.4 eV. Here peaks are present below the band gap region and the peak position varies with respect to HCl volume. The presence of this sub-band gap is negligible in the case of A5 and almost absent for A2.

Figure 4.4 presents transmittance spectra in the wavelength range 300 to 2500 nm. The fringes obtained confirm uniformity of prepared films.
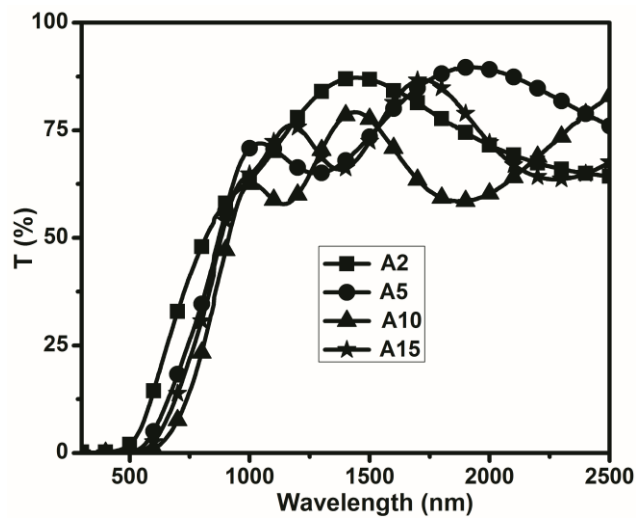
Figure 4.4 Transmittance spectra obtained for A2 to A15 samples

4.2.3 Electrical studies

Electrical properties such as carrier concentration, resistivity and mobility were investigated through Hall measurement (Figure 4.5). initially, resistivity falls rapidly and then increases slightly with an increase in concentration of HCl from sample A5 onwards. The minimum resistivity is obtained for samples prepared with 5 ml of HCl. All samples retained the n-type polarity.
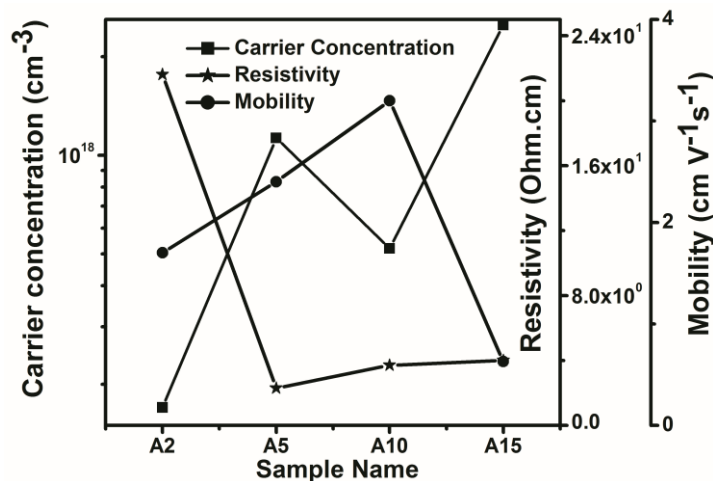
Figure 4.5 Results of electrical measurements on samples A2 to A15

Hence from the above characterization studies, it is clear that even with doping, optimum quantity of precursor solvent required is same as 5 ml. Since A5 sample was found to have highest conductivity with good structural (XRD peak along (111) plane) and optical properties (band gap value of 1.34 eV), the same was used for further investigations. Surface morphology, chemical bonding state and composition of A5 sample was studied using AFM , SEM and XPS.

4.2.4 Morphological and compositional analysis

Surface morphology of A5 sample is studied using AFM and SEM techniques and the images are represented in Figure 4.6 (a) and 4.6 (b) respectively. Both images confirm uniformity of the sample, which again validates the data obtained from transmission spectra.
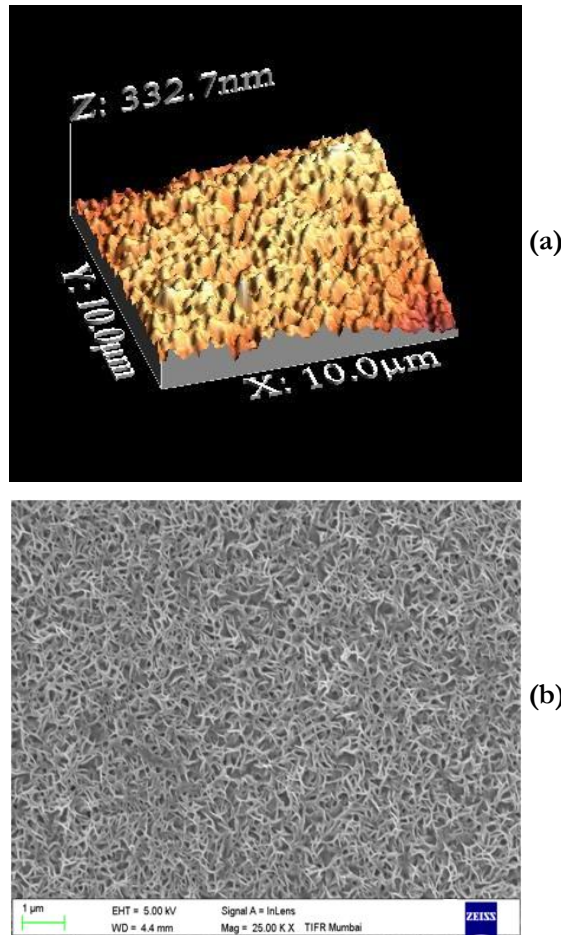
Figure 4.6 (a) and (b) Morphological analysis done
on A5 sample using AFM and SEM

The sample is adherent to substrate surface with uniform "needle-like or wormlike" crack-free surface nature, which is quite natural for SnS films and is devoid of any pinholes [11]. The grains were of more or less same size, uniformly covering the entire substrate surface. The RMS value of surface roughness was found to be ~ 40 nm.

Compositional analysis of this sample was carried out using XPS technique. In order to confirmthe compound formation of SnS, we calculated Binding Energy (B.E) from the spectra obtained using XPS (Figure 4.7).
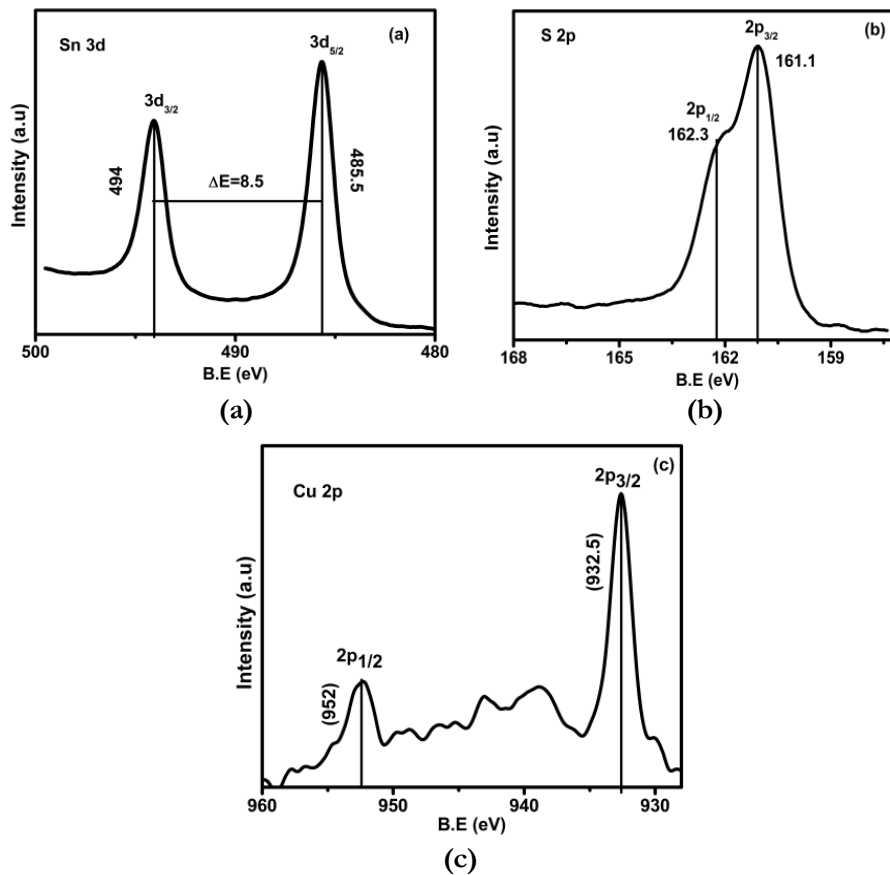
Figure 4.7 The narrow scan XPS spectra for Sn, S and Cu respectively

In the case of tin, peaks of Sn3d$_{3/2}$ and Sn3d$_{5/2}$ are obtained at 494 eV and 485.5 eV respectively and for sulfur S2p$_{3/2}$ and 2p$_{1/2}$ peak are obtained at 161.1 eV and 162.3 eV respectively [12]. For copper, the

binding energies at 952 eV and 932.5 eV correspond to that of $Cu2p_{1/2}$ and $Cu2p_{3/2}$ respectively and are due to the presence of Cu^{2+} [13,14]. Presence of peaks at 485.5 eV for $Sn3d_{5/2}$ and 161.1 eV for $S2p_{3/2}$ confirm formation of Sn^{+2} and S^{-2} in SnS. Absence of Sn^{+4} peak at 486.3 eV confirms that the SnS sample is phase pure [12]. Atomic concentration of each element is also calculated (Sn-53.4%, S-30.4%, Cu-3.48% and O-12.72%). Hence it becomes clear that n-type polarity for SnS:Cu is due to excess tin concentration that has been observed by other researchers as well [11,15,16]. From all these studies, we fixed the solvent quantity required for SnS:Cu preparation as 5 ml.

4.3 Effect on post-deposition annealing

Even though we could deposit SnS:Cu thin films via cost-effective method without any other impurity phase, it is important to check whether any further improvement in properties of deposited films can be achieved by employing anypost-deposition treatments. Variouspost-deposition treatments such as vacuum annealing, air annealing, varying annealing time, inversion etc. can modify the material properties due to recrystallization of the amorphous and/or unreacted portions of the film [17-21]. It can also reorient the existing crystallites and can help in Chemisorption (Oxygen desorption at grain boundaries). In order to exploit these effects, an initial trial is done. For this, the prepared films were annealed in vacuum as well as in air at 125 ^{o}C for 90 minutes (possible temperature that can be attained with our present vacuum heating setup) and were compared with unannealed samples.

4.3.1 Effect due to vacuum and air annealing

Three sets of SnS:Cu samples were prepared with the above-mentioned conditions. One set of samples was taken from heater soon after deposition and was named as "unannealed (U.A)". Of the other two sets of samples, one set was transferred immediately to the vacuum chamber and was annealed at 125 ^{o}C for 90 minutes, and the other set was air annealed by transferring it to a heater maintained at same temperature and time as that of vacuum annealing. These samples were named as "vacuum annealed (V.A)" and "air annealed (A.A)" respectively. Then the changes in structural, morphological, optical and electrical properties of annealed samples were compared with those of the unannealed samples (U.A).

4.3.1.1 Structural analysis

A)   XRD

X-ray diffractograms of U.A, A.A and V.A films are depicted in Figure 4.8. Among these, U.A samples were found to be amorphous and for air and vacuum annealed samples, their characteristic peaks appeared with considerable enhancement in intensity. Peaks at 2θ value 15.84, 21.9°, 27.4°, 31.5°, 39° and 44.7° correspond to (002), (011), (102), (111), (113) and (114) planes of orthorhombic SnS (JCPDS:75-0925).
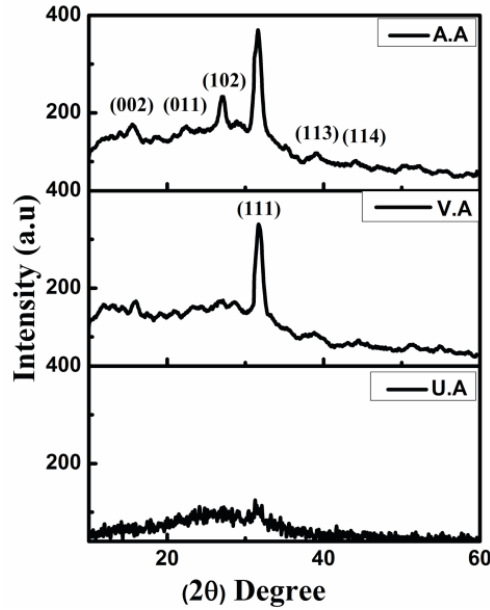
Figure 4.8 X-Ray Diffractograms of A.A, V.A and
U.A SnS:Cu thin films

The weak (102) plane observed at 2θ value 27.3° is reoriented on vacuum annealing along with enhancement of (111) plane, confirming reorientation of grains in the film. Mean grain size was calculated for V.A and A.A samples using Scherrer's formula and found to be 15 nm and 10 nm respectively. Number of grains per unit area (N) is also calculated and found to be around $2*10^{13}$ (per cm^2) on vacuum annealing and $8*10^{13}$ (per cm^2) on air annealing indicating that vacuum annealing can better orient the grains of SnS:Cu film along (111) plane.

B)   Raman analysis

In order to confirm phase purity of SnS:Cu, room temperature Raman spectra of the films were recorded using exciting radiation of 632.8 nm and is shown in Figure 4.9.
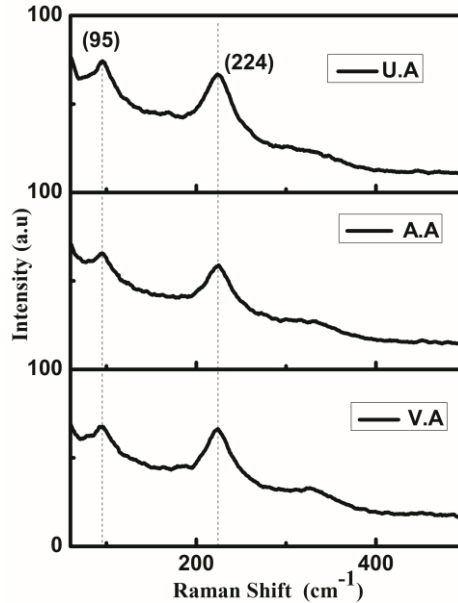
Figure 4.9 Raman analysis of U.A, A.A and V.A SnS:Cu thin films

Two Raman peaks were clearly observed (at 95 cm^{-1} and 224 cm^{-1}) for all the annealed and unannealed SnS:Cu samples. Even though in XRD U.A sample was amorphous, here Raman shifts of SnS:Cu was obtained. This is because Raman analysis can detect chemical phases present even in its amorphous state. Absence of other phases like SnS_2 at 315 cm^{-1} and Sn_2S_3 at 307 cm^{-1}, 251 cm^{-1} confirm that the formation is pure SnS:Cu [8].

4.3.1.2 Optical studies

For studying optical properties of SnS:Cu thin films, absorption measurements of U.A, A.A and V.A were recorded in the wavelength range of 190–2500 nm. Optical band gap of all the thin films were

estimated by extrapolating the linear region in the plot of $(\alpha h\nu)^2$ against energy $(h\nu)$ (Figure 4.10).
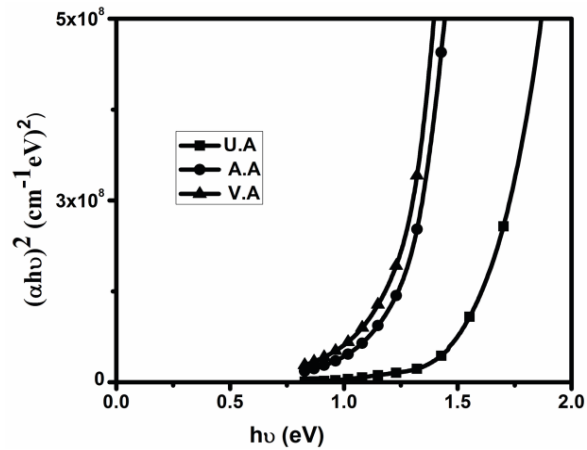
Figure 4.10 $(\alpha h\nu)^2$ versus $(h\nu)$ graph of U.A, A.A and V.A SnS:Cu thin film

There was a reduction in band gap value on annealing due to improvement of crystallinity [22]. It is found that unannealed SnS:Cu has a band gap of 1.5 eV which decreased to 1.3 eV on air annealing and to 1.2 eV on vacuum annealing. The required band gap around 1.3 eV is thus obtained by air annealing. Here also no sub-band gap is observed for samples.

4.3.1.3 AFM

Surface topography and roughness of the U.A, A.A and V.A films were investigated using atomic force microscopy (AFM) which is shown in Figure 4.11.
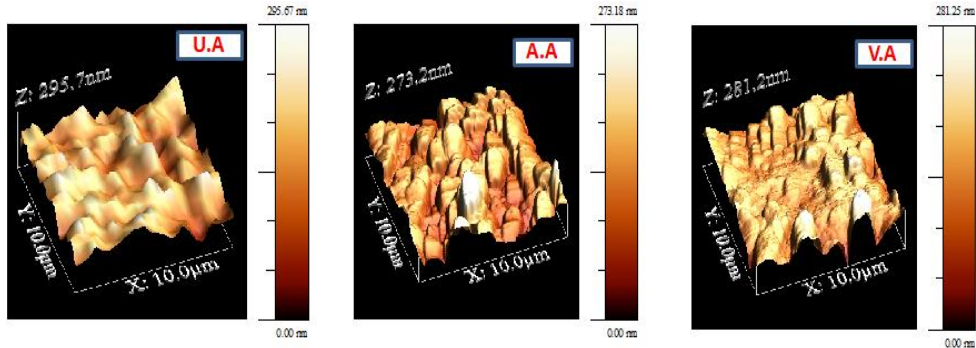
Figure 4.11 AFM analysis of U.A, A.A and V.A SnS:Cu thin film

All films were found to be free of pinholes and cracks. Root mean square (RMS) values of surface roughness of U.A samples were around 43 nm while that of A.A and U.A samples were found to be 38 nm and 30 nm, respectively.

4.3.1.4 Electrical studies

Electrical studies on both unannealed and annealed samples were carried out using Hall measurements and the results obtained are tabulated in Table 4.1. There is a reduction in resistivity with annealing when compared to unannealed samples, but there is no appreciable change in resistivity between air annealed and vacuum annealed samples. Though all SnS:Cu films exhibited n-type behaviour, mobility of air annealed samples was found to be enhanced.

Table 4.1 Electrical measurements done on U.A, A.A and V.A samples

Sample Name	Carrier Concentration ($/cm^3$) $10*^{17}$	Resistivity (ohm.cm)	Mobility ($cm^2/V.s$)
U.A	4.6	12	1.05
A.A	7	2.3	3.90
V.A	42	1.1	1.30

On comparing properties, air annealed samples have near optimum energy conversion band gap of 1.3 eV and enhanced (111) plan, which is considered to be beneficial for device fabrication. The post deposition annealing at deposition temperature can assure complete pyrolytic reduction over the sample after deposition. Hence as next step, a trial was done by increasing annealing temperature to 375 °C, which is the deposition temperature optimized for the present study. Because of the difficulty to attain annealing temperature ~ 375 °C in vacuum and also from the "point of view", of reduction of energy consumption during sample fabrication process, we used an alternate method to attain the same goal. We had developed another method viz., "inversion technique" that can improve the material properties comparable to vacuum annealing [17, 23] through an easier process. Hence we decided to try the "inversion technique" on the air-annealed samples that were heated for an optimized time period at the deposition temperature.

4.3.2 Optimization of annealing time

Post-deposition annealing at deposition temperature can assure complete pyrolytic reduction over the sample after deposition, only if we could optimize the post-deposition annealing time. Because longer annealing time can result in either formation of other phases (by reacting with the elements present in the atmosphere) or re-evaporation of material elements [24]. If post-annealing time is very small, complete pyrolytic reduction will not take place and may adversely influence the material properties. We raised air annealing temperature to deposition temperature and then varied annealing time (by increasing it in steps of 15 minutes) from 15 to 60 minutes. Four sets of samples were deposited

and one by one these were removed from the heater in intervals of 15 minutes and were compared with the unannealed samples. They were named PA15, PA30, PA45 and PA60 respectively. Structural, optical and electrical results obtained are now discussed.

4.3.2.1 Structural characterizations

Figure 4.12 represents the XRD pattern obtained for samples annealed for different time periods.
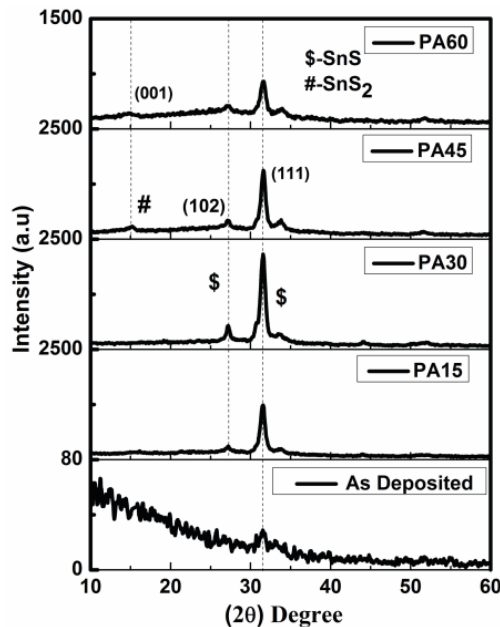
Figure 4.12 X-Ray Diffractograms of as deposited and PA15 to PA60 samples

It is seen that longer annealing time resulted in formation of SnS_2 phase, another binary compound of tin. Formation of SnS_2 phase on long term annealing is already reported for p-type SnS [6]. It is to be noted that intensity of preferred peak also enhanced from hundreds to thousands with annealing at deposition temperature. From XRD analysis, samples annealed

for 30 minutes were found to have enhanced intensity for the preferential peak with no visible impurity phases. Grain size was calculated and found to be ~ 22 nm for all annealed samples except PA60, which had ~ 18 nm.

4.3.2.2 Optical characterizations

The $(\alpha h\nu)^2$ versus hν plot of "as deposited "and annealing time varied samples (PA15 to PA60) are shown in Figure 4.13 (a).Here also no formation of sub-band gap is observed. Figure 4.13 (b) represents corresponding band gap obtained in each case.
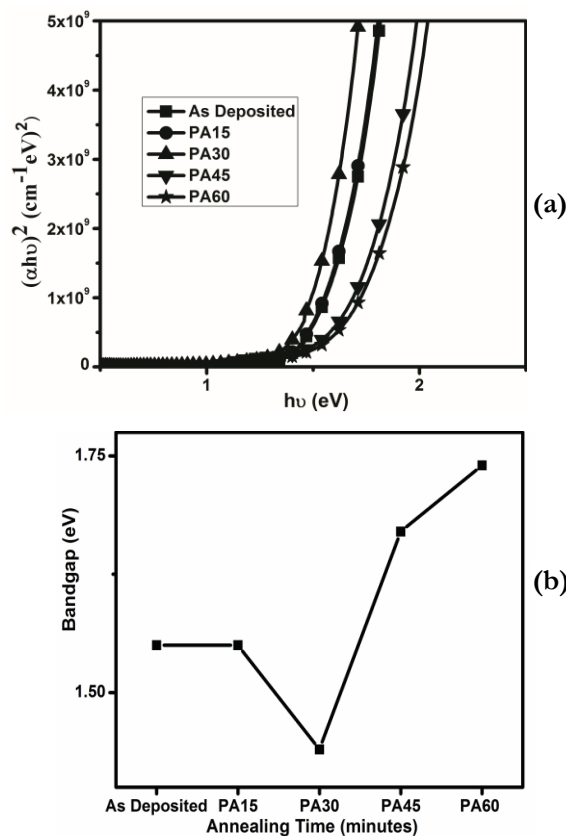
Figure 4.13 (a) $(\alpha h\nu)^2$ versus (hν) graph
(b) band gap obtained for all samples

With an increase in annealing time, optical band gap decreased initially and then increased slightly in comparison to "as deposited" film. Increase in band gap might be due to the presence of SnS_2 phase (confirmed from XRD, Figure 4.12). Minimum band gap of ~ 1.4 eV was obtained for 30 minutes of annealed samples.

4.3.2.3 AFM

AFM analysis was done on all annealed samples (PA15 to PA60) and surface roughness was calculated. Surface topography obtained is shown in Figure 4.14 and the roughness obtained is tabulated in Table 4.2. It is clear that all the samples are crack free.
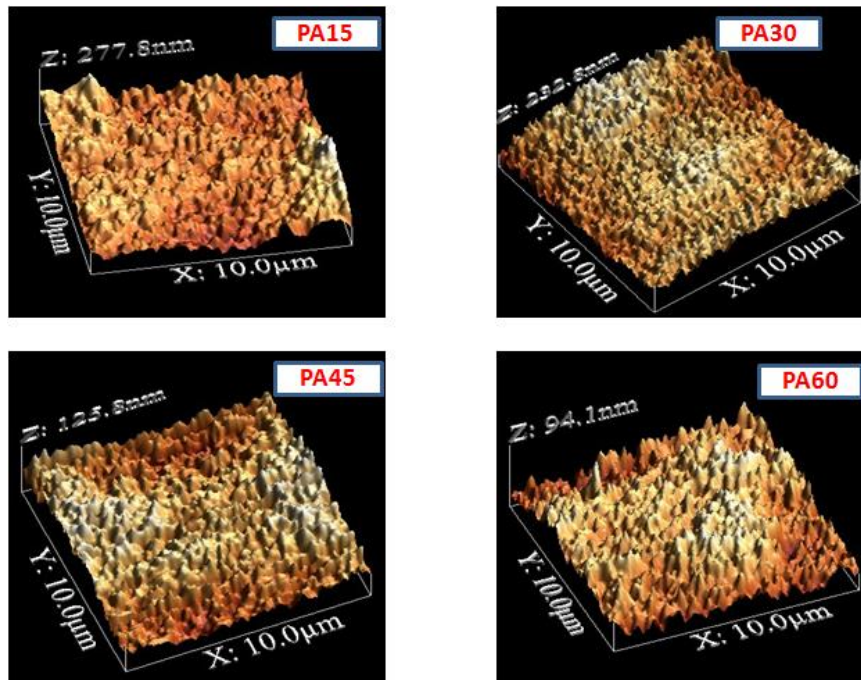
Figure 4.14 AFM images of PA15 to PA60 samples

RMS value of surface roughness was calculated for annealed samples and compared with that of the "as deposited" (unannealed) sample obtained in the earlier section. The roughness of "as deposited" sample was found to be around 43 nm. From Table 4.2, it is clear that the roughness decreases with increase in annealing time.

Table 4.2 Surface roughness obtained for annealed samples

Sample name	RMS surface roughness (nm)
PA15	32.2
PA30	29.2
PA45	20.4
PA60	14.2

4.3.2.4 Electrical studies

Figure 4.15 shows variation in carrier concentration, resistivity and mobility with an increase in annealing time.
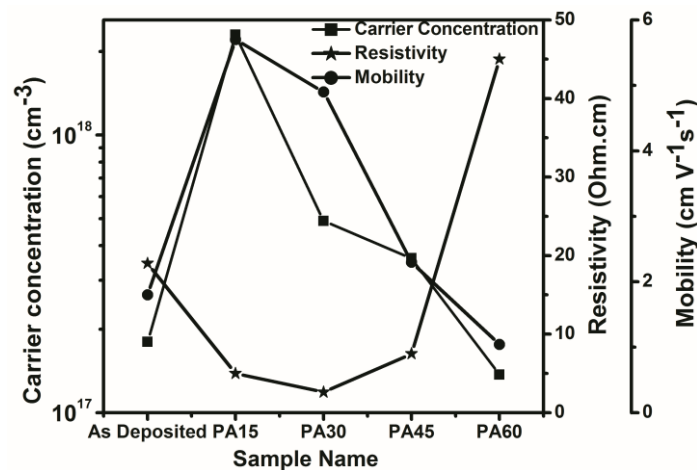
Figure 4.15 Electrical measurements done on as deposited and PA15 to PA60 samples

It is seen that resistivity starts decreasing with increase in annealing time and reached a minimum value for 30 minutes annealing. Further increase in annealing time resulted in an increase in resistivity, which may be due to a decrease in carrier concentration. Carrier concentration and mobility showed an opposite trend to that of resistivity with increasing annealing time. Both values increased initially and then started decreasing with annealing time. From the results obtained from various characterization studies done, 30 minutes of post-deposition annealing time is found to be better for further studies.

4.3.3 Inversion of sample

By varying air annealing time, film properties in general improved. In this session, effect due to anotherpost-deposition technique, namely "inversion", is described [17]. Usually, samples taken after post-deposition air annealing (by keeping it over the heater at deposition temperature for 30 minutes) are allowed to cool down to room temperature before storing. During this time, there is every chance for oxygen to enter the film and affect the orientation of different planes. This can be minimized if we reduce contact between the film surface and atmosphere when it is cooled. Thus after post-annealing, the samples are quickly removed using a holder and placed over a piece of "New wood" with the film surface facing the base material until it cools down. This is compared with the sample, which was allowed to cool in an open atmosphere. The "inverted samples" were named as 'I' and non-inverted samples as 'UI'. The choice of "New wood" was made because among various base materials like metal sheet, cardboard, thick chart paper, new

wood etc."New wood" was found to be the best base material for post-deposition cooling [23].

4.3.3.1 Structural analysis

The X-ray diffraction pattern of inverted (I) and non-inverted (UI) samples are depicted in Figure 4.16.
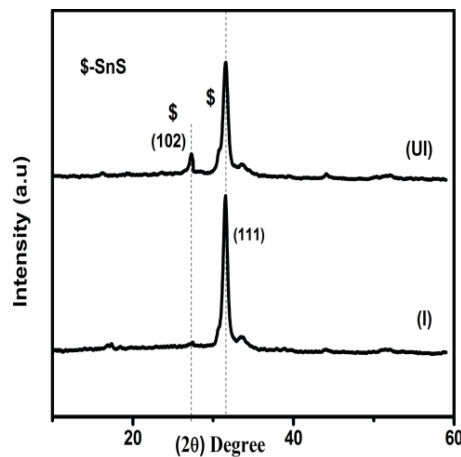
Figure 4.16 XRD of non-inverted and inverted sample

From the XRD analysis, [25] structural changes after the inversion process were very clear. For non-inverted samples, peaks were present at 2θ value 27.4° and 31.5° respectively, which correspond to the (102) and (111) planes of orthorhombic SnS (JCPDS:75-0925). On inverting, the (102) plane vanished and grains reoriented towards (111) plane, thereby enhancing intensity of XRD peaks corresponding to this plane. Similar result is observed in vacuum annealing also and therefore, this new process of cooling can be considered equivalent to vacuum annealing.

The prepared SnS:Cu films have enhanced (111) plane that is known to yield maximum efficiency for SnS based solar cells [1,2,5].

4.3.3.2 Optical studies

Absorption spectra for both inverted and non-inverted samples were recorded, and the corresponding band gap was determined from $(\alpha h\nu)^2$ versus $h\nu$ plot (Figure 4.17).
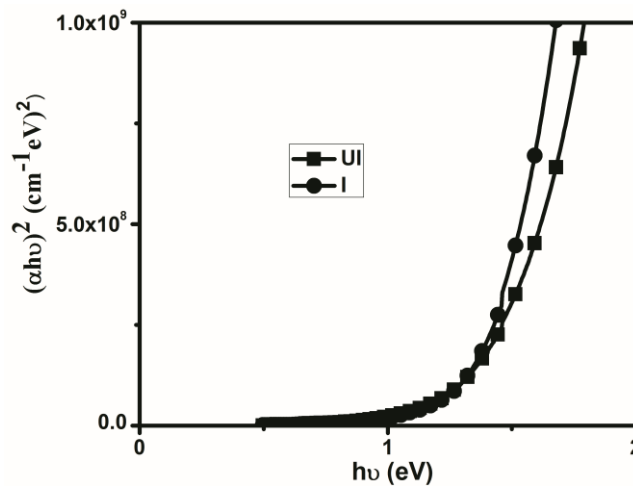
Figure 4.17 $(\alpha h\nu)^2$ versus $h\nu$ plot of non-inverted and inverted sample

The graph showed direct transition and the "inversion process" did not show noticeable variation in band gap. A band gap value ~ 1.36 eV is obtained for both samples without any sub-band gap formation.

4.3.3.2 Electrical and compositional studies

Electrical measurements were carried out using Hall measurements and carrier concentration, resistivity and mobility for both samples were noted. The values obtained are tabulated in Table 4.3.

Table 4.3 Electrical properties obtained for non-inverted and inverted samples

Sample Name	Carrier Concentration (/cm^3) 10*^{17}	Resistivity (ohm.cm)	Mobility (cm^2/V.s)
UI	6.3	2.8	3.5
I	10	1.6	3.7

From electrical measurements, resistivity is lower for the inverted samples with enhanced mobility and carrier concentration. Here, apart from increase in carrier concentration, mobility also increased when compared with vacuum annealing done in previous section. To verify whether there is any change in material composition due to inversion, EDAX measurements were carried out, and the percentage of tin, sulfur and copper concentration were obtained (Figure 4.18).
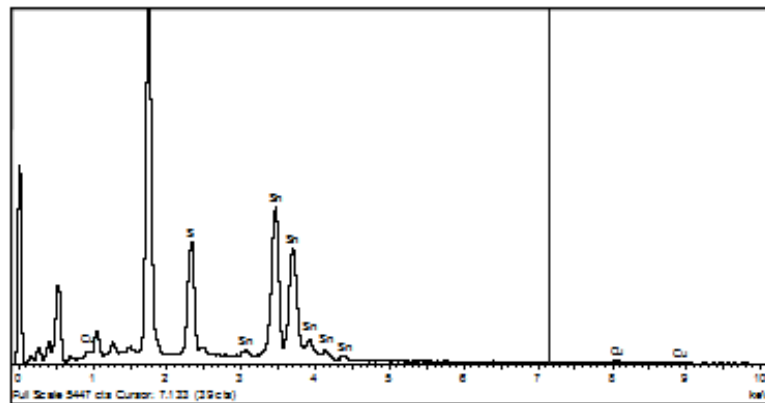
Figure 4.18 EDAX measurement of inverted sample

It was found that concentrations of tin was around 55.80 %, sulfur was around 41.02 % and copper was around 3.18 % in agreement with concentrations reported for n-type SnS [26].

Thus the inversion process was found to be an effective method to isolate the film surface from the atmosphere through a non-vacuum and "zero-energy" technique. Hence hereafter all deposited films were inverted after post-deposition annealing. This method can be adapted easily even for large area deposition. The procedures are environmental friendly and can be incorporated easily in the production line.

4.4 Stability of sample properties due to variation of precursor solution temperature:

4.4.1 Varying precursor preparation temperature

Here the effect of environmental temperature conditions while preparing the precursor solution and its influence on the film formation is investigated. Since we saw a change in material properties due to post-deposition annealing, preparation ambience may be significant. For the study, the precursor solution for depositing optimized samples was prepared by varying temperatures from 15 °C to 40 °C (as 15 °C, 25 °C, 30 °C and 40 °C). Temperatures were maintained by keeping it in set temperature baths. When the temperature is above 40 ^{o}C, there was a slight change in colour due to precipitation, making it difficult to spray. The samples (air annealed at deposition temperature for 30 minutes and is inverted) were named G15, G25, G30 and G40 respectively.

4.4.1.1 Structural analysis

Structural characterization was done using XRD analysis and the graphs are shown in Figure 4.19. It is found that all the samples had preferred (111) orientation without any other phases.
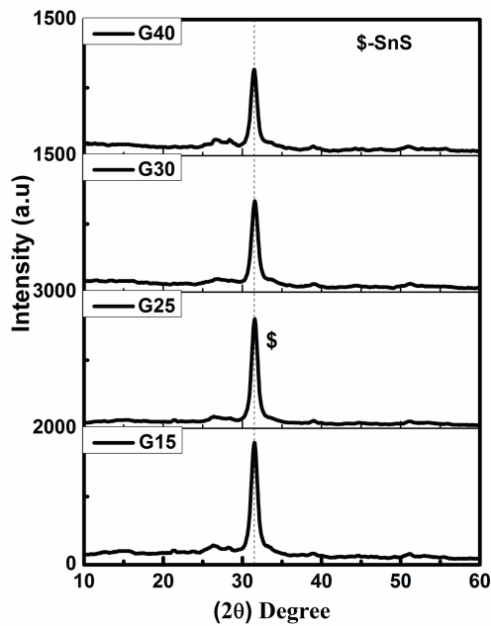
Figure 4.19 XRD pattern obtained for samples G15 to G40

Intensity was found to be maximum for the lowest temperature, and it slightly decreased with increase in temperature. Hence we concluded that the precursor preparation ambience did not affect the material structural properties.

4.4.1.2 Optical studies

The band gap was calculated from the "tau plot" and shown in Figure 4.20 (a).
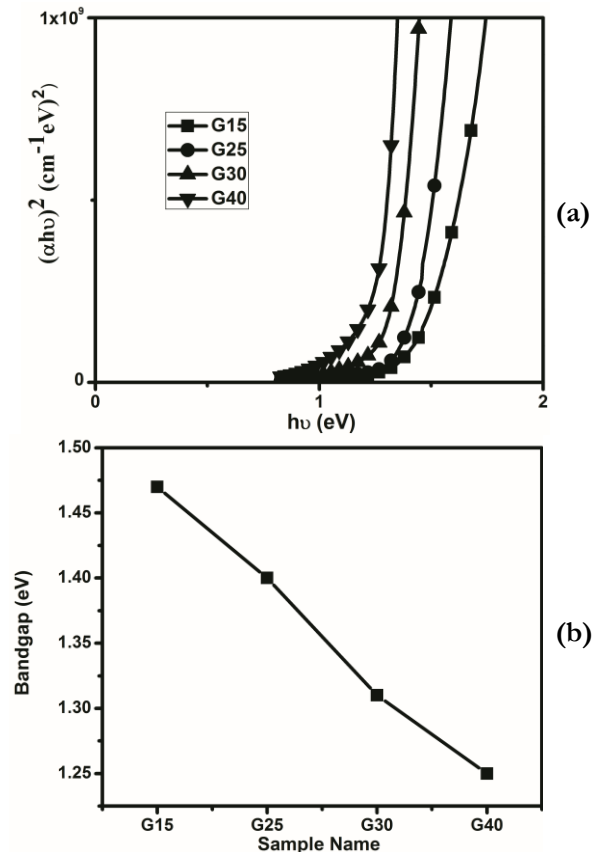
Figure 4.20 **(a)** $(\alpha h\nu)^2$ versus $(h\nu)$ graph **(b)** band gap obtained for all samples

Surprisingly, band gap of the prepared sample showed evident variation with the change in preparing conditions. Band gap was found to be decreasing with increase in preparation temperature (from 1.25 eV to 1.47 eV) and is shown in Figure 4.20 (b). The sample prepared at

25 °C was found to have the desired band gap around 1.4 eV. Thus we found that the optical properties can be even tuned (to an extent) by even changing solution temperature.

4.4.1.3 Electrical studies

Carrier concentration, resistivity and mobility were calculated using Hall measurements and the obtained values are shown in Figure 4.21.
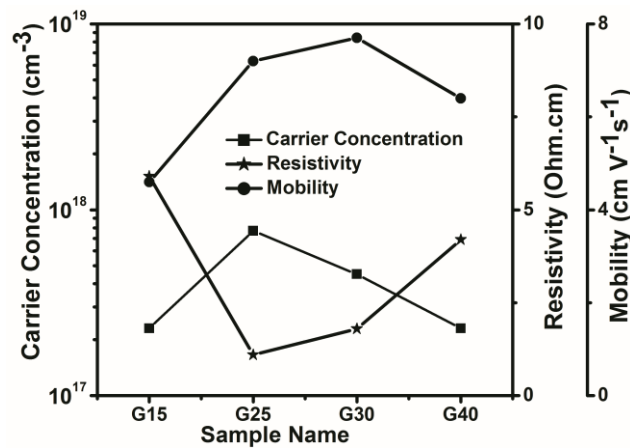
Figure 4.21 Electrical properties obtained for the samples

Resistivity was found to be in same order for all the samples, and minimum value was for the samples prepared at room temperature. Mobility increased initially and then remained almost constant. Carrier concentration also increased initially and then decreased with an increase in solution temperature. The highest carrier concentration was obtained for G25 sample. It is to be noted that all the electrical properties are stable over the varied preparation temperatures. Thus we could conclude that this material can withstand the variations in precursor preparation

temperature, without compromising its material properties. This becomes very useful in the case of device fabrication.

4.4.2 Stability with time

To understand the stability with time, two samples of the same nature (prepared at substrate temperature 375 ^{o}C, spray rate 2 ml/min, Sn:S ratio 1:2 with 4 % Cu doping with 30 minutes of post-deposition annealing at deposition temperature and is inverted) were prepared and were kept in inert condition. One sample was taken out at the end of one week for characterization. After the characterization study, the sample is again annealed at 375 ^{o}C for 30 minutes and was inverted. All the characterizations done before was again repeated over this annealed and inverted sample. The other sample was kept for 30 weeks, and similar material characterizations were done on it before and after the annealing and inversion process. Samples characterized after one week and 30 weeks were named 1W and 30W, respectively. The samples characterized after giving post-deposition annealing and inversion treatment were named A1W and A30W respectively.

4.4.2.1 Structural analysis

XRD pattern obtained for time varied annealed and unannealed samples are shown in Figure 4.22. This result confirms formation of prominent material plane along (111) even after 30 weeks. This can be considered as an indicator, which proved that SnS:Cu is good stable material.
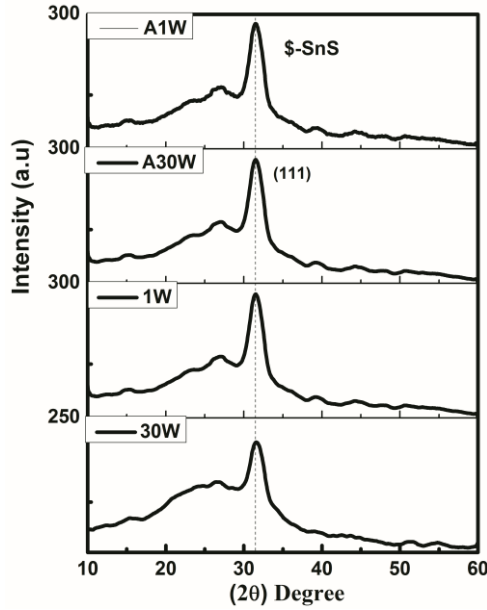
Figure 4.22 XRD pattern obtained for 30W, 1W,
A30W and A1W samples

On annealing, a slight increase in the intensity of (111) plane was observed, and that was more prominent for the annealing done on samples, aged for 30 weeks after deposition. For samples after 1 week, any improvement in structural property due to post-annealing was not much evident.

4.4.2.2 Optical studies

Optical characterization was done by calculating the material band gap, which is a determining factor to confirm the formation of a particular material. The $(\alpha h\nu)^2$ versus $(h\nu)$ graph is drawn and is shown in Figure 4.23.
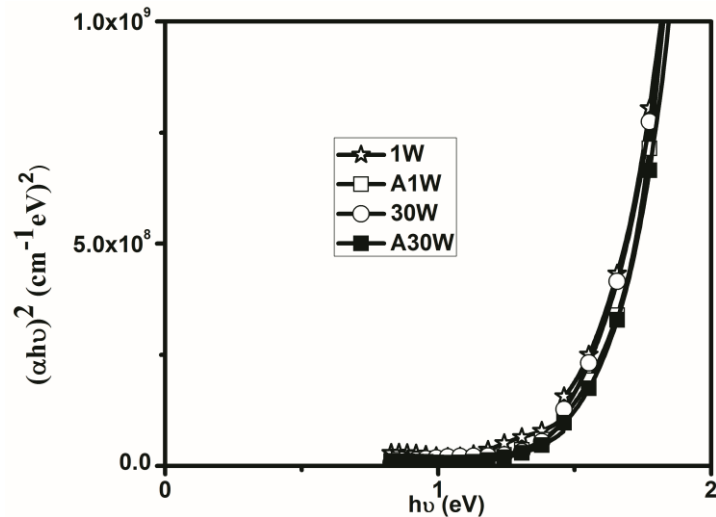
Figure 4.23 $(\alpha h\nu)^2$ versus $(h\nu)$ graph obtained for 30W, 1W, A30W and A1W samples

The corresponding band gap is calculated in each case. Not much variation was observed with ageing of the deposited sample and with post-deposition annealing. Band gap around 1.5 eV was obtained for all the samples.

4.4.2.3 Electrical studies

Electrical measurements were done using Hall measurement, and the results obtained are tabulated in Table 4.4. This showed an increase in resistivity by an order in the first week, and it remained unchanged for the next 30 weeks. Nevertheless, the post-deposition annealing treatment brought it back to the deposition range.

Table 4.4 Electrical properties obtained for aged annealed and unannealed samples

Sample Name	Carrier Concentration (/cm³) 10^{*17}	Resistivity (ohm.cm)	Mobility (cm²/V.s)
1W	0.24	55	4.9
A1W	3.2	7.2	2.7
30W	0.25	55	4.6
A30W	9.6	8.4	0.78

Mobility remained almost constant with ageing, but after giving post-deposition annealing, it decreased further. In the case of carrier concentration, there was a decrease in its value with ageing but it could be brought back to deposition range by giving post-deposition annealing treatment.

4.3 Conclusion

The present work investigated various post-deposition techniques so as to improve the material properties. Five milliliter (ml) of precursor solvent (HCl) for dissolving the $SnCl_2.2H_2O$ for the deposition SnS:Cu films was found to be optimal. Then effects on material properties due to air annealing and vacuum annealing were analysed and were compared with the unannealed samples. Air annealing was found to be more suitable and economic. As the next step, improvement is made by systematically varying the annealing time to 30 minutes. Zero energy process, namely "inversion" was also tried and found to be an effective method for preparing SnS:Cu with (111) orientation, which is very much suited for device fabrication. The resistivity is obtained lower for the inverted samples along with enhancement in mobility and carrier concentration. In the final section, the ability of material to withstand

variations in precursor preparation temperature and also the material stability with time were checked. Possibility of bringing resistivity back to its deposition order by simply applying post-deposition annealing treatment is a notable phenomenon. Material stability and capability to regain material properties confirmed that SnS:Cu is a potential candidate for solar cell fabrication.

References

[1] Reddy, N. Koteswara, KT Ramakrishna Reddy, G. Fisher, R. Best, and P. K. Dutta. "The structural behaviour of layers of SnS grown by spray pyrolysis." *Journal of Physics D: Applied Physics* 32, no. 9 (1999): 988.

[2] Reddy, KT Ramakrishna, N. Koteswara Reddy, and R. W. Miles. "Photovoltaic properties of SnS based solar cells." *Solar energy materials and solar cells* 90.18-19 (2006): 3041-3046.

[3] Reddy, N. Koteeswara. "Growth-temperature dependent physical properties of SnS nanocrystalline thin films." *ECS Journal of Solid State Science and Technology* 2, no. 6 (2013): P259-P263.

[4] Bashkirov, S. A., V. F. Gremenok, V. A. Ivanov, V. V. Lazenka, and K. Bente. "Tin sulfide thin films and Mo/p-SnS/n-CdS/ZnO heterojunctions for photovoltaic applications." Thin Solid Films 520, no. 17 (2012): 5807-5810.

[5] Guneri, E., C. Ulutas, F. Kirmizigul, G. Altindemir, F. Gode, and C. Gumus. "Effect of deposition time on structural, electrical, and optical properties of SnS thin films deposited by chemical bath deposition." *Applied Surface Science* 257, no. 4 (2010): 1189-1195.

[6] Sajeesh T.H, PhD Thesis, Cochin University of Science and Technology, India (2012).

[7] Chaki, Sunil H., Mahesh D. Chaudhary, and M. P. Deshpande. "SnS thin films deposited by chemical bath deposition, dip coating and SILAR techniques." *Journal of Semiconductors* 37.5 (2016): 053001.

[8] Mathews, N. R., C. Colín García, and Ildefonso Z. Torres. "Effect of annealing on structural, optical and electrical properties of pulse electrodeposited tin sulfide films." *Materials Science in Semiconductor Processing* 16.1 (2013): 29-37.

[9] Seo, Wondeok, Seokyoon Shin, Giyul Ham, Juhyun Lee, Seungjin Lee, Hyeongsu Choi, and Hyeongtag Jeon. "Thickness-dependent structure and properties of SnS2 thin films prepared by atomic layer deposition." *Japanese Journal of Applied Physics* 56, no. 3 (2017): 031201.

[10] Reddy, N. Koteswara, and KT Ramakrishna Reddy. "Optical behaviour of sprayed tin sulphide thin films." *Materials research bulletin* 41.2 (2006): 414-422.

[11] Sajeesh, T. H., Anita R. Warrier, C. Sudha Kartha, and K. P. Vijayakumar. "Optimization of parameters of chemical spray pyrolysis technique to get n and p-type layers of SnS." *Thin Solid Films* 518, no. 15 (2010): 4370-4374.

[12] Reddy, Vasudeva Reddy Minnam, Sreedevi Gedi, Chinho Park, RWc Miles, and Ramakrishna Reddy KT. "Development of sulphurized SnS thin film solar cells." *Current Applied Physics* 15, no. 5 (2015): 588-598.

[13] Avendaño, CA Meza, Nini Rose Mathews, Mou Pal, F. Paraguay Delgado, and X. Mathew. "Structural evolution of multilayer SnS/Cu/ZnS stack to phase-pure Cu_2ZnSnS_4 thin films by thermal processing." *ECS Journal of Solid State Science and Technology* 4, no. 3 (2015): P91-P96.

[14]   Zhao, Min, Fengjiao Shang, Ying Song, Feng Wang, Zhitao Zhou, Jianguo Lv, Zhenfa Zi et al. "Surface morphology, composition and wettability Cu 2 O/CuO composite thin films prepared by a facile hydrothermal method." *Applied Physics A* 118, no. 3 (2015): 901-906.

[15]   Sharon, Maheshwar, and Krishnan Basavaswaran. "Photoelectrochemical behaviour of tin monosulphide." *Solar cells* 25.2 (1988): 97-107.

[16] Huang, Chung-Cheng, Yow-Jon Lin, Cheng-Yu Chuang, Chia-Jyi Liu, and Yao-Wei Yang. "Conduction-type control of SnSx films prepared by the sol–gel method for different sulfur contents." *Journal of Alloys and Compounds* 553 (2013): 208-211.

[17]   Vimalkumar, T. V., N. Poornima, C. Sudha Kartha, K. P. Vijayakumar, T. Abe, and Y. Kashiwaba. "Enhancement of electrical conductivity in sprayed ZnO thin film through zero-energyprocess." *Physica B: Condensed Matter* 405, no. 24 (2010): 4957-4960.

[18]   Banai, R. E., J. C. Cordell, G. Lindwall, N. J. Tanen, S-L. Shang, J. R. Nasr, Z-K. Liu, J. R. S. Brownson, and M. W. Horn. "Control of Phase in Tin Sulfide Thin Films Produced via RF-Sputtering of SnS 2 Target with Post-deposition Annealing." *Journal of Electronic Materials* 45, no. 1 (2016): 499-508.

[19]   Truong, Nguyen Tam Nguyen, Ha Hai Thi Hoang, Thanh Kieu Trinh, Viet Thanh Hau Pham, Ryan Patrick Smith, and Chinho Park. "Effect of post-synthesis annealing on properties of SnS nanospheres and its solar cell performance." *Korean Journal of Chemical Engineering* 34, no. 4 (2017): 1208-1213.

[20]   Gotoh, Tamihiro. "Control of carrier concentration in SnS films by annealing with S and Sn." *physica status solidi (a)* 213.7 (2016): 1869-1872.

[21] Di Mare, Simone, Andrei Salavei, Daniele Menossi, Fabio Piccinelli, Paolo Bernardi, Elisa Artegiani, Arun Kumar, Gino Mariotto, and Alessandro Romeo. "A study of SnS recrystallization by post deposition treatment." In *2016 IEEE 43rd Photovoltaic Specialists Conference (PVSC)*, pp. 0431-0434. IEEE, 2016.

[22] Barreau, Nicolas, J. C. Bernede, H. El Maliki, S. Marsillac, Xavier Castel, and Jacques Pinel. "Recent studies on In2S3 containing oxygen thin films." *Solid State Communications* 122, no. 7-8 (2002): 445-450.

[23] Vimalkumar T.V, PhD Thesis, Cochin University of Science and Technology, India (2011).

[24] Ray, Sekhar C., Malay K. Karanjai, and Dhruba Das Gupta. "Structure and photoconductive properties of dip-deposited SnS and SnS$_2$ thin films and their conversion to tin dioxide by annealing in air." *Thin Solid Films* 350.1-2 (1999): 72-78.

[25] Sharma, Ravi, D. P. Bisen, Usha Shukla, and B. G. Sharma. "X-ray diffraction: a powerful method of characterizing nanomaterials." *Recent research in science and technology* 4, no. 8 (2012).

Chapter 5

DEMONSTRATION OF SnS:Cu BASED
PHOTOVOLTAIC HETEROJUNCTION

5.1 Introduction

In recent years synthesis of n-type SnS and fabrication of solar cell using this material as the absorber layer have been an area of active research. Even though various trials on the device fabrication are still going on, not yet a single technique has been reported as the favored fabrication technique. In this chapter we describe solar cell fabrication using chemical spray pyrolysis (CSP) technique, which posses many advantages as mentioned in the previous chapters. In the present study, the cell is having 'superstrate configuration' in which all the layers of solar cell are deposited above a transparent conducting layer (for present study we used ITO) and is illuminated through the substrate side. Here ITO (tin doped indium oxide) is coated over glass substrate which can act as the window for illumination. There are two possible configurations that can be followed while fabricating solar cell devices and they are 'Glass/ITO/n-layer/p-layer/electrode' and 'Glass/ITO/p-layer/n-layer/electrode'. In general, most of the reported works deal with p-type SnS layer along with various n-layers like CdS, ZnO [1-4]. It is really important to find a suitable non toxic material which can transfer photo generated electrons before recombining, within the material itself. Thus an attempt on fabricating device using n-type SnS:Cu layer and p-type CZTS (copper zinc

tin sulfide) is described in this chapter. It should be emphasized that present work is a preliminary study of the novel architecture CZTS/SnS:Cu and so far no works have been reported with this device configuration.

5.2 Device fabrication

In order to fabricate a solar cell, several steps have to be followed and the following section briefly describes importance and need for each step. Firstly, for a solar cell to perform well, we have to tackle various loss mechanisms, mainly the optical loss mechanism and electronic loss mechanism. Efficiency in absorbing light and creation of minority carriers controls the optical loss mechanism whereas how effectively these created minority carriers can be collected at the required contacts decides the electronic loss mechanism [5]. Hence materials with required material properties and optimum thickness should be chosen for device fabrication. We used the above optimized SnS:Cu as n-type layer and CZTS (a well studied material in our lab) as p-type layer [6,7]. ITO and silver were used as bottom and top electrodes respectively. Figure 5.1 shows the schematic diagram of the fabricated solar cell.
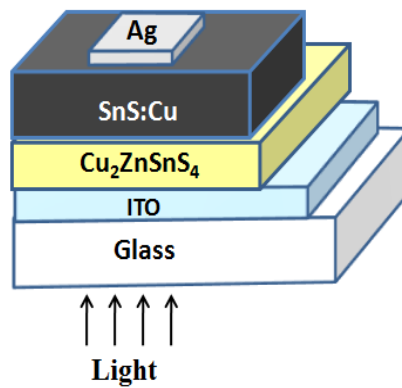
Figure 5.1 Schematic diagram of device fabricated

We used commercially available ITO coated glass plate (GEOMATEC, Japan, with optical transmission 82 %, sheet resistance ~12 $\Omega/\square$ and thickness ~ 200 nm). The heterojunctions have certain advantages over the homojunction devices and one such advantage is the possibility of using materials of different band gaps such that, there is a window layer with large band gap allowing the passage of most of the solar radiation, and an absorber layer which has a relatively narrow band gap to absorb the incoming solar radiation. Here in our case, it may be noted that we have used two different materials a p-type CZTS having a band gap of ~ 1.5 eV and an n-type SnS:Cu having a band gap of ~ 1.4 eV. Moreover, because of the peculiarity of our device structure (Glass/ITO/CZTS/SnS:Cu/Ag) and illumination through the ITO, the role of SnS:Cu is not just as a window layer, but it also functions as the n-type buffer and at the same time absorbs any of the transmitted light from CZTS [7-9]. Hence, it was expected that the configuration could improve the short-circuit current density. Moreover, such a structure has an added advantage of absorbing light from both the sides, thus functioning as a "bifacial solar cell" [10,11]. In addition to the advantages of the device structure as stated above, it is important to point out that both CZTS and SnS:Cu use eco-friendly and earth-abundant materials in contrast to CdTe, CIGS, CdS or In_2S_3 that are often used. Hence, there is more room for improvement, and it deserves special attention because of the use of eco-friendly and earth-abundant materials for cost-effective thin-film solar cells.

5.2.1 Deposition of SnS:Cu (n-layer), CZTS (p-layer) and Ag (Electrode)

As mentioned above, here both layers play the role of absorber, and hence, it is vital to optimize the material thickness and other properties. It is in this absorber layer(s) the electron-hole pairs are created after absorbing the electromagnetic energy. For successful transfer of energy, certain criteria have to be followed. The most three important criteria are:

1) The spectral region where the cell operate should match with the material band gap

2) For the successful absorption of light energy within the thin layer, the optical absorption coefficient should be very high

3) The minority carriers should posses required diffusion length and life time so as to cover the distance through the cell. By reducing the crystalline impurities and defects which produce recombination levels near to the middle of band gap, the diffusion length can be increased.

Initially, for device fabrication, optimized preparation condition for the n-type layer is used as described in previous chapters. Precursors were tin chloride ($SnCl_2.2H_2O$), thiourea [$CS(NH_2)_2$] and copper chloride ($CuCl_2.2H_2O$). Optimized deposition parameters (such as substrate temperature of 375 ^{o}C and spray rate of 2 ml/min with Sn:S in the ratio 1:2 with 4 % of Cu doping) were already fixed for the n layer deposition, as described in earlier chapters.

CZTS is an excellent p-layer for n-type SnS:Cu due to its comparable band gap of 1.5 eV. The material properties of spray

deposited CZTS, and its optimized deposition conditions are well studied [6,12-14]. The CZTS was prepared using precursors copper chloride ($CuCl_2.2H_2O$), zinc acetate ($Zn(CH_3COO)_2$), stannic chloride ($SnCl_4.5H_2O$) and thiourea ($CS(NH_2)_2$) and deposition parameters were already optimized as substrate temperature of 350 ^{o}C and spray rate of 6 ml/min with ratio Cu:Zn:Sn:S as 2.5:1:0.7:12 [15].

For the device fabrication, we selected vacuum evaporated silver (Ag) (about 50 nm thickness coated over an area of 0.03 cm^2) as top electrode. Ohmic contact between the film and silver electrode was also optimized during fabrication.

5.3 Device structure

There are two possible device structures that can be followed and as an initial trial, we fabricated solar cells with "ITO/SnS:Cu/CZTS/Ag" and "ITO/CZTS/SnS:Cu/Ag" structures. Their schematic diagrams are shown in Figure 5.2 (a) and (b) and are named as C1 and C2 respectively.
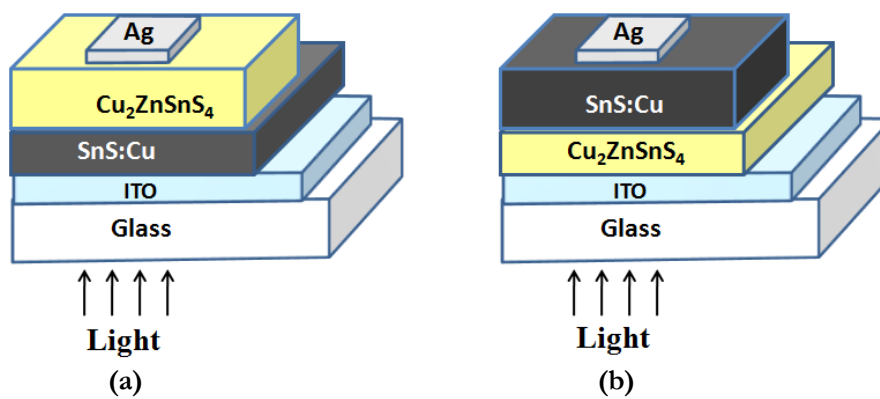
Figure 5.2 Schematic diagrams of both (a) C1 and (b) C2 device structures

In both cases, ITO is used as bottom electrode over which both p-type and n-type layers are deposited using the spray technique. Ratio of SnS:Cu was kept as 1:2 with 4 % Cu doping and the ratio of CZTS as Cu:Zn:Sn:S=2.5:1:0.7:12 (as mentioned above). The spraying time were kept fixed as 12'30'' (12 minutes and 30 seconds; thickness ~ 480 nm) for CZTS and 10' (thickness ~ 650 nm) for SnS:Cu. Above these layers, silver was vacuum evaporated for the top contact. Six silver electrodes were deposited as an array over the device, each with a thickness of 50 nm over an area of 0.03 cm^2. Top view of the device is shown in Figure 5.3 (a) and (b) and each electrode was isolated by scribing using 'doctor-blade edge'.

(a)   **(b)**
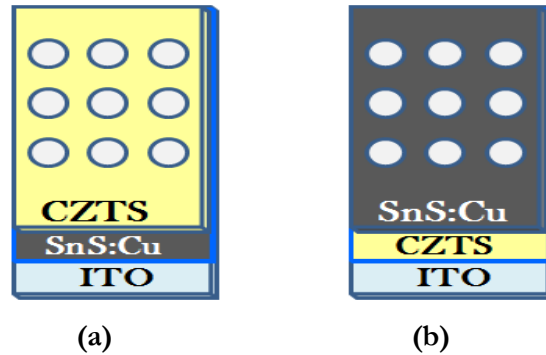
Figure 5.3 Top views of both (a) C1 and (b) C2 devices

The J-V characteristics (dark and illuminated) were checked in each case and even after various trials, no light activity was obtained. This was probably due to large thickness of the n-layer and low resistivity of p-layer. In the case of C1 structure, higher molarity (0.1M SnCl$_2$,0.2 M TU) and thickness of SnS:Cu made the film very dark so that it probably blocked the light reaching the junction. The J-V

characteristic obtained was a straight line, which means the device got shorted. In the case of C2 structure, the J-V characteristic of the device showed diode nature which confirmed the junction formation, but no light activity was observed. The thick SnS:Cu n-layer and the absorption in CZTS layer might be blocking light from reaching the electrode in the case of C2 structure. Hence as the next step, thickness of n-layer and resistivity of p-layer were reduced. In the case of CZTS, this could be achieved by reducing copper to zinc ratio in CZTS. For SnS:Cu, the thickness could be reduced by decreasing molarity of $SnCl_2.2H_2O$ and also by varying its spray time. Thickness of SnS:Cu should be such that recombination probability of photo-generated carriers within this layer is significantly reduced so that it promotes the efficient charge collection at the external contacts. Thus the limits due to low mobility of carriers and the inevitable defects formed can be minimized. But care should be taken to find the optimum thickness so that the absorption of light is not compromised.

5.3.1 Device fabrication with low copper CZTS and molarity fixation of SnS:Cu

As mentioned above, solar cells were fabricated in both device structures using CZTS in the ratio Cu:Zn:Sn:S = 2.5:1:0.7:12 and SnS:Cu using 0.1 M $SnCl_2.2H_2O$. Now as the next step, devices were fabricated in both architectures using CZTS layer with less copper to zinc ratio (Cu:Zn:Sn:S = 1.5:1:0.7:12) and SnS:Cu layer with reduced molarity of $SnCl_2.2H_2O$ and also by varying the spraying time. Thus the molarity of $SnCl_2.2H_2O$ was varied from 0.1 M to 0.01 M and the molarity of thiourea was varied accordingly so as to maintain the ratio

Sn:S = 1:2. The doping percentage of Cu was same as before (4 % of the tin concentration in precursor solution). The CZTS layer was sprayed for 12'30'' (12 minutes and 30 seconds; thickness ~ 450 nm) with the above ratio for all devices. SnS:Cu was sprayed for each molarity for time periods as shown in Figure 5.4. Higher spray time is required for lower molarity and the time period was selected to obtain almost comparable thickness in all the cases.
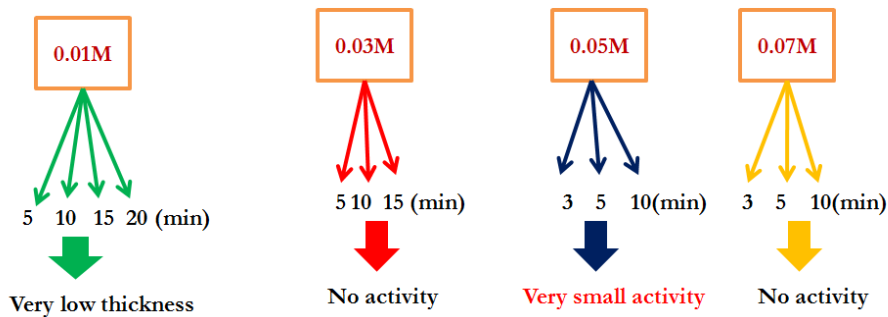
Figure 5.4 Molarity variation of $SnCl_2.2H_2O$ along with spray time variation of SnS:Cu

5.3.2 Measurement of J-V characteristics

Dark and illuminated J-V characteristics of the prepared devices and their performances were analyzed with the help of Keithley source measure unit "SMU" (NI PXI-1033) and Class AAA solar simulator (PET, model-SS50AAA; USA) was used for illumination. The measuring apparatus was so arranged that there was no temperature rise in the cell during measurement and also masked to avoid light falling on regions other than the required area. Light intensity of 100 mW/cm^2 was used. Voltage and current density were measured for each sample as discussed below.

For C1 structure, no activity was obtained. But for the C2 structure, light activity was observed for the first time, with the samples prepared using 0.05 M $SnCl_2$ irrespective of spraying time (Figure 5.4). Thickness for spray timings 3', 5' and 10' were around 230 nm, 255 nm and 420 nm respectively. The very low molarity (0.01 M and 0.03 M) and the very high molarity (0.07 M) did not come up to our expectation. Also the C1 structure did not respond to light with any of the above variations. Hence hereafter, C2 device architecture was followed for fabrication and analysis.

The samples were named C3, C5 and C10, respectively according to the spray time. The photovoltaic (PV) parameters like open circuit voltage (V_{oc}), short circuit current density (J_{sc}), fill factor (FF) and efficiency (η) were calculated in each case and these parameters are tabulated in Table 5.1. The corresponding J-V graphs obtained are shown in Figure 5.5
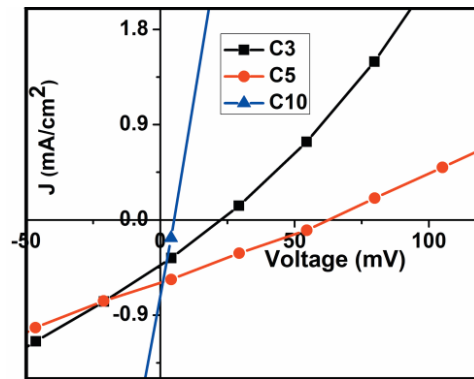
Figure 5.5 Illuminated J-V characteristics obtained for solar cell fabricated by varying spray time of SnS:Cu

Table 5.1 PV parameters obtained for solar cell fabricated by varying spray time of SnS:Cu

Minutes Sprayed	Cell Name	Thickness (SnS:Cu)	V_{oc} (mV)	J_{sc} (mA/cm^2)	Fill factor (%)	Efficiency (%)
3	C3	230± 10	22	0.42	16	0.0015
5	**C5**	**255± 08**	**63**	**0.55**	**27**	**0.0092**
10	C10	420± 12	4.7	0.65	20	0.0006

The best cell has V_{oc} = 63 mV, J_{sc} = 0.55 mA/cm^2, efficiency = 0.0092 % and fill factor = 27 %. The PV parameters observed were very low and so the future studies were naturally focused on improving the performance. The diffusion of silver electrode or series resistance offered by the top layer was first considered. In order to investigate this, modifications were made in the cell structure by introducing a very thin top layer. Here the entire solar cell fabrication except the electrodes and ITO were done using automated spray pyrolysis machine [16]. The molarity of SnCl$_2$.2H$_2$O was fixed as 0.05 M, thiourea as 0.1 M and copper doping (0.02 M) constrained to 4 % of tin molarity. The spray time was fixed as 5' for SnS:Cu and 12'30'' for CZTS.

The cross sectional SEM image of the best sample is taken and the layers obtained are marked in the Figure 5.6. The high series resistance which is mainly contributed by the top SnS:Cu layer (comparatively resistive than CZTS layer) resulted in very low J_{sc} and FF values. Moreover the silver from electrode that diffused into the SnS:Cu layer provided a recombination path for the carriers, resulting in an increase in leakage current, reducing throughput from the device. So as the next step, we tried to improve performance parameters of the device by modifying the top layer.
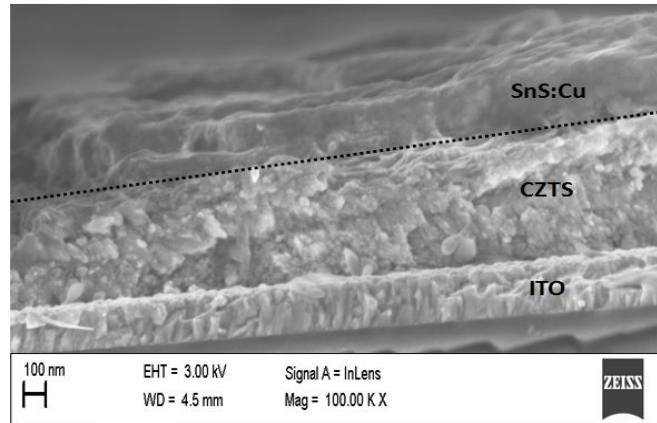
Figure 5.6 Cross-sectional SEM image of best device

This was done by introducing a thin layer of suitable material between the SnS:Cu layer and silver electrode done under the expectation that the layer can prevent the electrode diffusion and hence decreasing the recombination rate at the interface. There is also a possibility that this conducting layer atop can help to a greater extent in charge collection towards external contact. Thus the device structure was modified as ITO/CZTS/SnS:Cu/Top-layer/Ag. Here we deposited ZnO:Al (by CSP technique) as top layer. The effect of this top layer on the device performance is described below.

5.3.2 Introduction of ZnO:Al layer and its effect on solar cell performance

Ability of ZnO to become n-type and p-type makes it potential candidate for variousoptoelectronic applications. It is already reported that by doping with group III elements like Indium, Galium and Aluminium, n-type ZnO can be prepared [17]. Group VII elements like Cl and F though can also be used to make n-type ZnO by substituting for

the Oxygen atoms; however, these elements are toxic in nature and are thus not used in the study. Since our top layer (SnS:Cu) is n-type, we preferred n-type ZnO as carrier collective layer. To be cost-effective, instead of indium and rare earth metal gallium, we used aluminium as the dopant. ZnO:Al deposited by CSP technique is a well-studied material and by doping it with Al, its electrical conductivity can be improved [17-20]. The ZnO:Al was prepared by spraying a mixture of 0.1 M Zinc acetate doped with 2.56 % of 0.1 M aluminium pentanedionate at rate of 3 ml/min onto substrate (here the cell) maintained at fixed temperature of 300 $^{\circ}$C [17]. The structure followed is ITO/CZTS/SnS:Cu/ZnO:Al/Ag.

5.4 Optimization of each layer to improve the cell performance

As mentioned above the cell architecture is modified as "ITO/CZTS/SnS:Cu/ZnO:Al/Ag" and the schematic diagram is shown in Figure 5.7.
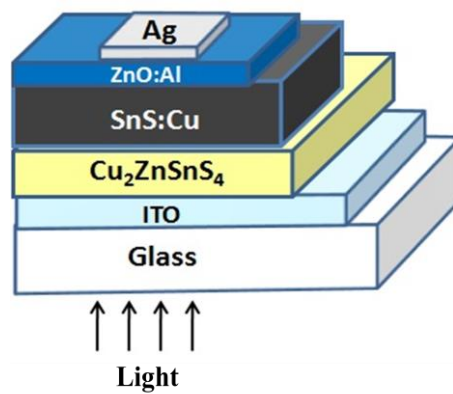
Figure 5.7 Schematic diagram of modified device structure

In order to achieve maximum device output parameters, we have to optimize thickness of each layer. This can be done by varying the spray time of each layer, keeping that of the other layers fixed. The optimum thickness of ZnO:Al was fixed by varying the spray time from 3' to 6'. The samples were named according to the spray time ZA3, ZA4, ZA5 and ZA6 respectively. The PV parameters obtained are tabulated in the Table 5.2 and the J-V characteristics are shown in Figure 5.8.

Figure 5.8 Illuminated J-V characteristics obtained
by varying spray time of ZnO:Al layer

Table 5.2 PV parameters obtained by varying spray time of ZnO:Al layer

Cell name	V_{oc} (mV)	J_{sc} (mA/cm^2)	FF (%)	Eff (%)
ZA3	245	0.454	39	0.04
ZA4	308	0.832	26	0.06
ZA5	**461**	**0.940**	**40**	**0.17**
ZA6	198	0.964	34	0.06

From Table 5.2, it is quite clear that there is increase in V_{oc} up to a particular spray time and further increase in spraying results in the decrease of V_{oc}. The current density however increased with the increase in top layer thickness. The best device parameters are obtained for the spray time of 5' that gives a thickness around 130 nm. The maximum values of fill factor and efficiency were 40 % and 0.17 % respectively. The top layer thickness hereafter is kept fixed at 130 nm. Figure 5.9 shows cross-sectional SEM image of the best solar cell that we could fabricate in this procedure. From the SEM image, presence of very thin zinc Oxide layer over surface of SnS:Cu is clear. When silver electrode is deposited over it, the diffusion of silver into SnS:Cu layer decreases and hence the shunt resistance is maintained. ZnO:Al can also help in carrier collection at the electrodes by band alignment, which results in increase of J_{sc} value (Table 5.2).
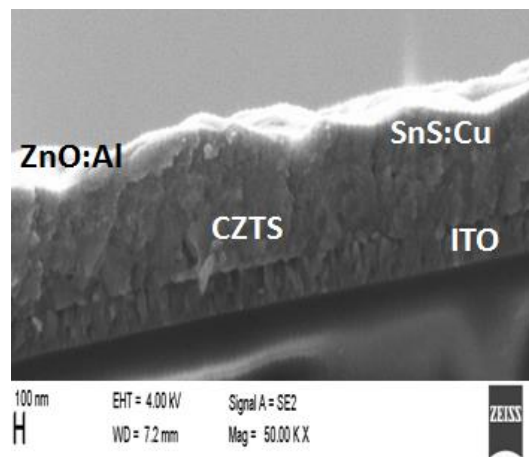
Figure 5.9 Cross-sectional SEM image of best device

Keeping ZnO:Al thickness constant, thickness of p-layer (CZTS) was varied next. For this, the spraying time of CZTS was varied,

keeping the deposition parameters of other layers fixed. This is important because, due to high thermal diffusivity of Cu ions, they will diffuse easily into SnS:Cu layer and as a result, there is a chance for impurity phase formation at the interface. This may destroy the optimized properties of SnS:Cu layer [21,22]. If the thickness of CZTS layer is very high, more and more Cu might get diffused to reach the top layer resulting in an electrical short circuit. Similarly, when the thickness of CZTS is very low, junction formation will not occur properly and the comparatively resistive top layer increases series resistance which adversely affects the J_{sc} [23,24]. Similar diffusion of Cu was observed and reported by Djessas, K. *et al.* [25]. To obtain optimum thickness of the p-layer for improving performance, spray time of CZTS was varied from 3'30'' to 15'30'' with 2' interval. The samples were named C3.5, C6.5, C9.5, C12.5 and C15.5 respectively. The output parameters are tabulated in Table 5.3 and Figure 5.10 represents the J-V characteristics.

Figure 5.10 Illuminated J-V characteristics obtained by varying spray time of CZTS layer

Table 5.3 Output parameters obtained by varying spray time of CZTS layer

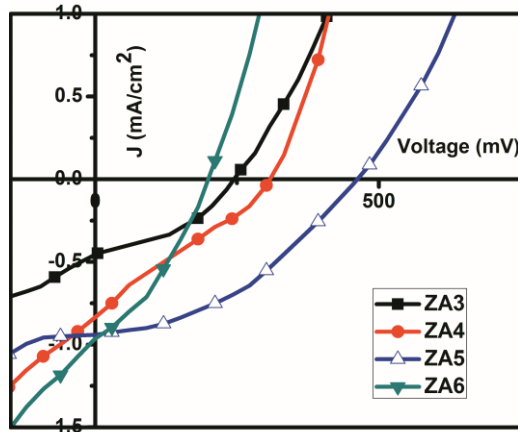| Cell name	V_{oc} (mV)	J_{sc} (mA/cm^2)	FF (%)	Eff (%)
C3.5	865	0.464	39	0.16
C6.5	604	0.791	37	0.17
C9.5	**557**	**0.837**	**42**	**0.19**
C12.5	404	0.842	38	0.12
C15.5	393	0.894	36	0.12

From the table, it is clear that V_{oc} decreases as CZTS thickness increases where as the J_{sc} always increases with increase in CZTS thickness. Fill factor and efficiency reached a maximum for 9'30'' spray time, which had thickness around 350 nm. Further increase in spray time resulted in decrease of the cell performance. As the CZTS layer thickness increases, total copper content present in this layer will be more and so the chances for diffusion towards the junction is comparatively high. This diffusion in turn decreases the effective thickness of pure SnS:Cu (forms extra impurity phases in between). This impurity phase makes the junction improper and thus V_{oc} decreases with increase in CZTS spray time. In the case of J_{sc}, with the present device structure, both CZTS and SnS:Cu will absorb light and generate carriers. So with the increase in CZTS layer thickness, absorption of light in this layer increases and hence total output current obtained will also increase. The increase in J_{sc} is not very large because this is contributed by those extra carriers produced from the increased CZTS layer thickness. The best sample under this study has V_{oc} = 557 mV, J_{sc} = 0.837 mA/cm^2, fill factor = 42 % and efficiency = 0.19 %. Figure 5.11 shows cross-sectional SEM of the best sample

with 0.2 % efficiency without the use of Ag electrodes. All the layers are well distinguished.
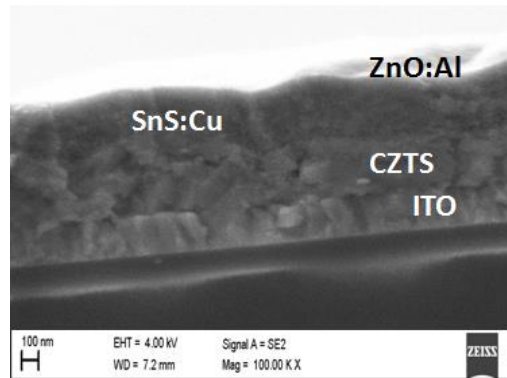
Figure 5.11 Cross-sectional SEM image of best device

Now the SnS:Cu thickness was adjusted without altering CZTS thickness (~ 350 nm) and ZnO:Al layer thickness (~ 130 nm). Silver electrode was used as the top contact, and an array of 6 electrodes, (each with area 0.03 cm^2 and thickness of 50 nm) were deposited. Each device was isolated from the other by using doctor-blade. Being an absorber layer, the thickness of SnS:Cu plays crucial role in absorbing the incident electromagnetic energy for the production of electron-hole pairs [26]. For the optimization of SnS:Cu thickness, the spray time was varied from 4' to 8' and the samples are named S4, S5, S6, S7 and S8 respectively. Thicknesses are measured by placing an extra soda lime glass plate along with the samples during the spray. The device photovoltaic parameters (V_{oc}, J_{sc}, fill factor and efficiency) were measured with respect to SnS:Cu spray time and is tabulated in Table 5.4. The J-V plot obtained in each case is shown in Figure 5.12.
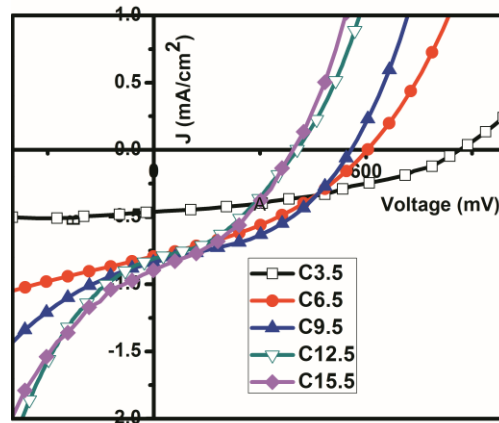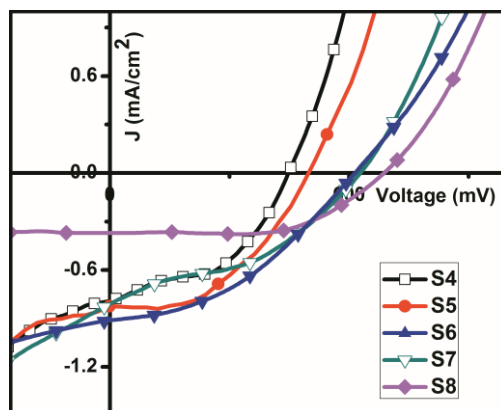
Figure 5.12 Illuminated J-V characteristics obtained
by varying spray time of SnS:Cu layer

Table 5.4 Output parameters obtained by varying spray time of SnS:Cu layer

Cell name	V_{oc} (mV)	J_{sc} (mA/cm^2)	FF (%)	Eff (%)
S4	448	0.790	45	0.16
S5	497	0.823	46	0.18
S6	**618**	**0.930**	**41**	**0.22**
S7	627	0.809	39	0.19
S8	688	0.372	60	0.15

As the spray time increases, there is considerable improvement in V_{oc} from 448 mV to 688 mV. With increase in spray time, the thickness of SnS:Cu layer increases and so the diffusion of Cu from CZTS layer below will not reach all through the SnS:Cu layer. Thus a comparatively resistive SnS:Cu layer is formed at the top, which in turn give good V_{oc}. Howeve, only up to 6' the J_{sc} value increased (from 0.790 to 0.930 mA/cm^2) and further increase in spray time resulted in a decrease of current density to 0.372 mA/cm^2. Efficiency also improved up to 6' of spray time and then

started decreasing. Fill factor of 60 % is obtained for higher spray time which confirms the formation of good junction. From the graph (Figure 5.12) good junction with better V_{oc} is observed, which means that all the carriers produced here will get collected and this result in better fill factor. However, reason for sudden hike in fill factor for S8 is unknown. But the J_{sc} obtained here is very low. This might be because, as the SnS:Cu layer thickness increases, light from the ITO side will not be able to reach the top portion of the absorber layer electrode to produce carriers and thus makes it more resistive. Increase in thickness enhances the series resistance and the recombination rate within the thick layer, which leads to the decrease of output current [23,24]. Even with enough production of carriers the low mobility of these carriers (from the electrical studies carried out in previous chapters) might be another reason for the low J_{sc} obtained. With higher spray time, the comparatively resistive SnS:Cu layer formed will give good V_{oc} but the current produced will be less (because as the thickness of resistive layer increases the series resistance and recombination rate within this thick layer increases) and hence efficiency also decreases. For very low spray time, voltage and current density are less due to the inefficient absorption of light. The best efficiency of 0.2 % is obtained for SnS:Cu thickness around 300 nm. Cross-sectional SEM of the best device is shown in Figure 5.13. SEM analysis is carried out without the top electrode. Thickness of SnS:Cu layer is found to be around ~ 290 nm which is in agreement with the thickness we obtained from the stylus profiler.
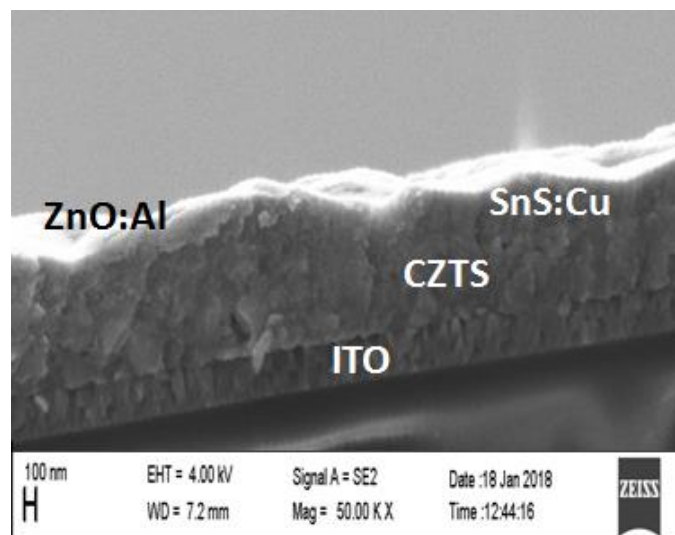
Figure 5.13 Cross-sectional SEM image of best device

Thus we conclude that for better performance of solar cells with ITO/CZTS/SnS:Cu/ ZnO:Al/Ag structure, the SnS:Cu thickness should be around 300 nm, CZTS thickness around 350 nm and ZnO:Al layer thickness around 130 nm.

5.5 The modified stoichiometry of n and p-layer

To find the best chemical composition of SnS:Cu layer which improves the efficiency, the following two strategies were tried.

1) The spray pyrolysis is done in normal air and XPS studies revealed presence of oxygen in the fabricated samples. Effect of replacing oxygen with sulfur by increasing the sulfur content in SnS:Cu was tried. Adjustment of Sn:S precursor ratio is a very effective method to achieve this. Proper care

was taken to maintain the structural, morphological, electrical and optical properties of the samples.

2) Reduce Cu to Zn ratio in CZTS to make it more resistive so as to increase the light activity at the junction.

5.5.1 Reduction of oxygen content present in n-layer

In the present study sulfur content in SnS:Cu is increased with the assumption that the oxygen content of the samples, (which is a determining factor in the performance of the device) can be decreased by this. Adjustment of Sn:S precursor ratio is a very effective method to achieve this. But care should be taken to see that, the structural, morphological, electrical and optical properties are not affected. Adjustment of S/Sn ratio in the precursor is achieved by varying the molarity of thiourea keeping the molarity of $SnCl_2$ constant. Films were prepared for S/Sn ratios of 1, 2, 4 and 6 in the precursor solution and the samples are named as T1, T2, T4 and T6 respectively. Thicknesses of all the samples were found to be around $\sim 310 \pm 20$ nm. Now, these samples were subjected to different studies to see if any variation has occurred in optical/optoelectronic properties and these results are presented below.

5.5.1.1 Structural analysis

X-ray diffractogram of SnS:Cu samples (T1, T2, T4 and T6) are depicted in Figure 5.14. All the samples have peak at 2θ value of 31.5^o (JCPDS: 75-0925) corresponding to SnS (111) plane.
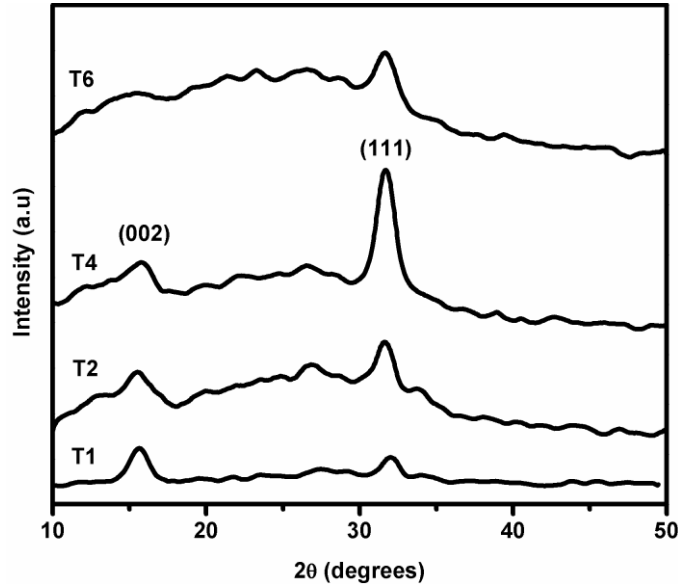
Figure 5.14 X-Ray diffractograms of SnS:Cu samples (T1-T6)

It is seen that, as sulfur concentration increases, the peak at 2θ value 15.84° (corresponding to (002) plane of SnS is getting diminished. Interestingly, even at higher sulfur concentration, there is no Cu_xS phase or any other compound of Sn and S. From the graph it is clear that sample T4 has the most intense (111) plane. The average value of grain size was found to be 14nm using Scherrer's formula D=0.9λ/ β Cosθ, where, D is the average grain size, λ is the X-ray wavelength, β is the full-width at half-maximum (FWHM) and θ is the Bragg angle. Using the equation $N = t/D^3$(per cm^2) where 't' is the film thickness, and 'D' is the grain size, the number of grains per unit area (N) is calculated. Average N value for all the samples is found to be $\sim 2 \times 10^{13}$ /cm^2.
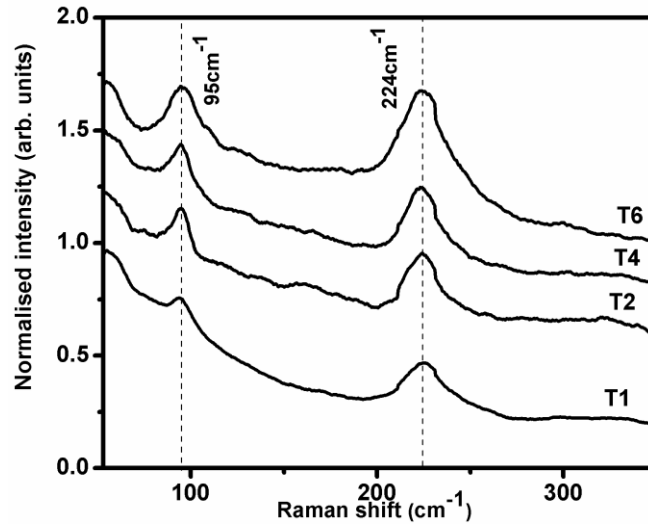
Figure 5.15 Raman Spectra of ratio varied SnS:Cu samples

To confirm the material purity (that is not visible in XRD), Raman analysis was carried out with excitation wavelength 632.8 nm. The results are presented in Figure 5.15. Raman shifts are observed at 95 and 224 cm^{-1}, which coincide with value reported for SnS in thin films as mentioned in previous chapters. Raman bands of SnS$_2$ (at 315 and 215 cm^{-1}) and Sn$_2$S$_3$ (at 307 and 251 cm^{-1}) are absent and hence phase purity of the prepared samples can be established. The full width at half maximum (FWHM) is calculated for all samples and are found to be 22.7, 20.7, 20.3 and 26.6 cm^{-1} for T1, T2, T4 and T6 respectively. The highest FWHM value obtained for T6 sample again confirms its mild amorphous nature which validates the XRD data.

5.5.1.2 Optical analysis

In order to estimate band gap of 'sulfur varied' samples, absorption measurements were carried out in the wavelength range of 190-2500 nm

and the corresponding $(\alpha h\nu)^2$ versus energy (hν) graphs are plotted (Figure 5.16 (a)). Direct band gap of 1.40, 1.42, 1.37 and 1.37 eV are obtained for the samples T1, T2, T4 and T6, respectively.
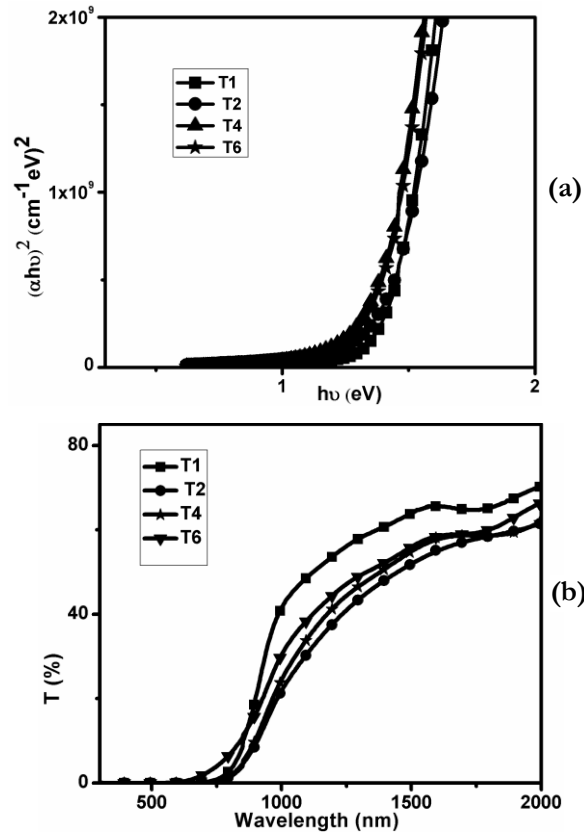
Figure 5.16 (a) $(\alpha h\nu)^2$ versus hν plot **(b)** Transmittance spectra of T1 to T6 samples

It may be noted that there is not much variation in band gap with variation in sulfur content. Transmittance spectra were also recorded in the wavelength range 300 to 2000 nm and are depicted in Figure 5.16 (b). Nature of transmittance remains almost same for all samples. It is clear that there is no transmittance in the visible wavelength range even

with this smaller thickness around 310 ± 20 nm whereas, it is above 40 % in the wavelength range greater than 1000 nm.

5.5.1.3 Morphological analysis of T4

Surface morphology is investigated with the help of SEM (Figure 5.17), with T4 sample indicating the presence of "worm-like or needle-like" structure characteristic of SnS [27].
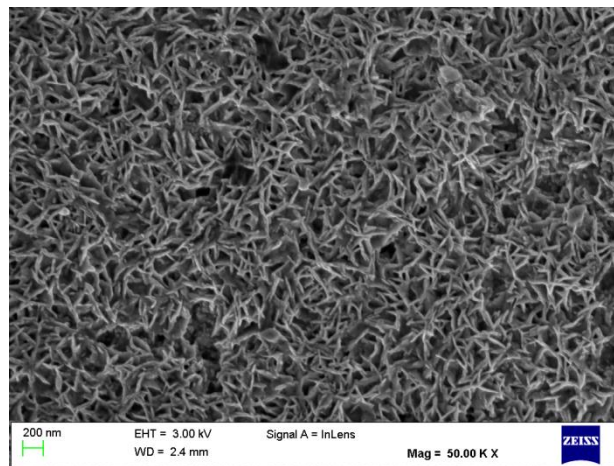
Figure 5.17 SEM image of sample T4

All samples have very good adhesion to substrate surface and are densely packed with uniform and pinhole-free surface.

5.5.1.4 Electrical studies

Electrical properties of SnS:Cu samples with different Sn/S ratio are investigated and the results are tabulated in Table 5.5. It can be seen that there is only minor change in carrier concentration, resistivity and mobility with change in sulfur concentration. Also, all the samples showed n-type nature.

Table 5.5 Electrical studies done on sulfur varied samples

Sample Name	Carrier Concentration (/cm^3) (*10^{18})	Resistivity (ohm.cm)	Mobility (cm^2/V.s)	Polarity
T1	4.5	3.2	0.4	n
T2	4.2	1.0	1.3	n
T4	6.1	1.1	0.7	n
T6	4.1	3.7	0.4	n

5.5.1.5 Compositional studies

Atomic concentration of each element in all the samples is calculated from the XPS spectra measured after etching a few surface layers of the sample and is tabulated in Table 5.6.

Table 5.6 Composition of sulfur varied films

Sample Name	O (%)	Sn(%)	S (%)	Cu (%)
T1	49.29	29.11	18.85	2.75
T2	21.25	51.35	24.64	2.76
T4	12.80	53.40	30.40	3.40
T6	7.96	51.08	37.09	3.87

From XPS, presence of excess tin concentration is confirmed for all the samples. It has already been reported that excess tin concentration leads to n-type conductivity in SnS thin films [28]. Thus the presence of excess tin in all samples as observed through XPS measurements confirms this. As shown in Table 5.6, oxygen concentration decreased from 49 % to 8 % as sulfur concentration is increased. Percentage of copper remained almost constant in all samples. Thus by varying precursor concentration, we succeeded in synthesizing SnS:Cu films with different

oxygen concentration without compromising structural, optical and electrical properties.

5.5.1.6 CZTS/SnS:Cu device characterization

Devices were fabricated using n-type SnS:Cu described in the previous section and p-type CZTS layer.
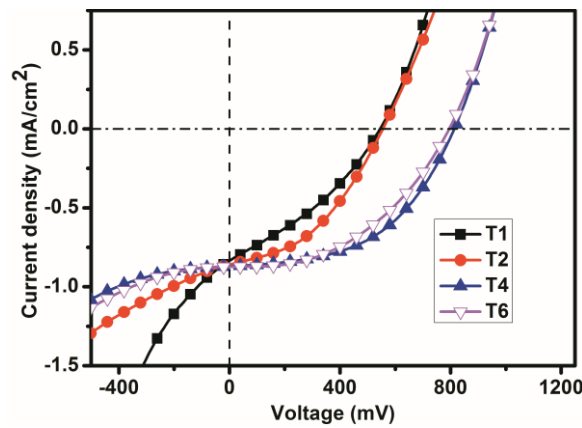
Figure 5.18 Illuminated J-V characteristics of CZTS/SnS:Cu devices

The J-V characteristics of the devices are depicted in Figure 5.18, and device parameters are shown in Table 5.7.

Table 5.7 Photovoltaic parameters of the CZTS/SnS:Cu device

Sample Name	V_{oc} (V)	J_{sc} (mA/cm^2)	Fill Factor (%)	Efficiency (η) (%)	R_{sh} (kΩ.cm^2)	R_s (Ω.cm^2)
T1	0.55	0.84	32	0.15	0.88	342
T2	0.56	0.86	42	0.20	2.44	289
T4	**0.81**	**0.87**	**51**	**0.36**	**11.76**	**247**
T6	0.80	0.87	46	0.32	41.67	287

Since the only difference in these devices is the change in composition of SnS:Cu layer, the variation in photovoltaic parameters may be correlated to change in composition of these films. For instance, it may be noted that, as oxygen percentage decreases below a certain level, there is a drastic improvement in open circuit voltage (V_{oc}) until it reaches a steady state. Fill factor and efficiency increased with decrease in oxygen concentration, reaching a maximum for the sample T4 and then decreased slightly. However, the short circuit current density (J_{sc}) remains almost constant for all devices. This may be due to high series resistance (R_s) that is roughly the same for all devices (see Table 5.7) that also accounts for the low value of J_{sc}. Ideally, series resistance should be around few ohms to get good J_{sc}.

Similarly from Table 5.7 it may also be noted that, for devices T1 and T2, the reverse current slopes down rapidly with increase in reverse voltage. This is clearly an indication of poor shunt resistance for these devices (Usually the R_{sh} comes around the order of ten thousand (10^4)) and suggests the presence of defects or recombination centers near junction. The shunt resistance (R_{sh}) is estimated for all devices and is given in Table 5.7. For devices T1 and T2, estimated values of R_{sh} are indeed quite small (lowest for T1 and about two orders less than for T4 and T6). Now considering the fact that oxygen percentage is higher for T1, the defects due to oxygen (such as O_i and O_S) near junction might be responsible for increased recombination, resulting in low value of shunt resistance. The decrease in shunt resistance due to increased recombination, in turn, lowers the V_{oc} of the devices, and this can be seen clearly for devices T1 and T2. The best cell (having SnS layer with oxygen content

~ 13 %) has achieved 0.36 % efficiency and 51 % fill factor. Hence improvement in cell parameters is obtained by varying the oxygen percentage present in the absorber layer.

5.5.2 Reducing Cu diffusion from CZTS

In the initial section of device study, we have seen an improvement in light activity in solar cells with reduction of Cu ratio in CZTS. To check the effect on further decreasing the Cu ratio, the CZTS layer is fabricated by reducing Cu content from 1.5 to 1, 0.5 and 0.25.
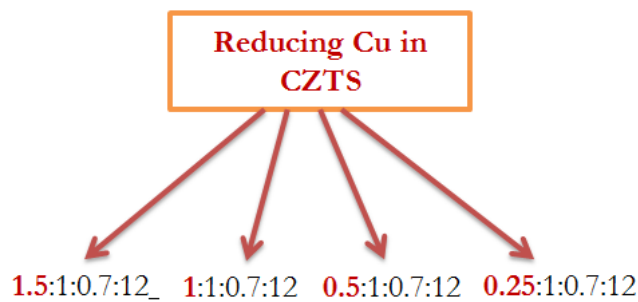
The reduction of Cu up to 0.25 was not found to affect the material properties [15]; however, decrease in Cu content makes CZTS more resistive and the resistive layer at the junction reduces the recombination probability of photogenerated charge carriers that helped charge carrier separation. In this way, the Cu diffusion and resistivity of CZTS can be manipulated to obtain maximum output. Solar cells were fabricated using CZTS with Cu ratio varied from 1.5 to 1, 0.5 and 0.25 keeping all other parameters constant. The cell parameters obtained (Table 5.8) and the J-V plot (Figure 5.19) is shown below. The optimization on 0.25 Cu

CZTS is neglected, since all its cell parameters observed are very low (graph is neglected).
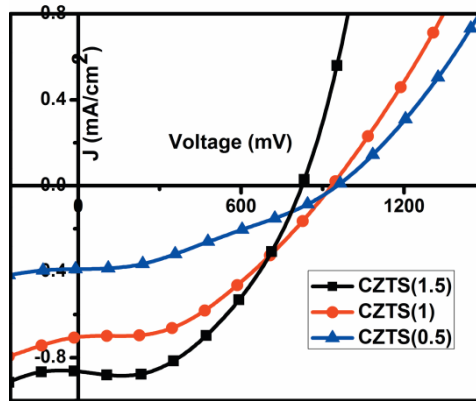
Figure 5.19 Illuminated J-V characteristics obtained by varying Cu ratio in CZTS

Table 5.8 Output parameters obtained by varying Cu ratio in CZTS

Cell name	Thickness (nm)	V_{oc} (mV)	J_{sc} (mA/cm^2)	FF (%)	Eff (%)
CZTS(1.5)	350	824	0.863	47	0.33
CZTS(1)	330	934	0.704	42	0.27
CZTS(0.5)	300	955	0.389	34	0.12
CZTS(0.25)	275	452	0.619	21	0.06

From the Table 5.8, it is seen that, with the decrease in Cu content in CZTS, V_{oc} increases but J_{sc} decreases. The increase in V_{oc} is probably due to the less copper diffusion to n-layer which reduces formation of impurity phases and makes the junction more perfect. The copper less resistive layer might also reduce the recombination rate of carriers generated and hence increase shunt resistance (R_{sh}) of the device.

However, there exists an optimum thickness below which all the device parameters are decreasing. Analyzing the J-V parameters described in the Table 5.8, we could neglect the 0.25 Cu CZTS since all its cell parameters were very low. Now it is to be noted that, due to the variation in Cu content of CZTS, thickness gets varied, and hence optimization of SnS:Cu thickness is required for each CZTS thickness and that has to be done next. Here also SnS:Cu optimization on 0.25 Cu CZTS is neglected since all its cell parameters observed are very low.

5.6 Thickness optimization of SnS:Cu for CZTS (1:1:0.7:12)

In order to optimize the thickness of n-layer, SnS:Cu (1:4 ratio with 4 % doping) is sprayed over the CZTS (1:1:0.7:12) by varying the spray time. The spray time is varied from 3' to 6' and the samples are named as SnS_3, SnS_4, SnS_5, SnS_6 SnS_7 respectively. The J-V characteristics are shown in the Table 5.9 below and the corresponding plot in Figure 5.20.

Figure 5.20 Illuminated J-V characteristics obtained by varying SnS:Cu thickness

Table 5.9 Output parameters obtained by varying SnS:Cu thickness

Cell name	V_{oc} (mV)	J_{sc} (mA/cm^2)	FF (%)	Eff (%)
SnS_3	316	0.996	25	0.07
SnS_4	462	0.939	28	0.12
SnS_5	466	0.814	45	0.17
SnS_6	**670**	**0.799**	**47**	**0.25**
SnS_7	681	0.339	69	0.15

The best performance is shown by the SnS_6 sample, which has thickness of 310 nm. This is the same thickness optimized for CZTS (1.5:1:0.7:12), but the maximum efficiency obtained here is less, compared to sample CZTS(1.5) and T4.

Similar explanation can be given as in the case of n-layer optimization (Section 5.4). Here also as the spray time increases, V_{oc} improves from 326 mV to 900 mV and J_{sc} decreases from 0.996 to 0.339 mA/cm^2.

5.7 Thickness optimization of SnS:Cu for CZTS (0.5:1:0.7:12)

The SnS:Cu thickness is varied from 3' to 6' so as to obtain the best thickness required for better performance. The CZTS (0.5:1:0.7:12) is coated over the ITO and then SnS:Cu is deposited over it by varying the spray time. The top ZnO:Al layer thickness and top electrode are kept same as in previous studies. The samples are named correspondingly as SnS:3, SnS:4, SnS:5, and SnS:6 respectively. The obtained parameters are shown in the Table 5.10 and J-V characteristics are shown in Figure 5.21.
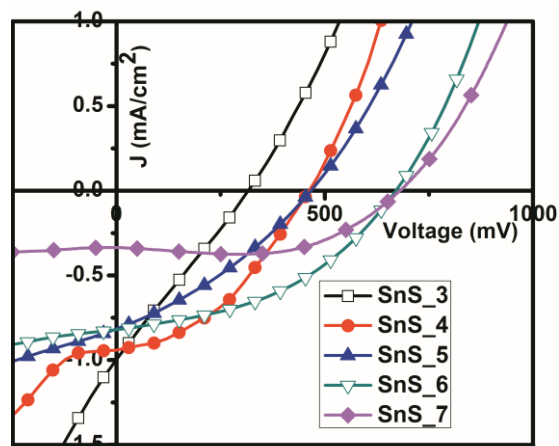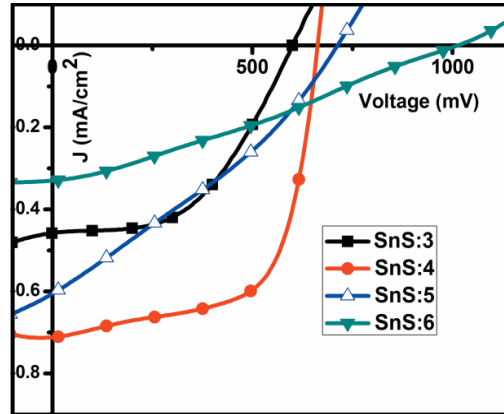
Figure 5.21 Illuminated J-V characteristics obtained
by varying SnS:Cu thickness

Table 5.10 Output parameters obtained by varying SnS:Cu thickness

Cell name	V_{oc} (mV)	J_{sc} (mA/cm^2)	FF (%)	Eff (%)
SnS:3	599	0.457	50	0.13
SnS:4	**662**	**0.711**	**64**	**0.30**
SnS:5	712	0.605	31	0.13
SnS:6	1013	0.328	29	0.09

Here also V_{oc} is found to be increasing with increase in SnS:Cu thickness but J_{sc} decreases accordingly and it is clear that the cell parameters are better for lesser thickness of SnS:Cu and the maximum efficiency (~ 0.3%) is obtained for 4' spray time which has a thickness 270 nm. Here the SnS:Cu thickness required is comparatively less and might be due to the effective less thickness of CZTS. Thus by optimizing the SnS:Cu thickness we could obtain almost similar efficiency of 0.3 % for both devices using CZTS (1.5:1:0.7:12) and CZTS (0.5:1:0.7:12) asa p-type laye withr along with optimized SnS:Cu n-layer.

5.8   Effect due to post-annealing:

From the above study, (Table 5.7 and Table 5.10) we observed that with optimized n layer thickness we could obtain almost similar efficiency (0.36 % and 0.3 %) with CZTS (1.5:1:0.7:12) and CZTS (0.5:1:0.7:12) p-layers respectively. Hence on these two devices, a new approach of post-annealing was done to check the possibility for further enhancement in efficiency. Here both CZTS(1.5) and CZTS(0.5) devices with highest efficiency configuration were taken and post-annealed separately. The post-annealing was given at different stages of fabrication in order to precisely understand its effect. Here the post-annealing temperature was kept as 375 $^\circ$C for 30 minutes, which we have optimized and found to be good from our earlier characterization studies (chapter 4). Post-annealing is given at three different stages of solar cell fabrication.

1) Samples are annealed before electrode deposition and ZnO:Al deposition and is named as BZBE

2) Samples annealed after ZnO:Al layer deposition and before electrode deposition and is name as AZBE

3) Samples annealed after complete fabrication of device ie after ZnO:Al and electrode deposition and is named as AZAE.

Hence depending on the annealing given, the devices with CZTS (1.5:1:0.7:12) layer were named as BZBE(1.5), AZBE(1.5) and AZAE(1.5) respectively and CZTS (0.5:1:0.7:12) devices were named BZBE(0.5), AZBE(0.5) and AZAE(0.5) respectively. The cell parameters obtained after three types of annealing given for these devices with CZTS (0.5:1:0.7:12) and CZTS (1.5:1:0.7:12) are shown in Table 5.11

and Table 5.12 respectively. The corresponding J-V plot is described in Figure 5.22 and Figure 5.23.
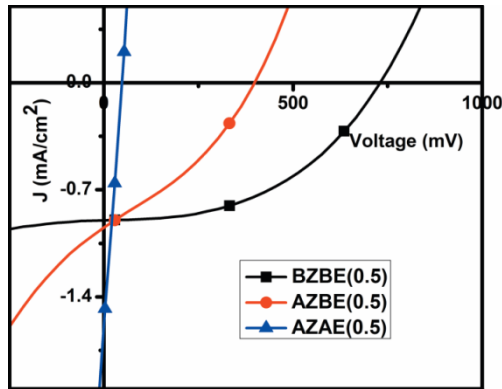
Figure 5.22 Illuminated J-V characteristics obtained after annealing for CZTS(0.5) device

Table 5.11 Output parameters obtained after annealing for CZTS(0.5) device

Cell name	V_{oc} (mV)	J_{sc} (mA/cm^2)	FF (%)	Eff (%)
BZBE(0.5)	**731**	**0.903**	**47**	**0.31**
AZBE(0.5)	397	0.945	32	0.12
AZAE(0.5)	470	1.600	24	0.01
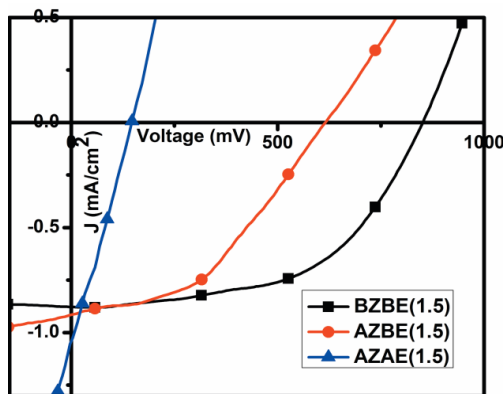
Figure 5.23 Illuminated J-V characteristics obtained after annealing for CZTS(1.5) device

Table 5.12 Output parameters obtained after annealing for CZTS(1.5) device

Cell name	V_{oc} (mV)	J_{sc} (mA/cm^2)	FF (%)	Eff (%)
BZBE(1.5)	**852**	**0.876**	**53**	**0.40**
AZBE(1.5)	614	0.910	43	0.24
AZAE(1.5)	146	1.040	27	0.04

From Table 5.11 and Table 5.12, it is clear that in both the cases similar trend is followed with the post-deposition annealing. The effect due to post-deposition annealing is quite convincing. We could see that in both devices, the annealing before the ZnO:Al deposition and electrode deposition (BZBE) resulted in an improvement in both V_{oc} and J_{sc} values compared to similar unannealed devices (Table 5.10 and Table 5.7). This increase in V_{oc} and J_{sc} might be due to the proper junction formation and increased production of carriers resulting from the annealing. This annealing effect is more pronounced in the case of devices fabricated using CZTS (1.5:1:0.7:12) that enhanced the efficiency to 0.4 % which is the highest efficiency reported so far with this configuration. For the devices fabricated by annealing after ZnO:Al layer deposition and before electrode deposition (AZBE) there was increase of current density with voltage drop. The reason for this voltage drop is probably due to the higher diffusion of copper into the SnS:Cu layer causing enhancement of the formation of more impurity phases. At the same time, with annealing, more free carriers are also generated resulting in an increase in current. But in the case of annealing after the complete fabrication (AZAE), the results (Table 5.11 and Table 5.12) show a drastic decrease in voltage with good enhancement in current density. Here the decrease

in voltage might be due to the diffusion of silver from electrode into the layers below which gives a recombination path for the carriers formed. Because more carriers are being formed due to annealing, the current is increased. Thus from the studies we selected devices with BZBE CZTS (1.5:1:0.7:12) composition as better one with SnS:Cu n-layer, to obtain maximum efficiency.

5.9 Conclusion

In the present study, trial work on CZTS/SnS:Cu heterojunction solar cells were carried out. Front and back contacts are made using Ag and ITO respectively. Initially, trials were carried out to optimize a suitable structure for the device and "ITO/CZTS/SnS:Cu/Ag was found to be the best. Later, the improvement of cell parameters were tried by introducing a top layer with ZnO:Al to get ITO/CZTS/SnS:Cu/ZnO:Al/Ag. The best cell had V_{oc} = 361 mV, J_{sc} = 0.866 mA/cm^2, Fill factor = 31 % and efficiency= 0.099%.

As the next step, thickness required for the top layer, p-layer and n-layer were optimized for improving the device performance. This is explored simply by varying the time required for spraying the respective precursor solutions. The best device fabricated has the cell parameters V_{oc} = 618 mV, J_{sc} = 0.930 mA/cm^2, Fill factor = 41 % and efficiency = 0.224 %.

To achieve further improvement in cell parameters, studies on ratiovariation and post-annealing treatment were tried and this could improve the cell parameters V_{oc} = 852 mV, J_{sc} = 0.879 mA/cm^2, Fill factor = 53 % and efficiency = 0.40 %. This study confirms the

possibility of preparing cells with compound semiconductors with eco-friendly and earth-abundant elements; moreover, these elements can be retrieved back from cells after their lifetime through simple chemical process.

References

[1]   Schneikart, A., H. J. Schimper, A. Klein, and W. Jaegermann. "Efficiency limitations of thermally evaporated thin-film SnS solar cells." *Journal of Physics D: Applied Physics* 46, no. 30 (2013): 305109.

[2]   Park.H. H, PhD Thesis, Harvard University, USA (2015)

[3]   Kawano, Yu, Jakapan Chantana, and Takashi Minemoto. "Impact of growth temperature on the properties of SnS film prepared by thermal evaporation and its photovoltaic performance." *Current Applied Physics* 15, no. 8 (2015): 897-901.

[4]   Wangperawong, Artit, Po-Chun Hsu, Yesheng Yee, Steven M. Herron, Bruce M. Clemens, Yi Cui, and Stacey F. Bent. "Bifacial solar cell with SnS absorber by vapor transport deposition." *Applied Physics Letters* 105, no. 17 (2014): 173904.

[5]   Hall, Robert Burton, and John D. Meakin. "The design and fabrication of high efficiency thin film CdS/Cu2S solar cells." *Thin Solid Films* 63, no. 1 (1979): 203-211.

[6]   Rajeshmon, V. G., C. Sudha Kartha, K. P. Vijayakumar, C. Sanjeeviraja, T. Abe, and Y. Kashiwaba. "Role of precursor solution in controlling the opto-electronic properties of spray pyrolysed Cu2ZnSnS4 thin films." *Solar Energy* 85, no. 2 (2011): 249-255.

[7] Rajeshmon, V. G., N. Poornima, C. Sudha Kartha, and K. P. Vijayakumar. "Modification of the optoelectronic properties of sprayed In2S3 thin films by indium diffusion for application as buffer layer in CZTS based solar cell." *Journal of Alloys and Compounds* 553 (2013): 239-244.

[8] John, Teny Theresa, Meril Mathew, C. Sudha Kartha, K. P. Vijayakumar, T. Abe, and Y. Kashiwaba. "CuInS$_2$/In$_2$S$_3$ thin film solar cell using spray pyrolysis technique having 9.5% efficiency." *Solar Energy Materials and Solar Cells* 89, no. 1 (2005): 27-36.

[9] Santhosh, M. V., D. R. Deepu, C. Sudha Kartha, K. Rajeev Kumar, and K. P. Vijayakumar. "All sprayed ITO-free CuInS2/In2S3 solar cells." *Solar Energy* 108 (2014): 508-514.

[10] Ge, Jie, Junhao Chu, Jinchun Jiang, Yanfa Yan, and Pingxiong Yang. "Characteristics of In-substituted CZTS thin film and bifacial solar cell." *ACS applied materials & interfaces* 6, no. 23 (2014): 21118-21130.

[11] Kim, Jung-Sik, Jin-Kyu Kang, and Dae-Kue Hwang. "High efficiency bifacial Cu$_2$ZnSnSe$_4$ thin-film solar cells on transparent conducting oxide glass substrates." *APL Materials* 4, no. 9 (2016): 096101.

[12] Tanaka, Kunihiko, Yuki Fukui, Noriko Moritake, and Hisao Uchiki. "Chemical composition dependence of morphological and optical properties of Cu$_2$ZnSnS$_4$ thin films deposited by sol–gel sulfurization and Cu$_2$ZnSnS$_4$ thin film solar cell efficiency." *Solar Energy Materials and Solar Cells* 95, no. 3 (2011): 838-842.

[13] Rajeshmon, V. G., MR Rajesh Menon, C. Sudha Kartha, and K. P. Vijayakumar. "Effect of copper concentration and spray rate on the properties Cu$_2$ZnSnS$_4$ thin films deposited using spray pyrolysis." *Journal of analytical and applied pyrolysis* 110 (2014): 448-454.

[14] Rajeshmon, V. G., Abin Kuriakose, C. Sudha Kartha, and K. P. Vijayakumar. "Effect of variation of tin concentration on the properties of Cu_2ZnSnS_4 thin films deposited using chemical spray pyrolysis." In *AIP Conference Proceedings*, vol. 1512, no. 1, pp. 1206-1207. AIP, 2013.

[15] Rajeshmon.V.G, PhD Thesis, Cochin University of Science and Technology, India (2013)

[16] Sebastian T, PhD Thesis, Cochin University of Science and Technology, India (2009)

[17] Vimalkumar T.V, PhD Thesis, Cochin University of Science and Technology, India (2011)

[18] Al-Ghamdi, Ahmed A., *et al.* "Semiconducting properties of Al doped ZnO thin films." *Spectrochimica Acta Part A: Molecular and Biomolecular Spectroscopy* 131 (2014): 512-517.

[19] Lee, Jin-Hong, and Byung-Ok Park. "Characteristics of Al-doped ZnO thin films obtained by ultrasonic spray pyrolysis: effects of Al doping and an annealing treatment." *Materials Science and Engineering: B* 106, no. 3 (2004): 242-245.

[20] Kim, Kyoung-Kook, Shigeru Niki, Jin-Yong Oh, June-O. Song, Tae-Yeon Seong, Seong-Ju Park, Shizuo Fujita, and Sang-Woo Kim. "High electron concentration and mobility in Al-doped n-ZnO epilayer achieved via dopant activation using rapid-thermal annealing." (2005): 066103.

[21] Cherian, Angel Susan, T. Abe, Y. Kashiwaba, C. Sudha Kartha, and K. P. Vijayakumar. "$CuInS_2/In_2S_3$ cells using a cost-effective technique: significance of precursor ratios on cell parameters." *Energy Procedia* 15 (2012): 283-290.

[22] Rau, Uwe, and Marion Schmidt. "Electronic properties of ZnO/CdS/Cu (In, Ga) Se$_2$ solar cells—aspects of heterojunction formation." *Thin Solid Films* 387, no. 1-2 (2001): 141-146.

[23] Aslan, Ferhat, Getachew Adam, Philipp Stadler, Abdullah Goktas, Ibrahim Halil Mutlu, and Niyazi Serdar Sariciftci. "Sol–gel derived In$_2$S$_3$ buffer layers for inverted organic photovoltaic cells." *Solar Energy* 108 (2014): 230-237..

[24] Hsiao, Yu-Jen, Chung-Hsin Lu, Liang-Wen Ji, Teen-Hang Meen, Yan-Lung Chen, and Hsiao-Ping Chi. "Characterization of photovoltaics with In$_2$S$_3$ nanoflakes/p-Si heterojunction." *Nanoscale research letters* 9, no. 1 (2014): 32.

[25] Djessas, K., S. Yapi, G. Massé, M. Ibannain, and J. L. Gauffier. "Diffusion of Cu, In, and Ga in In$_2$Se$_3$/CuGaSe$_2$/SnO$_2$ thin film photovoltaic structures." *Journal of applied physics* 95, no. 8 (2004): 4111-4116.

[26] Ryo, Toshihiro, Duy-Cuong Nguyen, Motohito Nakagiri, Noriaki Toyoda, Hiroaki Matsuyoshi, and Seigo Ito. "Characterization of superstrate type CuInS$_2$ solar cells deposited by spray pyrolysis method." *Thin Solid Films* 519, no. 21 (2011): 7184-7188.

[27] Sajeesh, T. H., K. B. Jinesh, C. Sudha Kartha, and K. P. Vijayakumar. "Role of pH of precursor solution in taming the material properties of spray pyrolysed SnS thin films." *Applied Surface Science* 258, no. 18 (2012): 6870-6875.

[28] Sajeesh, T. H., Anita R. Warrier, C. Sudha Kartha, and K. P. Vijayakumar. "Optimization of parameters of chemical spray pyrolysis technique to get n and p-type layers of SnS." *Thin Solid Films* 518, no. 15 (2010): 4370-4374.

Chapter **6**

SUMMARY AND FUTURE PROSPECTUS

With the growing energy demands of the current world, the need for photovoltaic device is inevitable. Advantages of solar energy like being a renewable energy source and surplus availability every day (as long as sun exists) makes it a better choice form other alternative energy sources. Solar energy is utilized for diverse applications other than producing electricity; it is a good source to generate heat, power satellites, distil water etc. Out of these, we mainly focus on solar cells which help to reduce the conventional electricity bills. It requires very low maintenance cost since there is no moving part, and more than that, each day the technological development for improvement for effectiveness of solar panels are going on. With all these advantages, like two sides of a coin, there are some disadvantageous also; but is negligible on comparing this with any other alternative energy resource. Some are initial purchasing cost of solar panel, dependence on weather conditions and unable to charge during night time, large space requirement for fixing panels, pollution due to use of toxic and hazardous products during cell manufacturing. Presently almost 90 % of solar panels are based on various types of silicon and hence, this material is considered as the 'king' among all photovoltaic materials. But the purification processes are very expensive and efficiency of panel

goes hand in hand with this purification. The Czochralski process of purification also results in significant wastage of silicon material. Moreover, due to indirect band gap and less absorption coefficient more than 100 microns of material is required to absorb light. Hence bulk amount of material is required for device fabrication. Comparing these drawbacks, thin films are more advantageous since all the manufacturing processes of Si wafer modules like Si purification, crystal growth, wafering, cell processing, cell encapsulation etc. can be effectively 'bundled' into one process in the case of the thin film. Also, the material cost can be reduced effectively as the thickness required is lesser by two or three orders than that required for Si wafer. But lot of improvement work has to be done to enhance efficiency. This includes choosing of materials, its deposition conditions, storing conditions etc. Hence choosing of thin film material for photovoltaic has to be done very carefully; it has to be earth abundant, non-toxic and stable. The method used for deposition also has similar importance and should be cost effective and simple. Tin chalcogenides are good choice which satisfies all the criteria. Thus the present thesis mainly focuses on complete characterization of n-type tin monosulfide material (SnS) and its device fabrication using economically viable technologically simple process viz., "chemical spray pyrolysis" (CSP). This n-type SnS can replace the toxic CdS which are currently used in solar cells. The idea of thesis was to first optimize preparation conditions of n-type SnS, then to optimize the deposition conditions of CSP technique for proper film deposition and finally to fabricate solar cell using this sprayed SnS:Cu as n- layer and CZTS as p- layer.

First, n-type SnS thin films were fabricated using tin chloride and thiourea in 1:2 ratio. The solvent quantity (HCl) for dissolving tin chloride is reduced in order to obtain the n-nature for SnS films prepared. From the structural and optoelectronic properties studied, 5 ml of HCl is found to be optimum. All these studies were done on "standard sample" which is prepared using "one day aged" tin chloride solution. Further improvement in material properties were obtained by In- situ doping with copper chloride and this is done by adding required percentages of 0.02 M $CuCl_2.2H_2O$. Doping percentage is varied and obtained 4 % of doping as the best.

As next step, deposition parameters of CSP were optimized in order to obtain good SnS:Cu films. Deposition parameters like substrate temperature, spray rate, cationic molarity and anionic molarity, which have significant influence on the properties of the material, were studied. Substrate temperature and spray rate are optimized to be 375 ^{o}C and 2 ml/min, respectively. The cationic to anionic ratio is optimized as 1:2 with molarity of tin and sulfur as 0.1 M and 0.2 M respectively.

As next step, various post-deposition techniques were investigated to further improve the material properties. Effects on material properties due to various type of annealing is checked and found air annealing at deposition temperature is more suitable and economic. Then the annealing time is varied systematically and found 30 minutes of annealing as best. The effectiveness of "inversion method" for preparing SnS:Cu with (111) orientation, which is very much suited for device fabrication, is checked. Ability of material to withstand variations in

precursor preparation temperature and also material stability with time were checked. Order of resistivity, which is found to be increasing with time, is brought back to its initial value by applying post-deposition annealing treatment. Hence n-type SnS:Cu thin films with required optoelectronic properties were synthesized, optimized and its effect on various environmental parameters were studied

The final chapter of this thesis deals with trials on fabrication of solar cells. Solar cells were fabricated using this eco-friendly SnS:Cu as n-layer and CZTS as p-layer. Through various modifications in device layers and cell configuration, performance of device was enhanced. For the deposition of these layers, automated CSP technique was employed. The figure below represents initial optimization done to fix device configuration and required thickness.
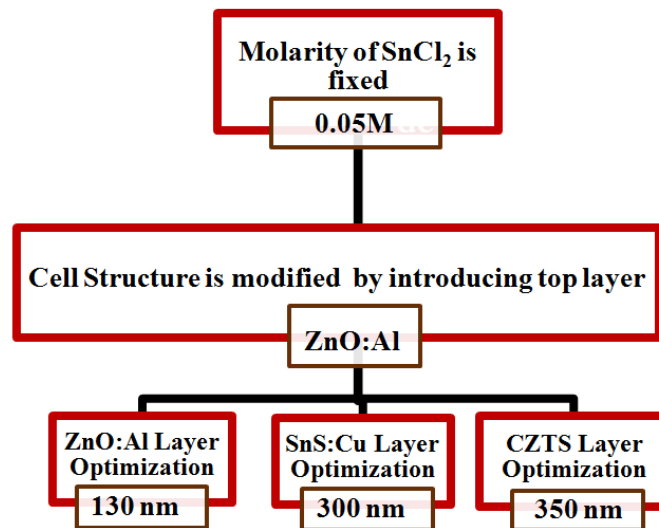
Thus CZTS/SnS:Cu hetero-junction solar cell were fabricated using Ag and ITO as front and back contact respectively. Molarity of $SnCl_2$ is reduced to 0.05 M for device layer. A suitable structure for the device "ITO/CZTS/SnS:Cu/Ag is selected for this study. Later, top layer of ZnO:Al is introduced to improve the cell parameters and structure is modified as ITO/CZTS/SnS:Cu/ZnO:Al/Ag. The best cell had V_{oc} = 361 mV, J_{sc} = 0.866 mA/cm^2, fill factor = 31 % and efficiency = 0.099 %. Now thickness required for each layer was optimized by varying spraying time of respective precursor solutions. The best device fabricated with these optimized thickness has cell parameters V_{oc} = 618 mV, J_{sc} = 0.930 mA/cm^2, fill factor = 41% and efficiency = 0.224%.

Enhancement in efficiency could be achieved further by reducing oxygen content present in the prepared film by varying the Sn:S ratio and also by various post-deposition annealing treatment at various stages of device fabrication. Annealing processes are named as BZBE (annealed before electrode deposition and ZnO:Al deposition), AZBE (annealed after ZnO:Al layer deposition and before electrode deposition) and AZAE (annealed after complete fabrication of device). The diagram below gives a brief outline of variations done.
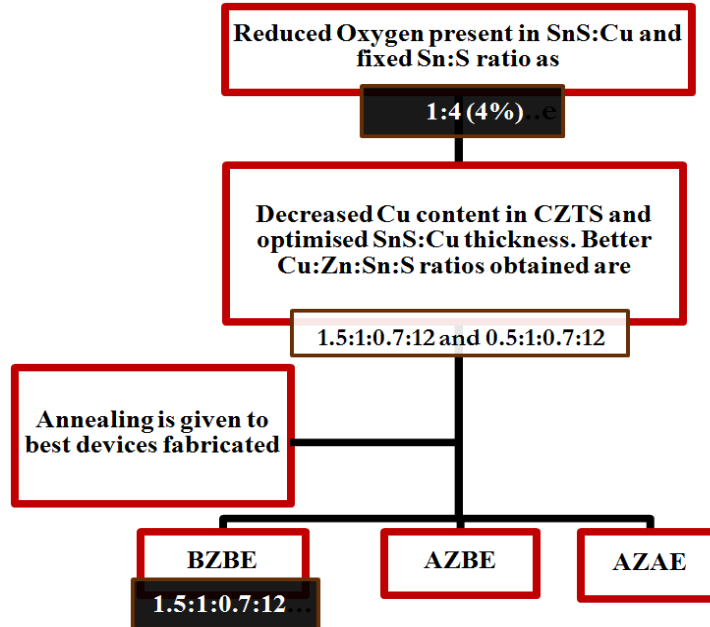
Out of various annealing given, the BZBE annealing on cells with SnS:Cu (1:4 (4 %)) and CZTS (1.5:1:0.7:12) is found to be best. This annealing could improve the cell parameters as V_{oc}= 852 mV, J_{sc}= 0.879 mA/cm^2, Fill factor = 53 % and efficiency = 0.40 %. This is the highest efficiency reported so far with this material and configuration. The possibility to deposit many solar cells with each batch of preparation, reduces the consumption of energy for a single solar cell fabrication.

Future prospects

SnS:Cu being a new material, a lot more investigation into material properties can be done further for better improvement of film properties. For example, SnS is having small grain size around 12-18 nm and has high resistivity around few hundred Ohm.cm at near stoichiometric compositions. Doping can help in overcoming this

limitation and very few works has been done in this direction. In the present work, only copper doping is attempted. The effect due to various other dopants like sodium, indium, zinc etc should be studied.

All the material studies and optimization in the present work is done on n-type SnS prepared using tin chloride solution dissolved in 5 ml of solvent HCl. Similar studies can be carried out by further decreasing the amount of tin precursor solvent HCl. Structural and optoelectronic properties for these films can be studied and these films can be used for device fabrication.

Diffusion of silver (electrode) towards bottom layer is the main challenge for SnS:Cu based solar cells, especially when prepared using CSP technique. For the present study, we used ZnO:Al top layer to prevent this diffusion. Various other top layer materials can be tried and continuous monitoring of diffusion should be done with XPS for comparing. In this way the leakage current can be minimized and can enhance the V_{oc} further.

Lower value of J_{sc} is another issue. To improve this, series resistance of the cell should be further minimized. This can be achieved by altering resistivity of both n and p layer. Resistivity of SnS can be manipulated easily by doping it with various dopants. With CSP technique this can be achieved very easily by incorporating the dopant salt with the precursor solution for SnS. Apart from this, type of in-situ doping, ex-situ doping can also be tried by depositing a dopant metal layer at top of the SnS layer followed by annealing. Similar modifications can be tried on p-layer and conducting top layer also. By doing so, device will have a

conducting layer near the electrode and a resistive layer near junction. This will help in effective carrier separation and carrier collection.

Fabrication of heterojunctions with other organic and inorganic materials can be tried. As an initial step, to show its possibility, devices were fabricated using organic polymer material (P3HT:PCBM) with structure ITO/SnS:Cu/Polymer/Ag and also with inorganic material CZS with structure ITO/CZS/SnS:Cu/ZnO:Al/Ag; efficiencies of ~ 0.08 % and 0.04 % respectively were achieved in these cases (Table 6.1).
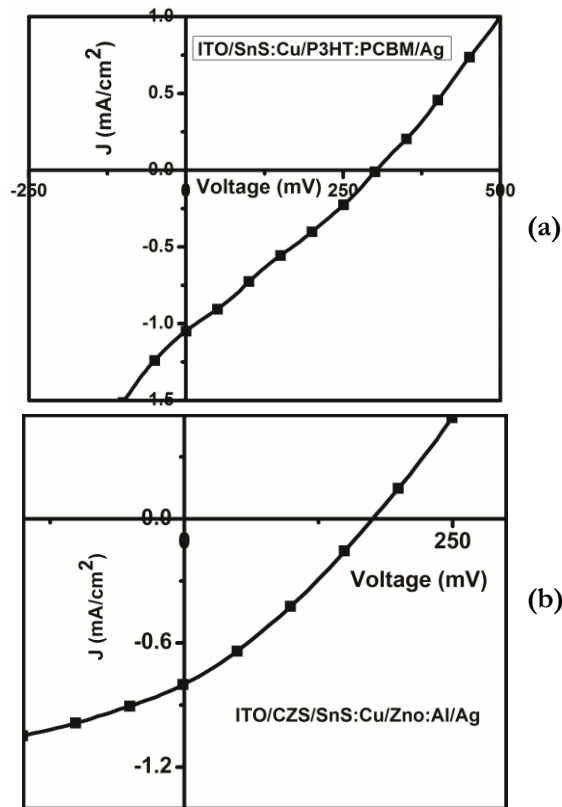
Figure 6.1 Illuminated J-V characteristics obtained for (a) Polymer based solar cell (b) CZS based solar cell

Table 6.1 PV parameters obtained from both organic and inorganic material based solar cell

Cell Name	V_{oc} (mV)	J_{sc} (mA/cm^2)	Fill factor (%)	Efficiency (%)
Polymer	304	1.03	26	0.08
CZS	176	0.79	29	0.04

Similarl, devices can be fabricated using alternative transparent conducting oxide materials like ZnO, SnO$_2$, FTO using spray technique. This can replace the imported ITO coated glass we used presently and can reduce cost of solar cells further. Possibility of solar cell fabrication using other earth-abundant non-toxic material can also be checked, which can be an alternative of this SnS:Cu material. Materials like Sn$_2$S$_3$, SnS$_2$, CZS, CuS etc. gain attention in this aspect. Studies on optimizing deposition conditions and material characterizations for cell fabrication can be pursued. Here is the table (Table 6.2) showing the highest efficiencies so far published by progress in photovoltaics.

Table 6.2 PV parameters obtained for various thin films reported to have highest efficiency

Cell Name	V_{oc} (mV)	J_{sc} (mA/cm^2)	Efficiency (%)
CdTe (Thin Film)	887	32	22
CZTSS (Thin Film)	513	35	13
CZTS (Thin Film)	730	21	11

On comparing the open circuit voltage and fill factor they obtained, we could say that we have almost reached near to these using our easy fabrication technique and also with thinner n and p-layers. But

the efficiency is very low due to very low J_{sc} we obtained and hence further enhancement of J_{sc} is required to bring about the complete potential of this material. The present work is a preliminary study and hence there is more room for further improvement. This thesis is only a small step for achieving this greater goal and lots of focused and determined efforts should be put forth to make this initiative a reality.

.....ജ്ഞ.....